AD-A037 252 AIR FORCE ARMAMENT LAB EGLIN AFB FLA F/G 17/5
EXPERIMENTAL RESULTS FOR HYDROCARBON EXHAUST INFRARED MODEL VER--ETC(U)
JUL 76 W J ROTHSCHILD, C W MARTIN
AFATL-TR-76-74

UNCLASSIFIED NL

1 OF 2
AD A037252

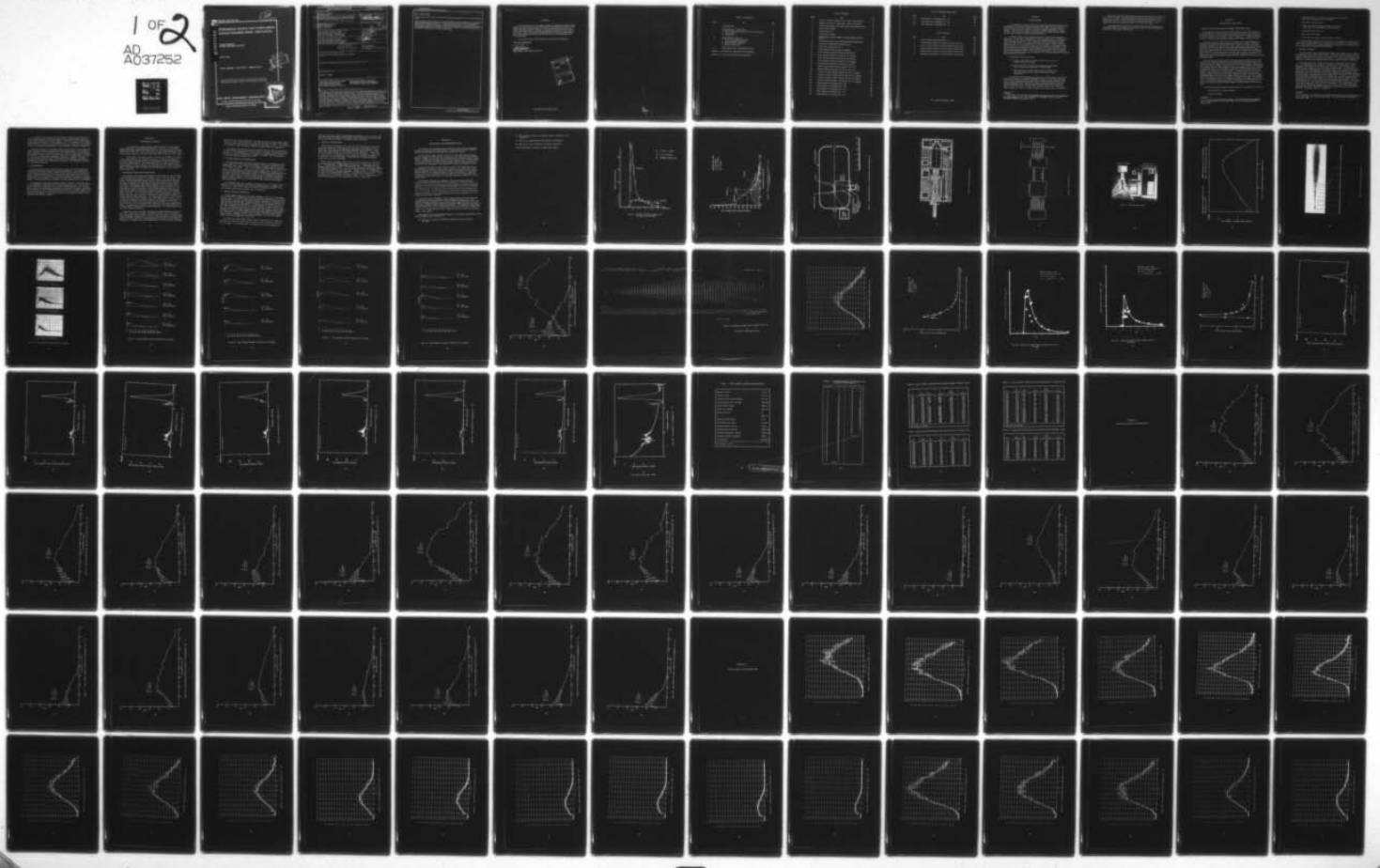

AFATL-TR-76-74

(12) NW

EXPERIMENTAL RESULTS FOR HYDROCARBON EXHAUST INFRARED MODEL VERIFICATION

TARGETS BRANCH
GUIDED WEAPONS DIVISION

JULY 1976

FINAL REPORT: JULY 1975 - MARCH 1976

AIR FORCE ARMAMENT LABORATORY
AIR FORCE SYSTEMS COMMAND • UNITED STATES AIR FORCE
EGLIN AIR FORCE BASE, FLORIDA

UNCLASSIFIED
SECURITY CLASSIFICATION OF THIS PAGE (When Data Entered)

REPORT DOCUMENTATION PAGE

READ INSTRUCTIONS BEFORE COMPLETING FORM

(14) 1. REPORT NUMBER: AFATL-TR-76-74 ✓

2. GOVT ACCESSION NO.

3. RECIPIENT'S CATALOG NUMBER

(6) 4. TITLE (and Subtitle): EXPERIMENTAL RESULTS FOR HYDROCARBON EXHAUST INFRARED MODEL VERIFICATION.

(9) 5. TYPE OF REPORT & PERIOD COVERED: Final Report, Jul 75 - Mar 76 ✓

6. PERFORMING ORG. REPORT NUMBER

(10) 7. AUTHOR(s): William J. Rothschild, Charles W. Martin

8. CONTRACT OR GRANT NUMBER(s)

(16) (17) 03

9. PERFORMING ORGANIZATION NAME AND ADDRESS
Guided Weapons Division (DLMI)
Air Force Armament Laboratory ✓
Eglin Air Force Base, Florida 32542

10. PROGRAM ELEMENT, PROJECT, TASK AREA & WORK UNIT NUMBERS
Project No. 1921
Task No. 03
Work Unit No. 01

11. CONTROLLING OFFICE NAME AND ADDRESS
Air Force Armament Laboratory
Armament Development and Test Center
Eglin Air Force Base, Florida 32542

(11) 12. REPORT DATE: Jul 1976

13. NUMBER OF PAGES: 126

14. MONITORING AGENCY NAME & ADDRESS (if different from Controlling Office)

(12) 128 p.

15. SECURITY CLASS. (of this report): UNCLASSIFIED

15a. DECLASSIFICATION DOWNGRADING SCHEDULE

16. DISTRIBUTION STATEMENT (of this Report)

Approved for public release; distribution unlimited.

17. DISTRIBUTION STATEMENT (of the abstract entered in Block 20, if different from Report)

18. SUPPLEMENTARY NOTES

Available in DDC.

P.E. 62602F

19. KEY WORDS (Continue on reverse side if necessary and identify by block number)

Hydrocarbon Exhaust Infrared Model
Infrared Simulation Technology
Hydrocarbon Exhaust Plumes
Plume Spectral Radiation Distribution
Plume Spatial Radiation Distribution
Hydrocarbon Exhaust Infrared Intensity
Plume Centerline Radiation Distribution

20. ABSTRACT (Continue on reverse side if necessary and identify by block number)

The objective of this effort was to evaluate a number of computer models used to predict infrared characteristics of hydrocarbon exhaust plumes. This report contains the experimental results obtained. Controlled plumes were generated using a small rocket operating at approximately 4 atmosphere chamber pressure and 5 grams per second total mass flow rate, exhausting into a large chamber held at 13.1 kilometers, static altitude conditions. Two liquid and two gaseous fuels were burned with gaseous oxygen at mixture ratios from 1.2 to 8.4. Engine performance was monitored with respect to combustion efficiency. Plume spatial radiation distributions were measured normal to the exhaust centerline by a scanning radiometer operating in the 4.1- to 5.1-micrometer band. Plume spectral radiation distributions were measured in a spot on the

DD FORM 1 JAN 73 1473 EDITION OF 1 NOV 65 IS OBSOLETE

400 936

UNCLASSIFIED
SECURITY CLASSIFICATION OF THIS PAGE (When Data Entered)

Item 20 (Concluded):

on the plume centerline by an interferometer spectrometer operating in the 2- to 5-micrometer region.

These results show that the degree of plume afterburning with the ambient air is the dominant factor controlling hydrocarbon exhaust infrared intensity in the 4.0- to 5.5-micrometer band. Mixture ratio, combustion efficiency, and propellant composition are the key parameters affecting plume afterburning processes. These data should provide a good basis for comparison with predicted results over a sufficiently broad range of conditions to allow thorough model verification and identification of model deficiencies.

PREFACE

The efforts described in this technical report were supported by Program Element 62602F and conducted under Project 1921, Task 03, and Work Unit 01, as part of the Infrared Simulation Technology program. The work was performed in-house by the Infrared Technology Team of the Targets Branch during the period from July 1975 to March 1976. Captain William Jollie provided assistance in obtaining the spectroscopic data. Other significant contributors were Mr Dale Fink, Mr Louis Weatherford, and Dr Davut Ebeoglu.

This technical report has been reviewed and is approved for publication.

FOR THE COMMANDER

JOHN W. JOHNSON
Deputy Chief, Guided Weapons Division

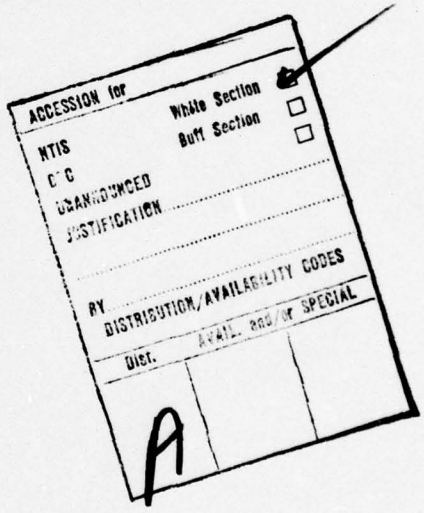

(The reverse of this page is blank)

blank
ii

TABLE OF CONTENTS

LIST OF FIGURES

LIST OF FIGURES (CONCLUDED)

LIST OF TABLES

(The reverse of this page is blank)

SECTION I

INTRODUCTION

The investigation of parameters influencing hydrocarbon exhaust plume infrared (IR) characteristics is of interest to the Air Force for air-to-air missile and target systems. IR seeker response during terminal guidance is driven by the spatial distribution of plume radiation. Target realism with respect to IR implies a detailed understanding of plume radiation. Valid, analytical models of hydrocarbon plume IR characteristics are essential for both seeker response and target simulation applications.

A detailed evaluation of one afterburning plume IR model has been reported in Reference 1. The calculations compared poorly with the measured data. The largest errors occurred for fuel-rich mixture ratios (O/F) where the measurements showed the highest radiant intensities (see Figure 1). The predicted and measured total radiant intensities agree near an O/F of 3.5. This agreement is fortuitous, as shown in Figure 2, since the spatial distribution of the data does not agree with the predictions. Considerable analysis has been done by many workers to explain these errors and improve the models. A new series of experiments and calculations were necessary to clarify these former discrepancies and evaluate the improved models. This activity has been organized as part of the Cooperative Plume Modelling Program under the auspices of The Technical Cooperative Programme/ Working Technical Panel No. 4.

The objectives of this effort were to:

- Provide a broad basis for verifying a variety of state of the art, afterburning plume IR models.
- Evaluate the effect of hydrocarbon propellant carbon/hydrogen ratio on afterburning exhaust plume IR characteristics.
- Assess the effects of rocket engine combustion efficiency and liquid versus gaseous fuels on afterburning exhaust plume IR characteristics.

The experiments were performed in a large vacuum chamber under a static pressure environment simulating 13.1-kilometer (40,000-foot) altitude. A small rocket engine was used to create a supersonic exhaust plume under controlled propulsive conditions. Mass flow rates were approximately 5 grams per second, and chamber pressures were approximately 4 atmospheres. Both mass flow and pressure were monitored as a measure of engine combustion efficiency. Kerosene (RP-1), ethylene (C_2H_4), methane (CH_4), and benzene (C_6H_6) were burned with gaseous oxygen at mixture ratios from 1.2 through 8.4.

Reference

1. D. B. Ebeoglu and C. W. Martin, Experimental Verification of Infrared Plume Predictions for a Rocket Engine, AFATL-TR-74-191 (Eglin Air Force Base, Florida: Air Force Armament Laboratory), 19 November 1974.

Spatially and spectrally resolved plume IR measurements were made normal to the plume axis of symmetry. A Bofors scanning radiometer (infrared scanner) was used to measure the plume spatial radiation distribution. This system was operated in the 4.1- to 5.1-micrometer region. A Block Engineering interferometer spectrometer was used to measure the plume spectral radiation over the 2- to 5-micrometer region.

Five independent sets of plume IR calculations were made for comparison with these measurements. The remainder of this report describes in detail the experimental arrangement, resulting data, and conclusions.

SECTION II

EXPERIMENTAL CONDITIONS

1. ROCKET ENGINE AND VACUUM CHAMBER INSTRUMENTATION

All measurements were conducted in a vacuum chamber at Eglin Air Force Base at a static altitude of 13.1 kilometers using the measurement geometry shown in Figure 3. The vacuum chamber, the rocket engine, engine control unit, and the engine instrumentation for the measurements are described in detail in Reference 2. A scale rocket drawing is shown in Figure 4, and the operating parameters of the engine are listed in Table 1.

The rocket control unit (RCU) illustrated in Figure 5 is an in-house designed and fabricated rocket control and instrumentation system described in detail in Reference 2. The RCU is composed of a valve box and a control console. The valve box houses a pressurized, liquid fuel tank, several solenoid valves, motor-driven metering valves, pressure transducers, flow rate transducers, and the interconnecting plumbing necessary to vary rocket input conditions and to monitor those conditions. The valve box is connected by an AC cable and a shielded signal cable to the RCU control console. The control console houses the manual switching network for rocket operation, transducer electronics, and a digital display panel which indicates pressures, flow rates, oxidizer-to-fuel ratio, and a banded radiometric reading.

The pressures were measured with thin film strain gauge-type transducers which were calibrated with pressurized nitrogen against helicoid Bourdon tube pressure gauges. The oxygen flow rate was measured with a thermal flowmeter calibrated against a variable area, glass flowmeter with a viscosity independent float. The liquid fuel flow rate was measured with a turbine flowmeter calibrated against a variable area, glass flowmeter with a spherical, constant density float. All the transducer outputs from the RCU control console were recorded on an eight-channel strip-chart recorder. The gaseous fuel flow rates were determined by visual readings from a variable area tube flowmeter identical to the oxygen reference standard. The test chamber pressure (altitude) was visually read from a mercury manometer calibrated in altitude. The pressure altitude was held at 13.1 ± 0.2 kilometers. Each of the pressure and flow rate system errors was less than 5 percent. The 5 percent errors in the flow rates result in a ± 10 percent uncertainty in the oxidizer-to-fuel mixture ratio. The experimental characteristic velocity (C^*) was determined by the product of nozzle throat area times measured chamber pressure divided by measured total mass flow rate.

The general experimental procedure used to achieve the data conditions is as follows:

- Set test chamber to altitude condition.
- Ignite rocket engine.

Reference

2. J. F. Long, Air Force Armament Laboratory Infrared Plume Simulation Capabilities, AFATL-TR-76-26 (Eglin Air Force Base, Florida: Air Force Armament Laboratory), 19 May 1976.

- Adjust flow rates to a desired O/F above stoichiometric mixture ratio and hold condition for data collection.
- Collect data during hold time.
- Adjust flow rates to a desired O/F below stoichiometric mixture ratio and hold condition for data collection.
- Collect data during hold time.
- Shut down rocket engine.
- Return the test chamber to ambient pressure conditions.

If it was determined that the engine conditions or the infrared data changed significantly during the data collection time, the data points were repeated. The data collection time for the infrared scanner data was approximately 10 seconds, and the collection time for the spectral data was approximately 20 seconds.

2. INFRARED SCANNER

The infrared plume spatial distributions and integral plume apparent radiant intensities were measured with an infrared scanner system. The infrared scanner system consists of a Bofors infrared camera and camera control monitor with a digital data acquisition system interfaced to a 9-track digital tape recorder (Figure 6). The data reduction software and calibration procedures were developed in-house and are reported in detail in Reference 3.

The infrared camera has a 25-degree (horizontal) by 12.5-degree (vertical) field of view. The instantaneous field of view of the scanner is 0.14 degree which is swept horizontally and vertically with scanning mirrors to produce a 94-line raster which is displayed on the cathode-ray tube of the camera control monitor. An oscilloscope was used to display the horizontal raster line (analog) nearest to the centerline of the exhaust plume with the detector/preamplifier voltage output displayed as the amplitude of the oscilloscope trace. The oscilloscope time base was adjusted such that the 600-microsecond line sweep extended completely across the oscilloscope scale (10 divisions). An oscilloscope camera was used to photograph this plume centerline data. Also, the complete picture was digitized line-by-line and recorded on the 9-track magnetic tape recorder to yield a two-dimensional matrix of 224 (horizontal) by 90 (vertical) picture elements. The digitizer system digitizes only every fourth point along a horizontal line for 56 points per line in a single picture scan of 94 lines (one file) in 0.35 second. On successive scans, every fourth point is digitized, then staggered over by 1, then 2, then 3. The four sequential, quarter-resolution, 56- by 94-element matrices can be interlaced to produce the 224- by 94-element full-resolution picture in 1.39 seconds.

Reference
3. C. W. Martin, et al, Operation of an Infrared Thermal Scanner for Plume Measurements, AFATL-TR-74-204 (Eglin Air Force Base, Florida: Air Force Armament Laboratory), 19 December 1974.

The infrared scanner 4.0-micrometer cut-on filter and photovoltaic InSb detector (at 77°K) combination viewing through the sapphire vacuum chamber window yields the system spectral response curve shown in Figure 7. The scanner system spectral bandpass, including sapphire window port, is approximately 4.1 to 5.1 micrometers. The bandpass is well centered on the CO_2 emission band and extends only slightly beyond the spectral cutoff of the interferometer spectrometer. (This is discussed in Section II, paragraph 3.)

The scanner alignment at the sapphire window was such that the rocket engine exit plane was several centimeters inside the left field of view extremity, and the horizontal center of the field of view was perpendicular to the rocket centerline and perpendicular to the sapphire window. Some of the plumes were found to extend beyond the scanner field of view at a front-of-camera distance of 2.18 meters. Subsequent data were taken at a front-of-camera distance of 2.97 meters to alleviate this problem. The spatial resolution of the digital matrix data at 2.18 meters is 5.2 millimeters horizontally by 6.3 millimeters vertically. At 2.97 meters, the resolution is 6.8 millimeters horizontally and 8.1 millimeters vertically.

3. SPECTROMETER

The infrared plume spectral distributions were measured with a Block Engineering interferometer spectrometer capable of 2 wavenumber resolution. The instrument uses a mini-computer for real-time data acquisition and fast Fourier transform data reduction. Both an uncooled PbSe detector and a cooled (77°K) InSb detector were used for the spectral range of 2 to 5 micrometers. The spectral response of the system is internally corrected in the mini-computer by comparisons with black-body calibration and background spectra. The data are plotted on an integral x-y plotter interfaced to the mini-computer.

The spectrometer measurement geometry is shown in Figure 8. The window used for the spectrometer measurements was a 14-centimeter-diameter calcium fluoride window whose transmission is accounted for in the system response (Figure 9). The maximum field of view of the interferometer spectrometer as used here was 5 degrees. The spectral data are reported in units of apparent spectral radiant intensity or spectral irradiance since all of the plume was not in the instrument field of view. At low O/F conditions (i.e., high radiance conditions), the spectrometer field of view was reduced to as low as 1.25 degrees to avoid electronic saturation.

SECTION III

EXPERIMENTAL RESULTS

The infrared plume radiation along the plume centerline, the total apparent radiant intensity, and the radiation spatial distribution in the 4.1- to 5.1-micrometer band and the radiation spectral distribution in the 2- to 5-micrometer band were measured for each of four fuels: RP-1, C_2H_4, CH_4, and C_6H_6 (commercial grade or better). These fuels were burned in the AFATL rocket with gaseous oxygen (commercial grade).

A photograph of the plume is shown in Figure 10 for O_2/RP-1 at an O/F of 2 and a total mass flow rate of 5 grams per second. The plume is exhausting from the rocket nozzle on the extreme left of the photograph, and the shock structure in the plume is readily apparent. The visible exhaust plume, as shown in Figure 10, is virtually identical for each of the fuels at an equivalent O/F (same fraction below or above stoichiometric mixture ratio) and varies little with changes in O/F. The following spatial plume radiation data is presented and discussed based on the plume geometry shown in Figure 10.

1. CENTERLINE RADIATION DISTRIBUTIONS

Three samples of the infrared plume radiation centerline data are shown in Figure 11 for O_2/CH_4 at three different O/F conditions: O/F = 2.3, 4.1, and 6.6. These traces are oscilloscope photographs of the infrared scanner center-of-plume raster line (analog). The oscilloscope was triggered such that only the desired line is displayed. This single line shows a 7mm high trace of the plume centerline radiance including the effects of self-absorption and scattering through the thin slice of plume along the line of sight. The horizontal field of view is adjusted to span 10 divisions on the oscilloscope scale which is equivalent to 105 centimeters along the plume axis. The camera shutter speed was 10 seconds, so approximately 28 sweeps of the centerline occur on each exposure. This number of sweeps is necessary at low O/F conditions (such as the O/F = 2.3 for CH_4 in Figure 11) since the afterburning in the plume causes a very ragged trace and must be integrated over several seconds to achieve an average radiation centerline distribution. The exhaust plume goes left to right as shown in Figure 10, with the shock structure in the plume clearly evident as spikes. Note that the high temperature, high radiance regions occur downstream of each shock. The strong Mach disc occurs at or near 1.6 centimeters downstream of the exit plane of the rocket, with up to six discernible weaker shocks out to about 12 centimeters downstream. The small signal just upstream of the exit plane is the ignition spark plug of the engine which is heated above the external temperature of the cooled engine by the high internal chamber temperature.

Figures 12, 13, 14, and 15 show the centerline radiation distributions for the four fuels: RP-1, C_2H_4, CH_4, and C_6H_6. These data were traced from the oscilloscope camera photographs (examples shown in Figure 11) with the physical axial distance scale. The data presented in Figures 12, 13, 14, and 15 were normalized to a constant amplitude scale such that each of the centerline distributions for any of the fuels may be compared on a consistent basis and are representative of the fifty centerline photographs

taken on the four fuels at various O/F. The total mass flow rate, which changed slightly from fuel to fuel, is indicated for each of the O/F data points. Figure 16 is an example of these centerline radiation traces in expanded scale for O_2/RP-1 at O/F = 4.7 and 1.7. The remainder of these expanded scale centerline radiation traces are in Appendix A.

The centerline data clearly show that the oxidizer-to-fuel ratio drastically affects the centerline radiation distribution for each of the fuels. The peak in the centerline radiation may occur at a point downstream half the length of the radiating plume at low O/F conditions or amid the shock structure at high O/F conditions. Also, the amplitude of the centerline radiation is affected by the O/F.

2. STATION RADIATION DISTRIBUTIONS

The digital data format of the infrared scanner system is a two-dimensional spatial matrix of 56 to 94 data elements (cells) representing a 25-degree horizontal and 12.5-degree vertical field of view. Figure 17 is a sample of a quarter resolution data printout for O_2/RP-1 at an O/F = 2.4. The pertinent experimental data is printed on the output. The background (in digital units) has been removed from the data, and only the nonzero matrix elements are printed in units of milliwatts per steradian per unit cell. The data is summed for a total radiant intensity in units of milliwatts per steradian. The data is also summed by columns or lines for units of milliwatts per steradian per column or line (see Table 2). The term station radiation (J/ℓ) will be used here to denote the radiant intensity per unit length (column sums divided by the horizontal distance per column).

Full resolution spatial data is recovered by interlacing four of the quarter resolution matrices in the proper sequence such that the horizontal increment is decreased by a factor of four. Figure 18 is a sample of this data for O_2/RP-1 at an O/F = 2.4. The remaining station radiation data are given in Appendix B.

3. SPECIFIC RADIANT INTENSITIES

The total radiant intensity (J) of the plume radiation in the 4.1- to 5.1-micrometer band is determined by integrating under the station radiation distributions or by summing the matrix data. In order to compare the total radiant intensities from different runs at slightly different mass flow rates, the radiant intensities are divided by the measured total mass flow rate for specific radiant intensity in units of joules per steradian per gram (or watts per steradian per gram per second). The complete sets of data for each of the four fuels are tabulated in Tables 3, 4, 5, and 6 and plotted in Figures 19, 20, 21, and 22. It can be determined from the data in these tables that there is an inverse relation between C* and specific radiant intensity and that these two parameters are highly dependent upon the O/F. It is also apparent that the peak specific radiant intensity occurs at a different O/F condition for each of the four fuels. This O/F for peak specific radiant intensity is dependent upon the carbon-to-hydrogen ratio, occurring at approximately one-half the stoichiometric mixture ratio.

The gaseous fuel specific radiant intensity curves in Figures 20 and 21 (C_2H_4 and CH_4) show more data point scatter than the liquid fuel curves (Figures 19 and 22 for RP-1 and C_6H_6). This increased scatter is attributed to the visual measurements of

gaseous fuel flow rates using a float-type glass tube flowmeter. Errors in the fuel mass flow rate can produce significant (±10 percent) errors in the O/F at low mixture ratios and can thus cause data scatter in the regions of steep curve slope.

4. SPECTRAL DISTRIBUTIONS

Plume spectra of O_2/C_2H_4 at O/F of 5.5, 3.9, and 2.5 are shown in Figures 23, 24, and 25, respectively. These spectra were taken using a PbSe detector with a 5-degree field of view centered 40 centimeters downstream of the nozzle exit. These spectra are virtually identical to those obtained for RP-1 (Reference 1). Figures 26 and 27 show spectra of O_2/CH_4 at O/F of 5.1 and 2.2, respectively. An InSb detector was used with a 1-¼-degree field of view centered 15 centimeters downstream of the nozzle exit. Note the appearance of unburned CH_4 in the fuel-rich spectrum (Figure 27) at 3.3 to 3.4 micrometers.

Plume spectra of O_2/C_6H_6 at O/F of 4.0, 2.0, and 1.5 are shown in Figures 28, 29, and 30, respectively. A PbSe detector was used with a 5-degree field of view for O/F = 4.0 (Figure 28), 2-½-degree field of view for O/F = 2.0 (Figure 29), and 1-¼-degree field of view for O/F = 1.5 (Figure 30). These fields of view were centered 40 centimeters downstream of the nozzle exit. At higher mixture ratios, C_6H_6 spectra are quite characteristic of the other fuels tested. However, at O/F = 2.0, the continuum portion of the C_6H_6 becomes important. At very fuel-rich conditions (O/F = 1.5), the C_6H_6 spectrum is dominated by continuum radiation. This is consistent with the observed sooty appearance of the C_6H_6 plumes at fuel-rich mixture ratios.

SECTION IV

CONCLUSIONS AND RECOMMENDATIONS

A large amount of high quality data on hydrocarbon plume infrared characteristics has been compiled under controlled conditions. These data should be very useful for evaluating the capabilities and limitations of existing plume IR models.

The peak specific radiant intensity in the 4.1- to 5.1-micrometer band has been found to increase as the fuel C/H ratio increases and as the fuel's combustion efficiency decreases. Regardless of fuel type, the most dramatic effect on specific radiant intensity is O/F. The peak specific radiant intensity has been found to occur at or near one-half the stoichiometric O/F. The specific radiant intensity decreases exponentially with increasing O/F and catastrophically with decreasing O/F relative to this peak O/F value.

The spatial distribution of plume radiation in the 4.1- to 5.1-micrometer band is also dramatically influenced by mixture ratio. Fuel-rich mixture ratios result in peak radiation intensities up to 60 centimeters downstream of the nozzle exit. Oxidizer-rich mixture ratios have peak radiant intensities at or near the nozzle exit. Plume shock structure exits up to 12 centimeters from the nozzle exit for all mixture ratios, with one Mach disc located approximately 1.6 centimeters downstream followed by up to six weaker shocks.

Plume spectral distributions at oxidizer-rich mixture ratios show characteristic vibrational-rotational bands for H_2O and CO_2 as expected in hydrocarbon flames. At fuel-rich mixture ratios, the infrared spectra indicate products of incomplete hydrocarbon combustion. For CH_4, the fuel-rich spectra show emissions at 3.3 to 3.4 micrometers from unburned CH_4. For C_6H_6, the fuel-rich spectra show continuum emissions from soot. The IR spectra of RP-1 and C_2H_4 do not yield clues to incomplete hydrocarbon combustion products. However, visual observation does show incandescent soot in the plumes of all four fuels at low O/F.

These results can be interpreted in terms of various effects on plume afterburning. The amount of combustible species for plume afterburning increases as O/F and C* efficiency decreases. However, there is a point at which further reduction in O/F, while adding more combustible species, brings the plume flame temperature below the flammability limits, resulting in drastic decreases in afterburning. The variation in specific radiant intensity with fuel C/H ratio can be explained in terms of the CO_2 which dominates the radiation in the spectral band of interest. Higher fuel C/H ratios yield more CO_2 which results in more radiation.

Many questions still remain unanswered about the IR processes of hydrocarbon plumes. These included but are not limited to:

- What are the products of incomplete combustion and how might they be varied?

- What role does soot play in the radiant transport processes at 4 to 5 micrometers?
- What are the mechanisms for soot production and oxidation?
- What are the specie, temperature, and velocity distributions?

Further experiments are necessary to clarify these questions.

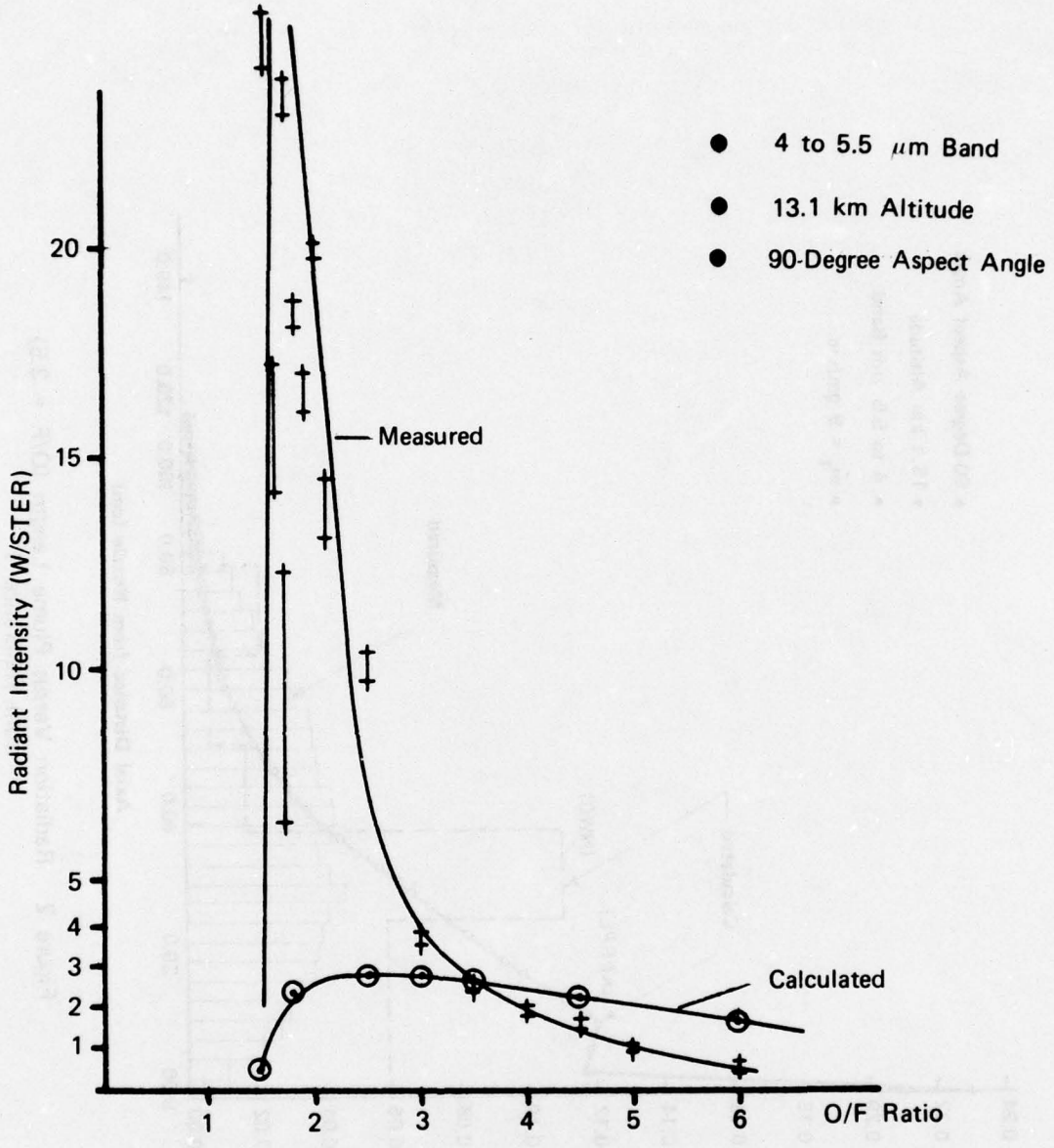

Figure 1. Variation of Radiant Intensity with O/F Ratio from Reference 1

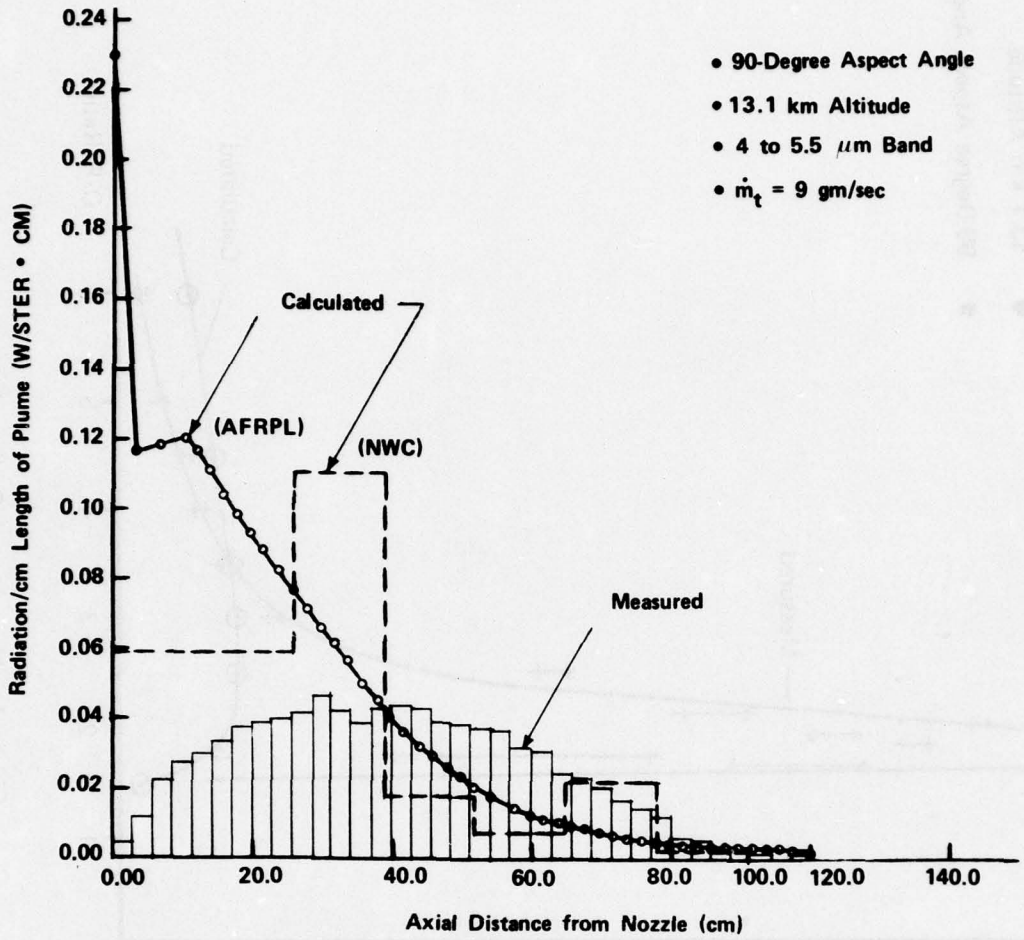

Figure 2. Radiation Versus Plume Length (O/F = 3.5) from Reference 1

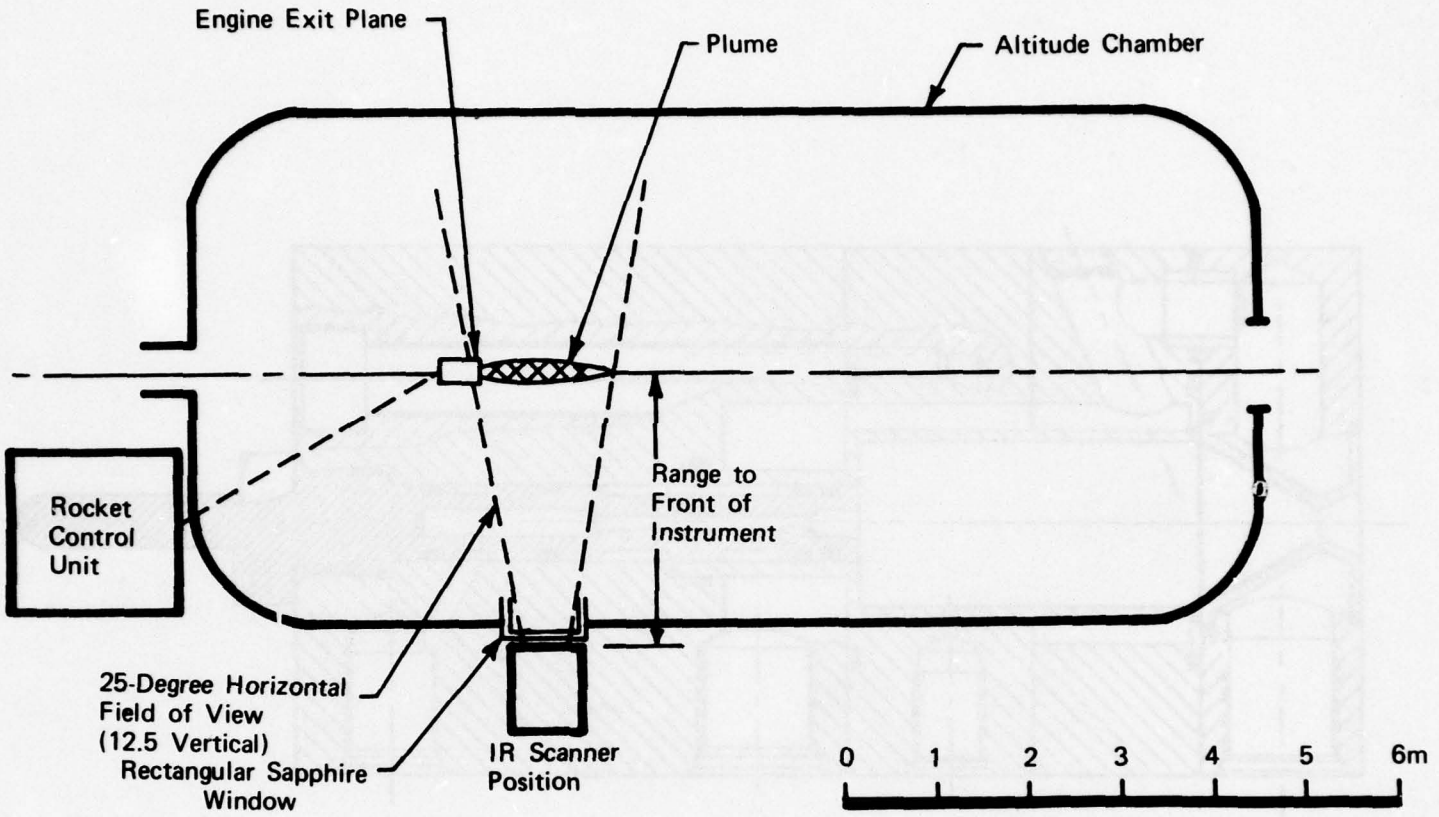

Figure 3. Experimental Geometry for Infrared Scanner Plume Measurements

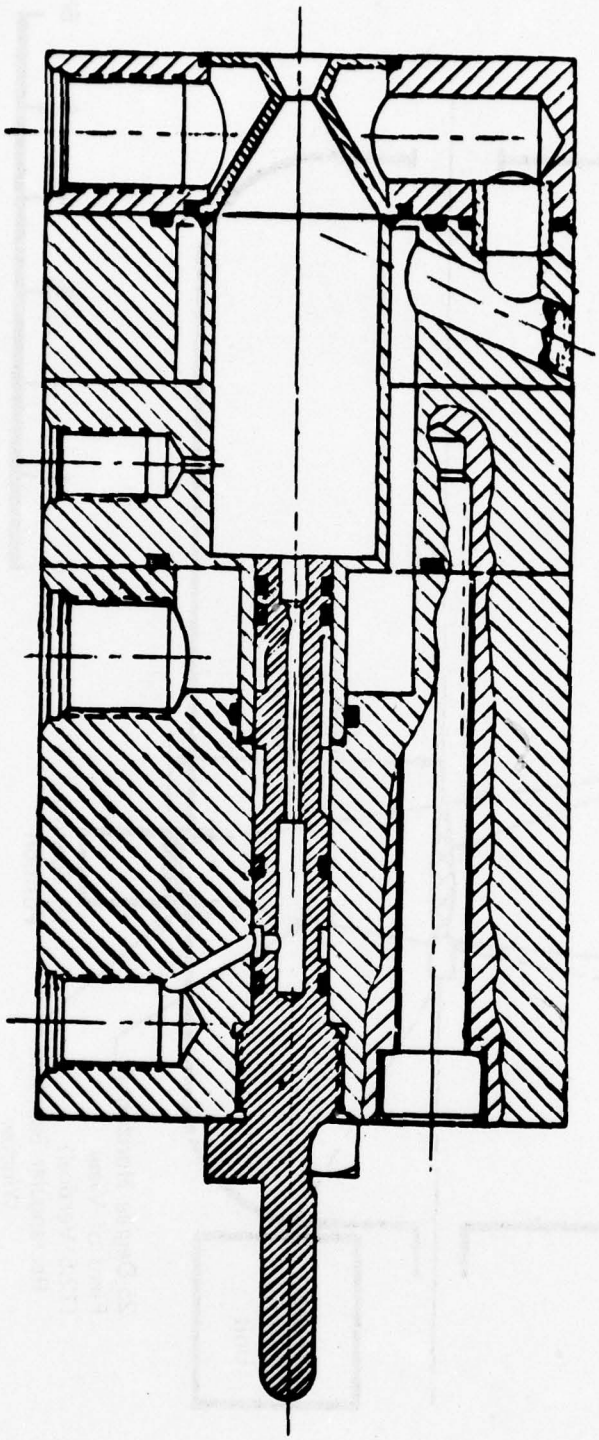

Figure 4. Rocket Engine Assembly

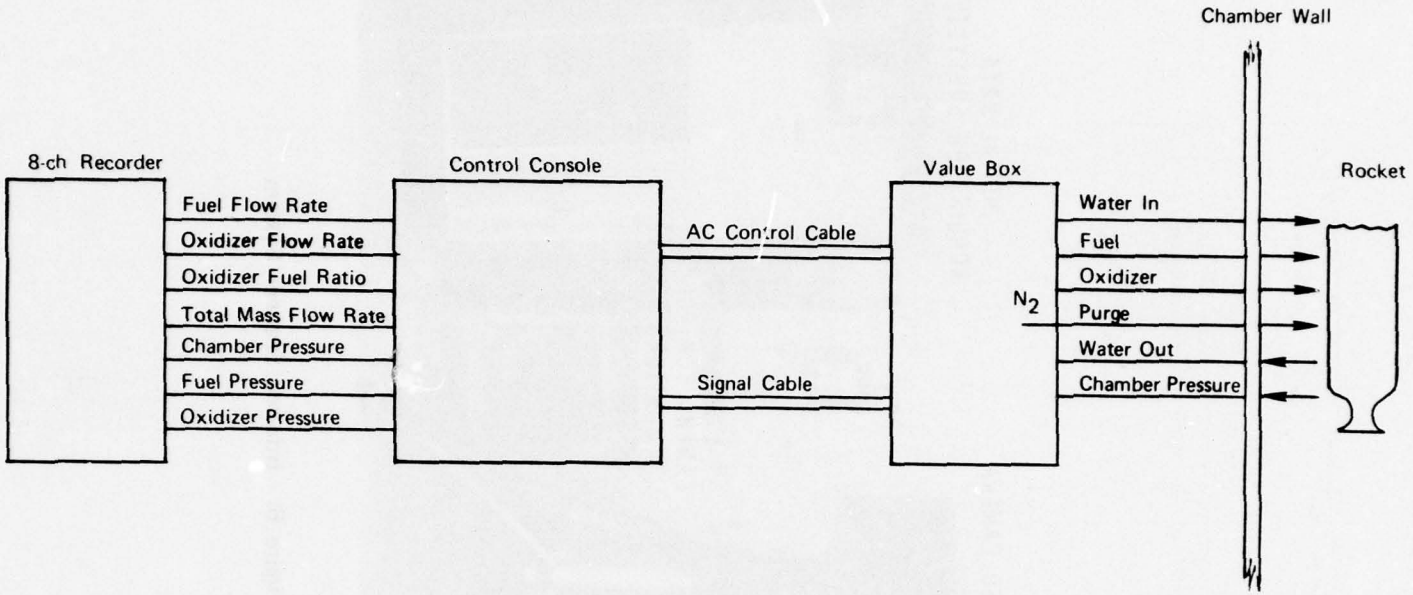

Figure 5. Rocket Control Unit

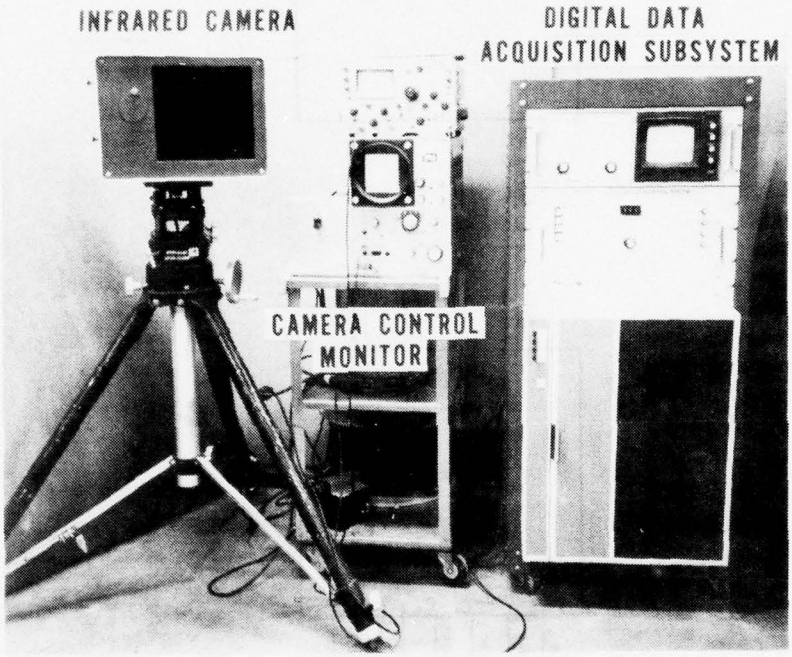

Figure 6. Infrared Scanner System

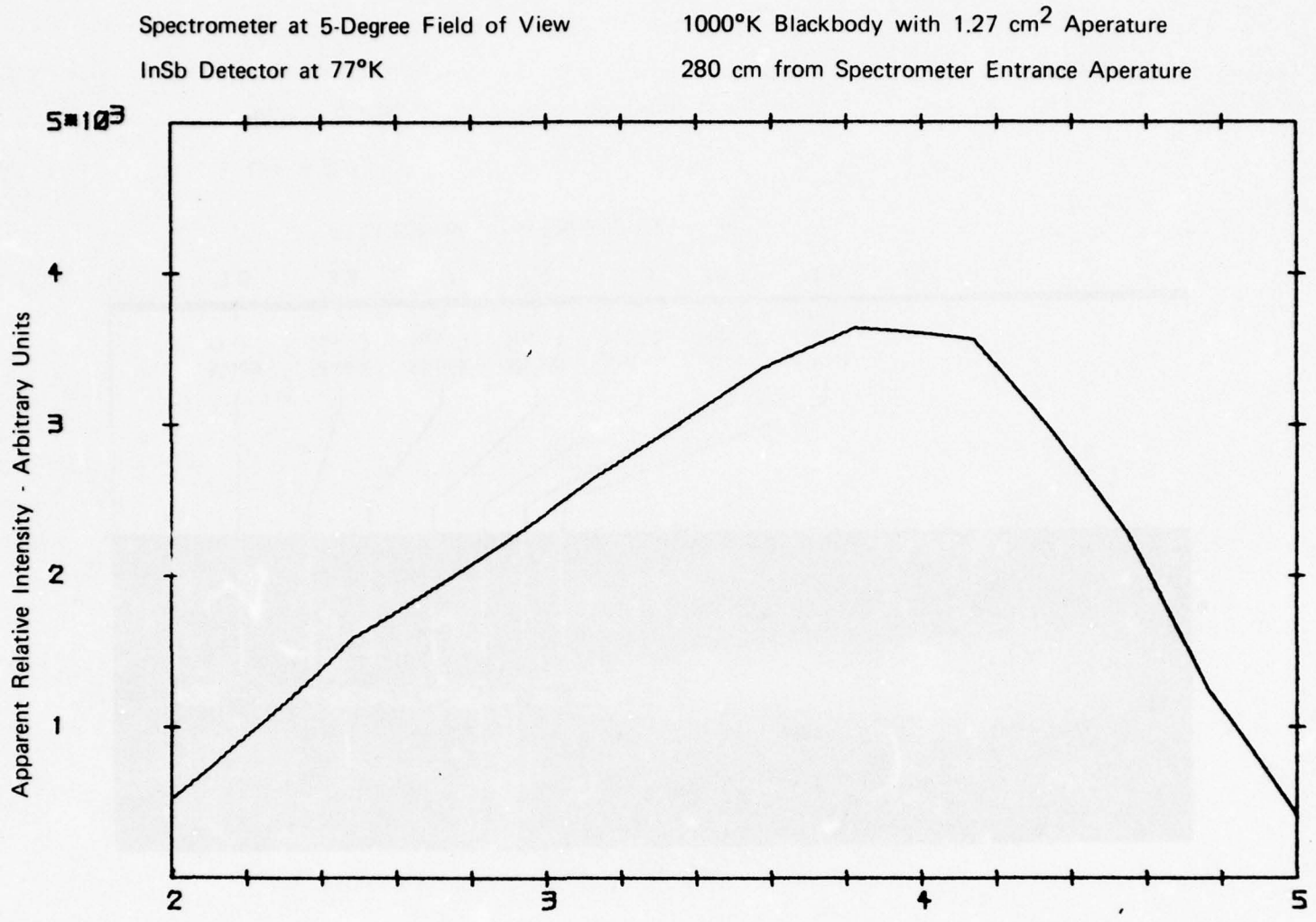

Figure 9. Interferometer Spectrometer Calibration Curve

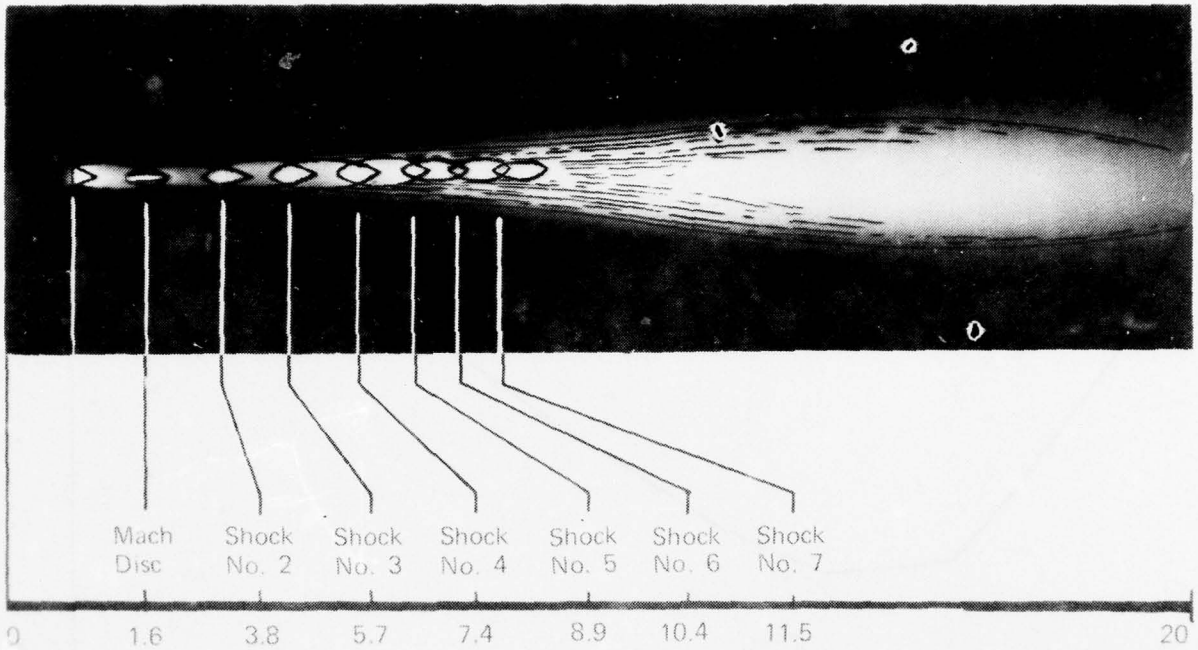

Figure 10. Visible Plume Structure for RP-1

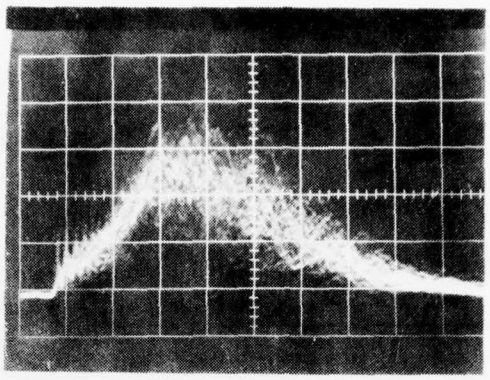

O/F = 2.3, $\dot{m}_t$ = 4.78 gm/sec

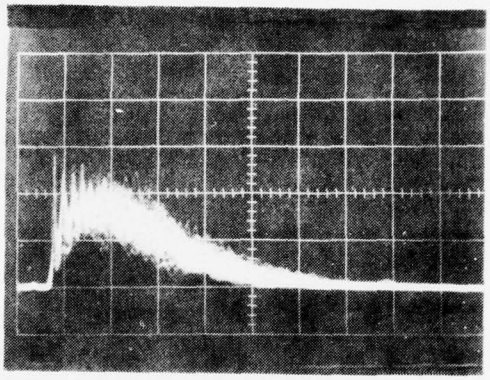

O/F = 4.1, $\dot{m}_t$ = 4.79 gm/sec

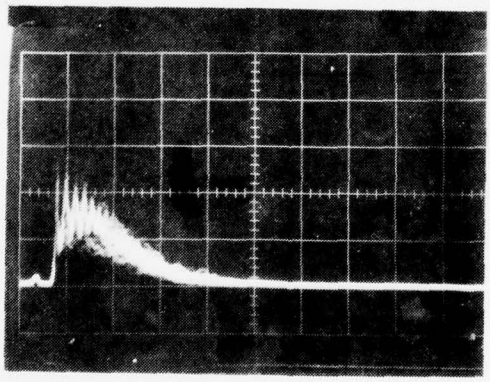

O/F = 6.6, $\dot{m}_t$ = 4.93 gm/sec

Figure 11. Infrared Scanner Centerline Data for O_2/CH_4

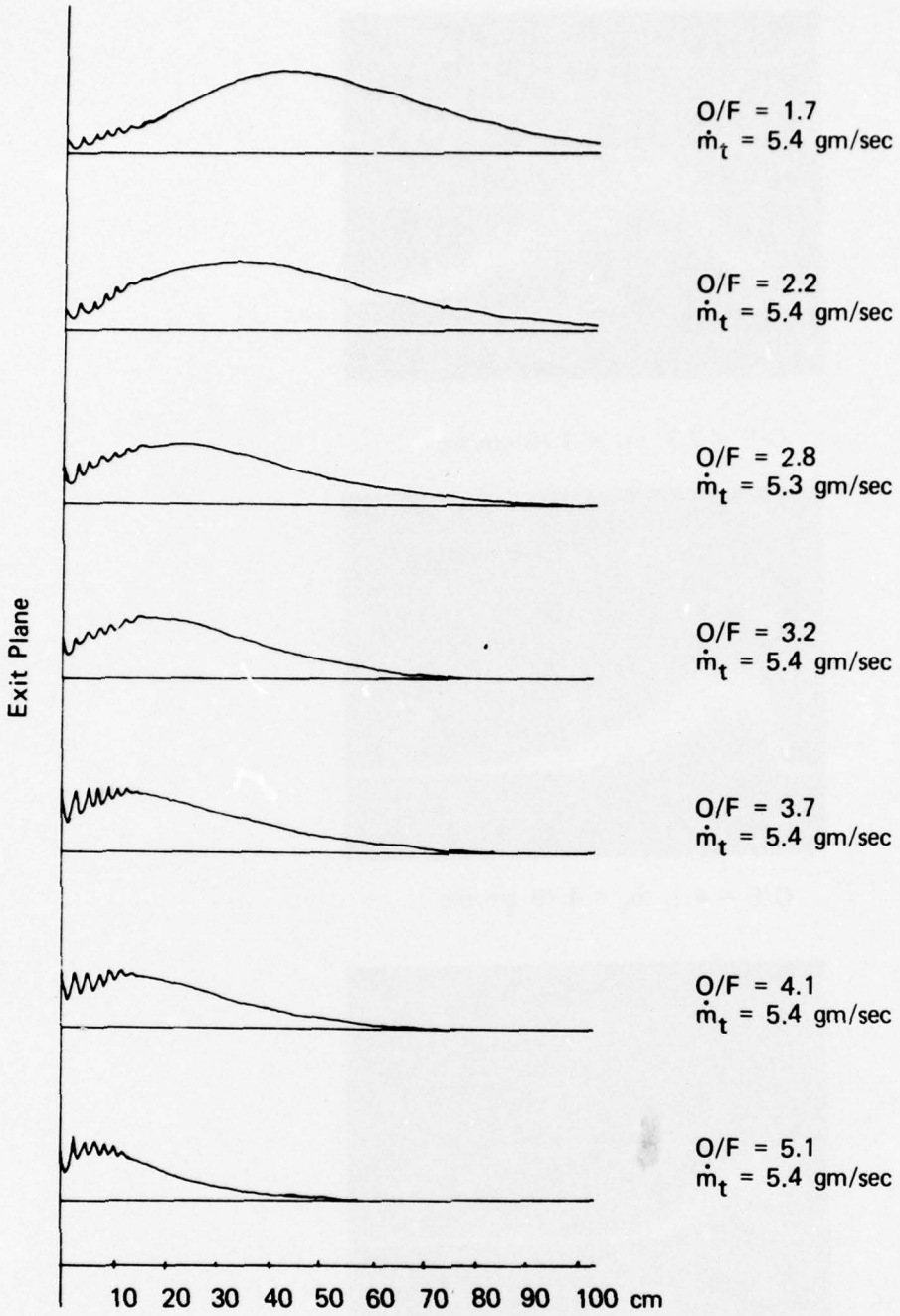

Figure 12. Plume Radiation Centerline Distributions for O_2/RP-1

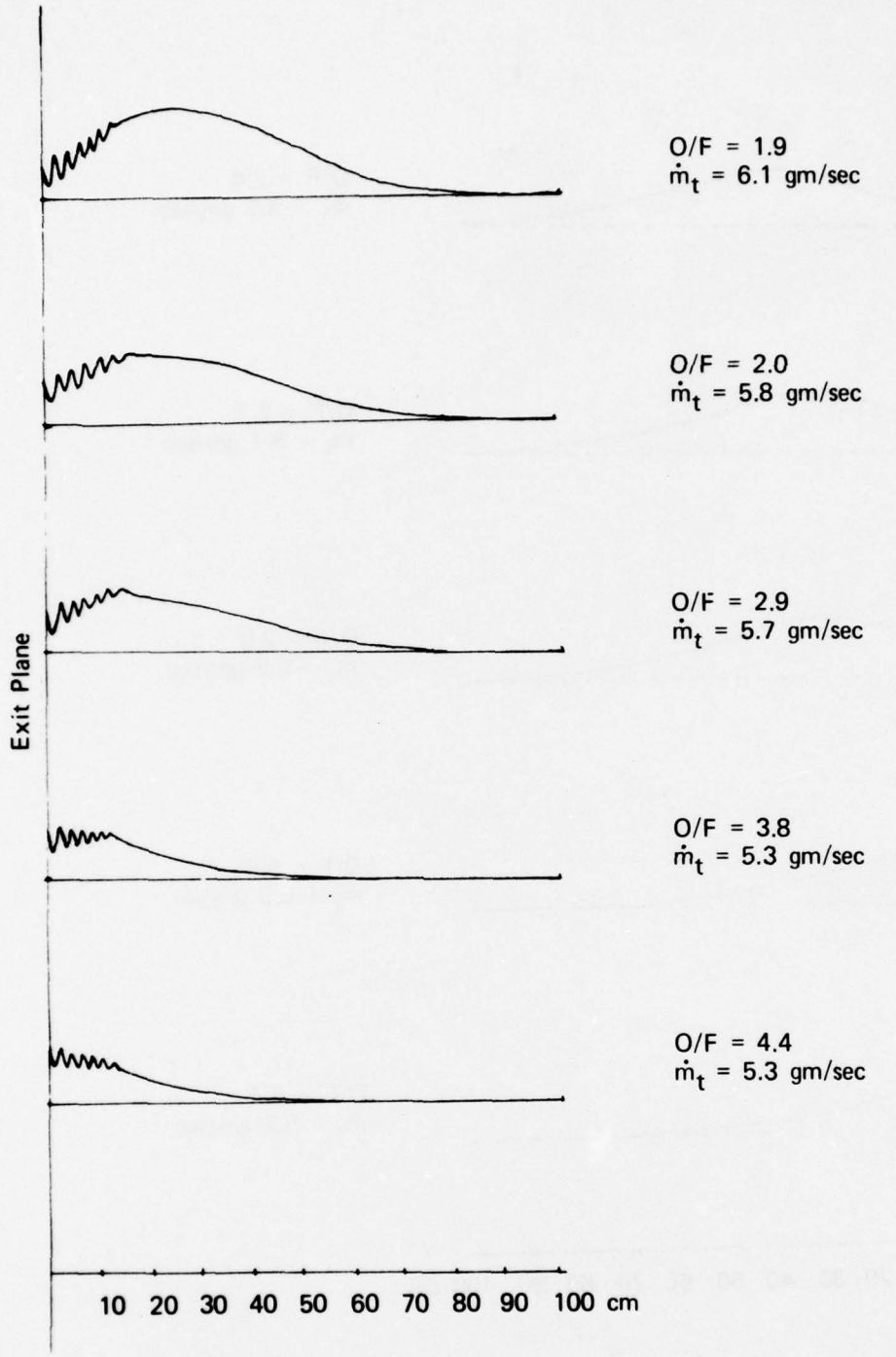

Figure 13. Plume Radiation Centerline Distributions for O_2/C_2H_4

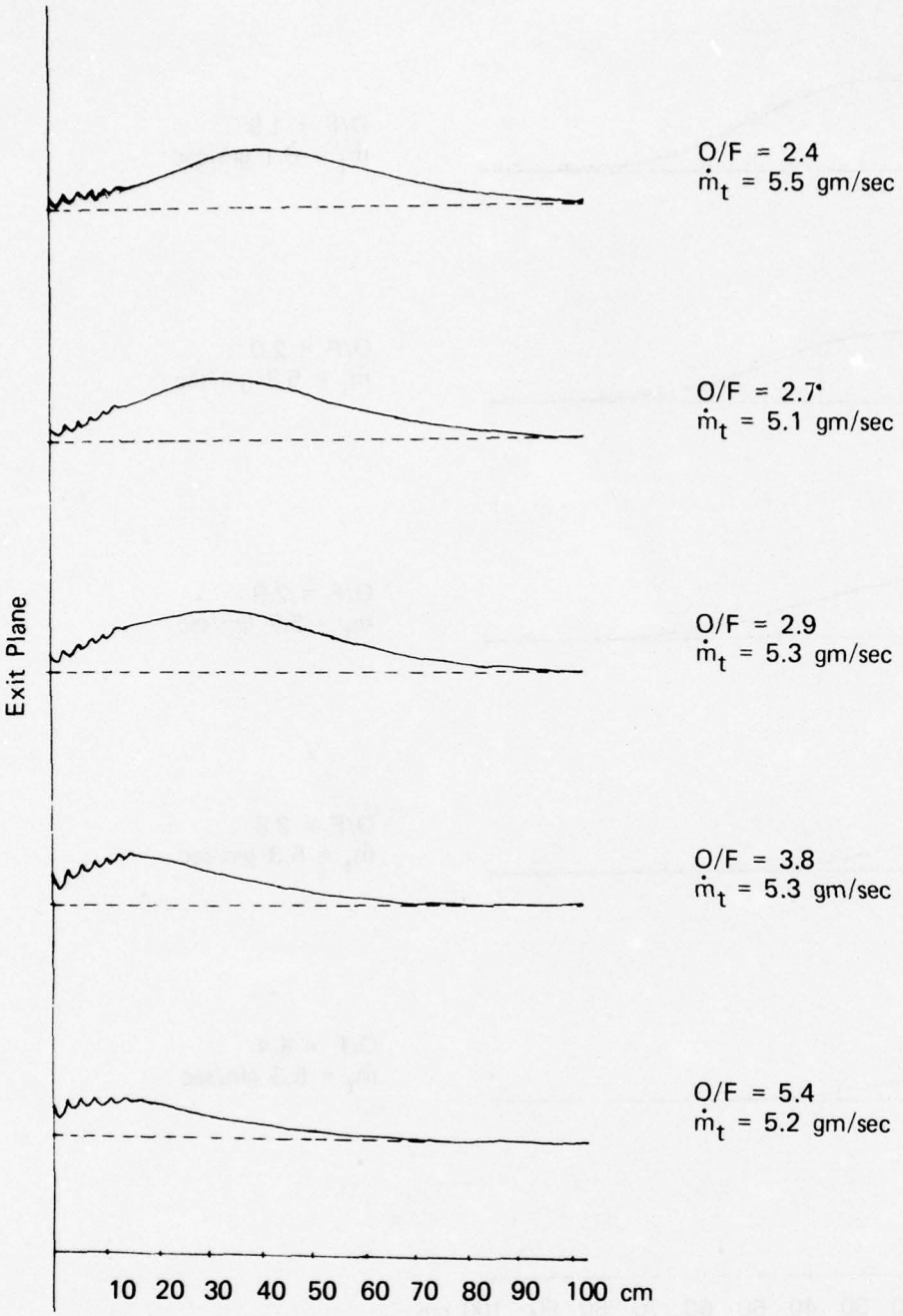

Figure 14. Plume Radiation Centerline Distributions for O_2/CH_4

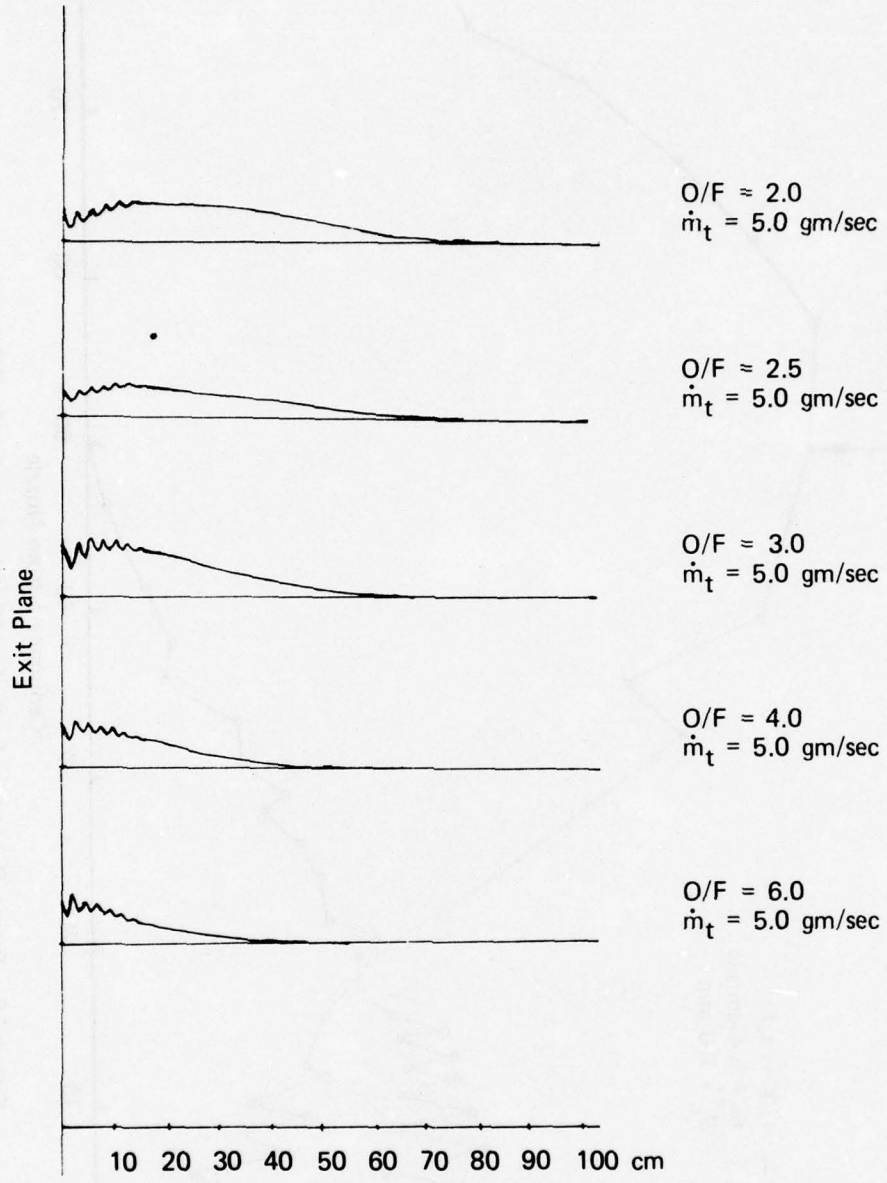

Figure 15. Plume Radiation Centerline Distributions for O_2/C_6H_6

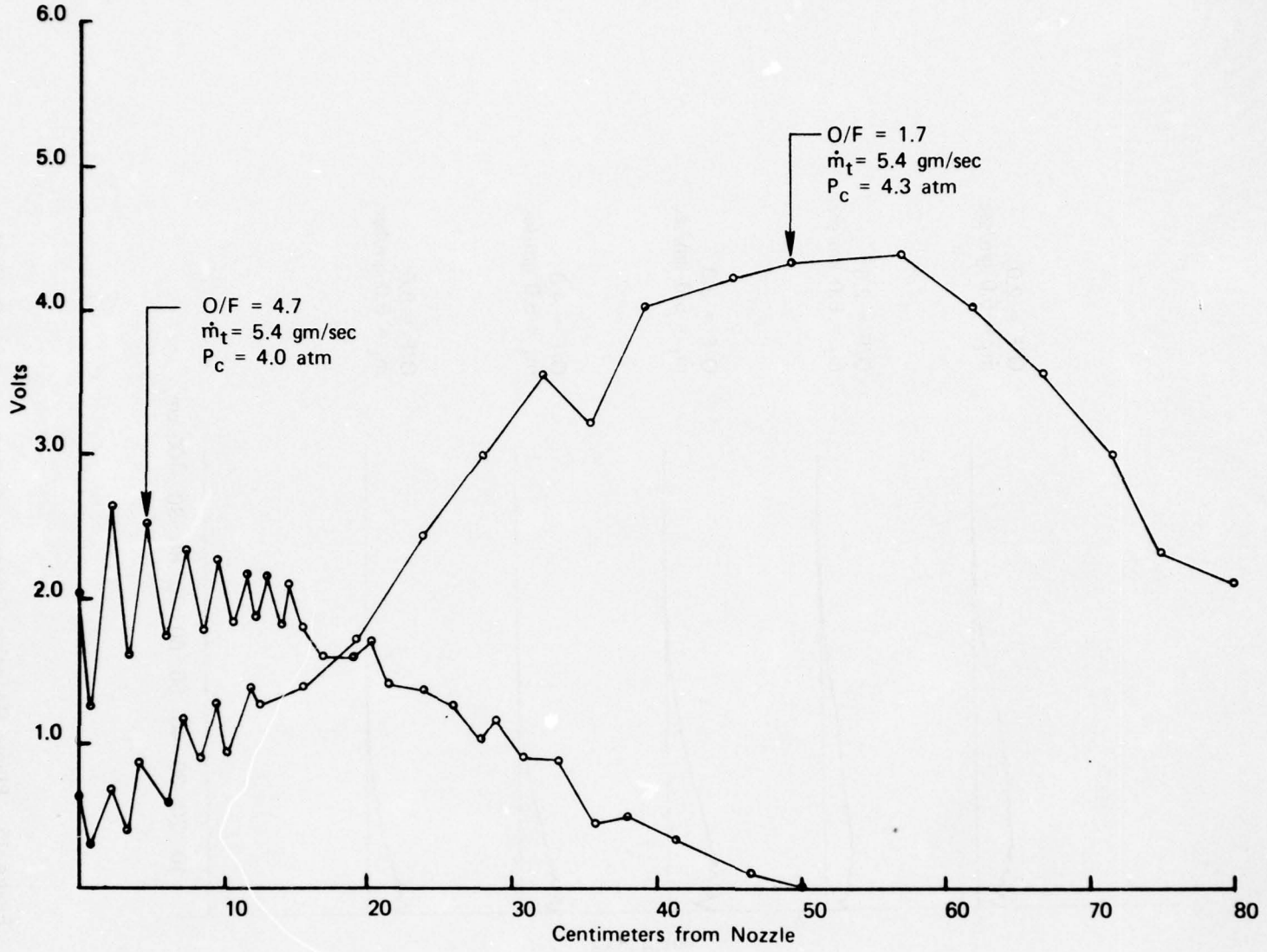

Figure 16. Plume Centerline Radiation Distributions for O_2/RP-1

RP-1/GOX ROCKET 5.4 GMS/SEC **13.1** KM ALTITUDE (STATIC) RANGE(DET)= 2.641 M UNITS=WATTS/STER

RUN= 9 FILE=162 RANGE (FRONT OF CAMERA)= 2.18 M SENSITIVITY= 50 ATTENUATION= 115 O/F= 2.4 BACKGROUND= 147

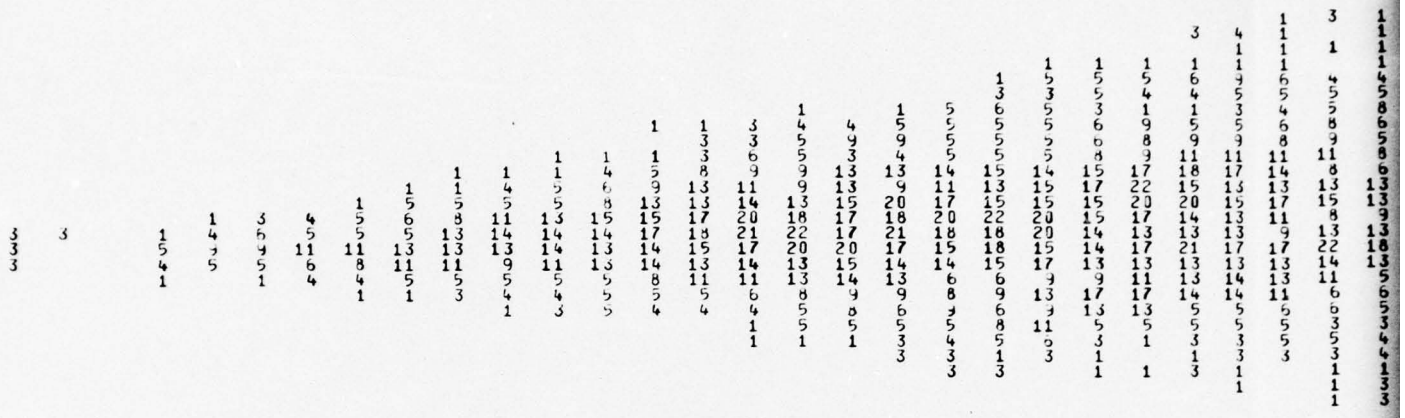

COLUMN NO.=

1	2	3	4	5	6	7	8	9	10	11	12	13	14	15	16	17	18	19	20	21	22	23	24	25	26	27	28	29	30
0.0	0.0	0.6	0.0	2.1	4.2	6.3	8.4	10.5	12.5	14.6	16.7	18.8	20.9	23.0	25.1	27.2	29.3	31.4	33.5	35.6	37.6	39.7	41.8	43.9	46.0	48.1	50.2	52.3	54.4

EXIT PLANE IS IN COLUMN 4,FIELD OF VIEW CENTER IS IN COLUMN 28 HORZ INCREMENT= 2.09 CM VERT INCREMENT= .63 CM

ER X .001 EXPERIMENT DATE 2 OCT 75

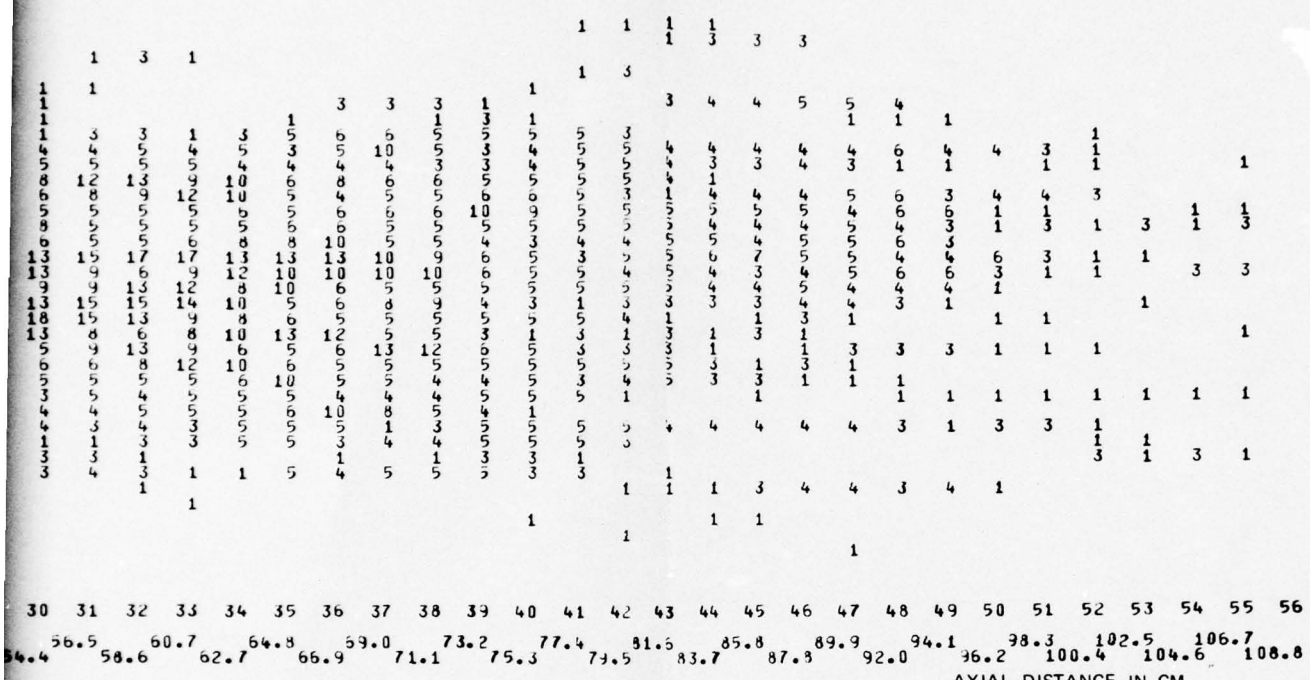

30 31 32 33 34 35 36 37 38 39 40 41 42 43 44 45 46 47 48 49 50 51 52 53 54 55 56

54.4 56.5 58.6 60.7 62.7 64.8 66.9 69.0 71.1 73.2 75.3 77.4 79.5 81.6 83.7 85.8 87.8 89.9 92.0 94.1 96.2 98.3 100.4 102.5 104.6 106.7 108.8

AXIAL DISTANCE IN CM

TOTAL SUM= 5310

Figure 17. Infrared Scanner Matrix Data for O_2/RP-1, O/F = 2.4

(The reverse of this page is blank)

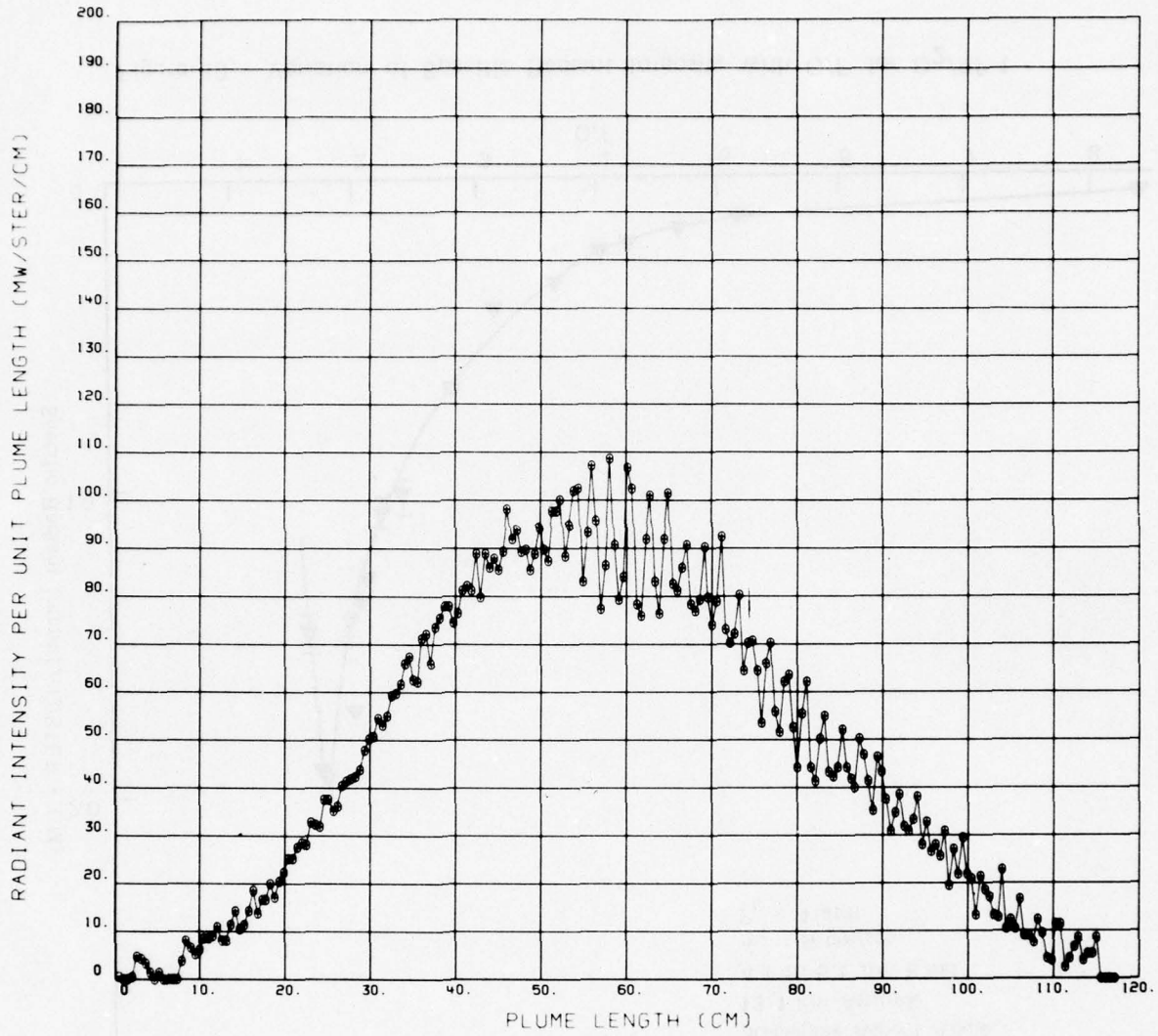

Figure 18. Station Radiation Distribution for O_2/RP-1, O/F = 2.4

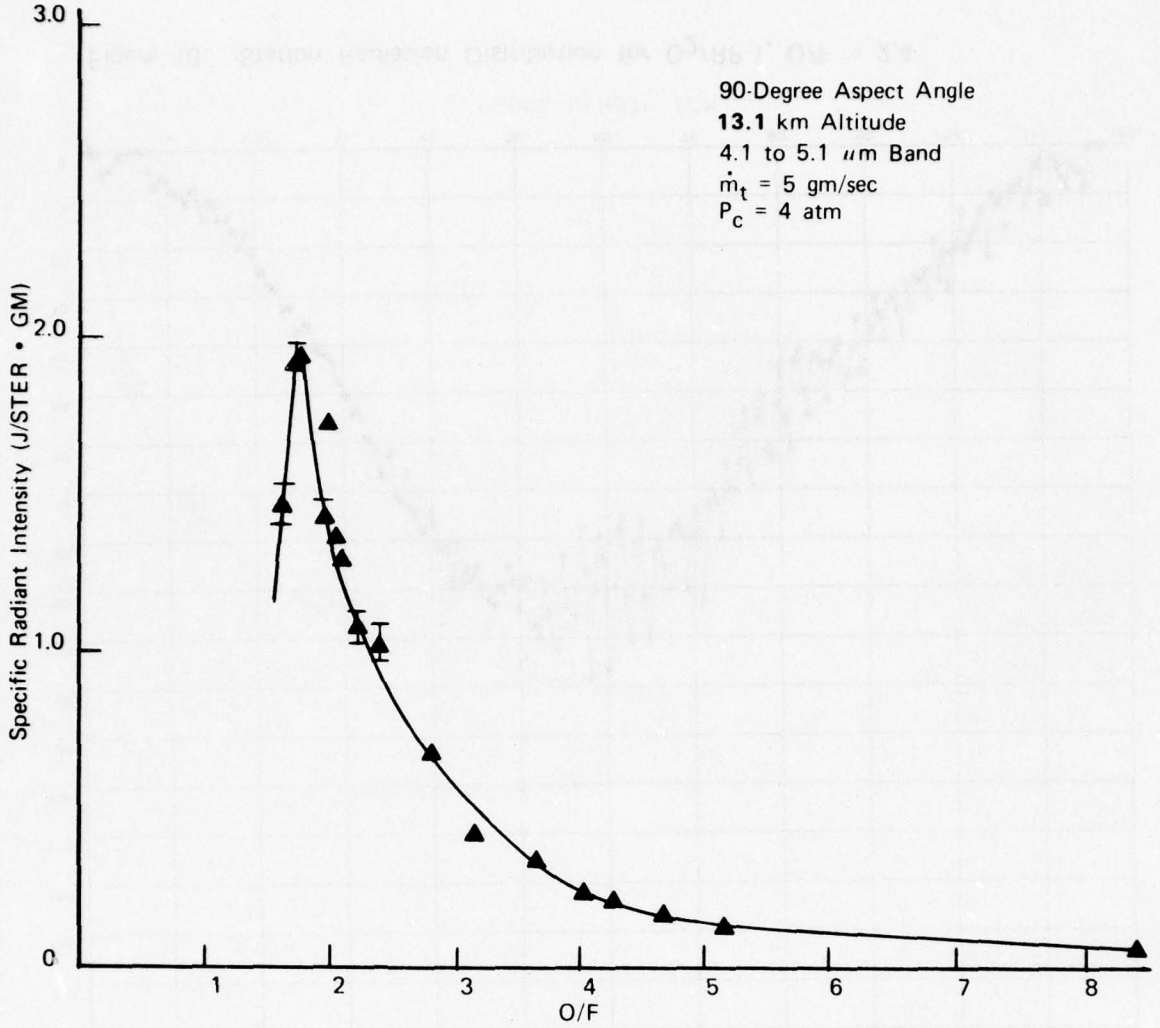

Figure 19. Variation of Specific Radiant Intensity with O/F for O_2/RP-1

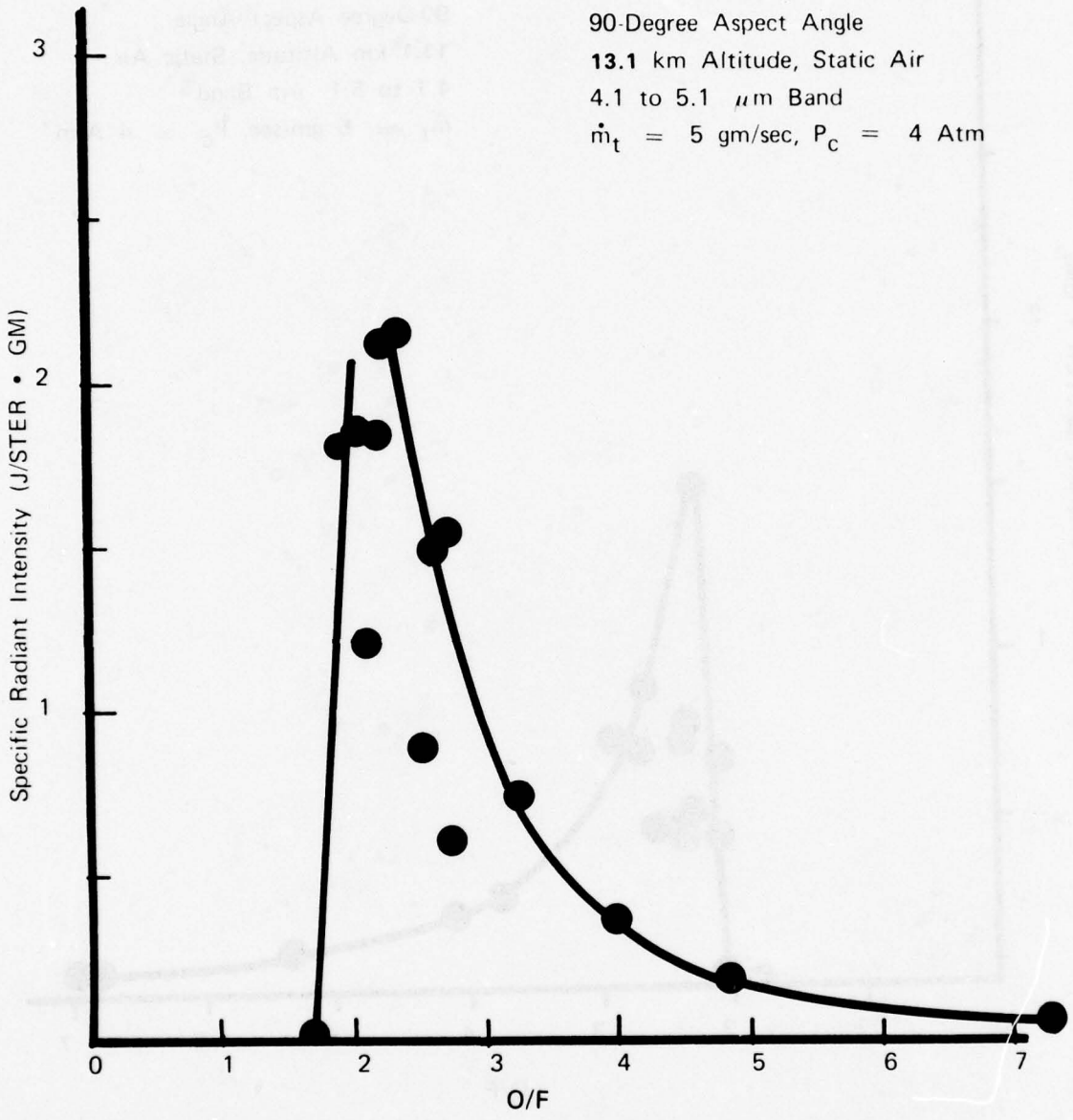

Figure 20. Variation of Specific Radiant Intensity with O/F for O_2/C_2H_4

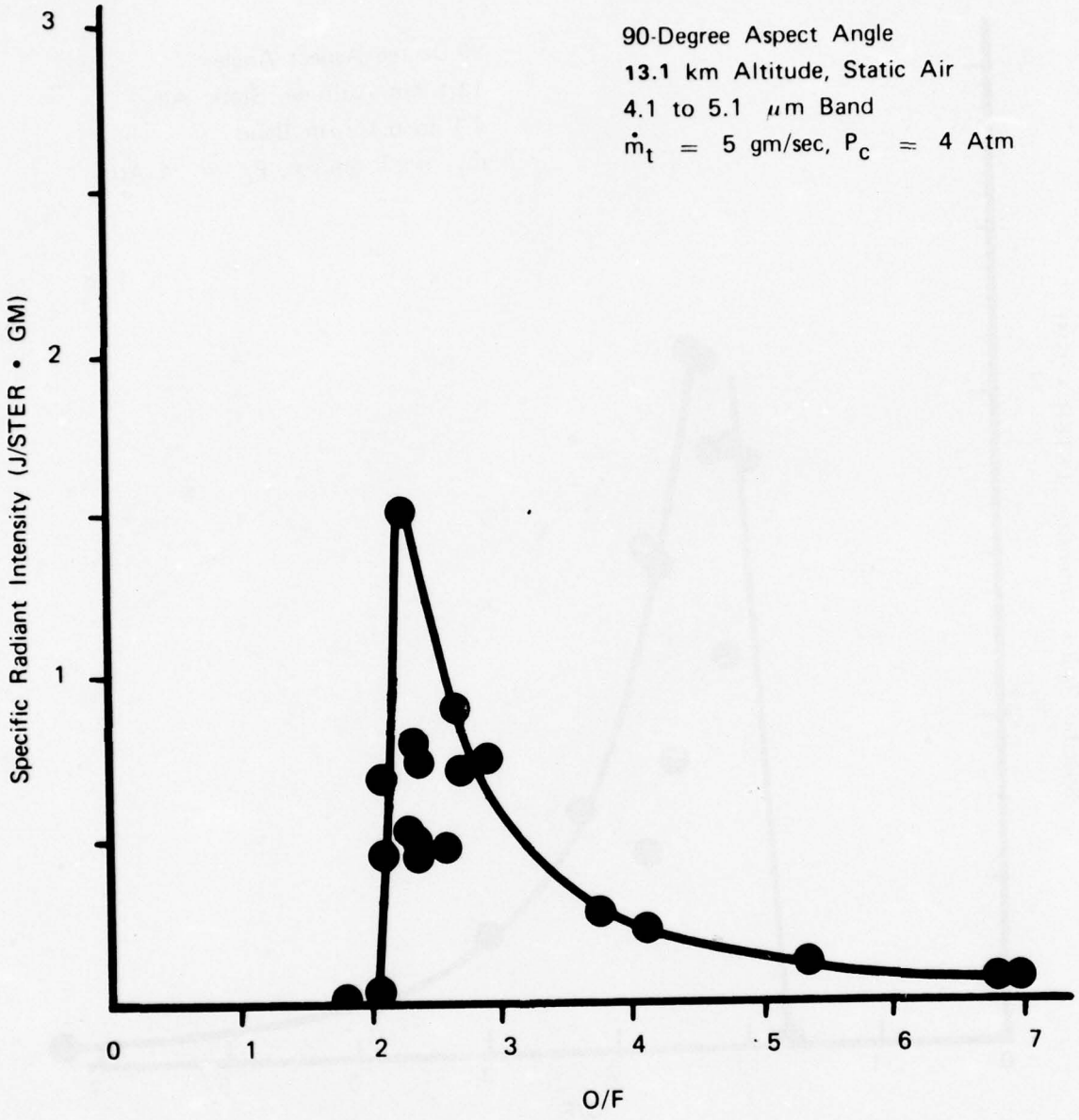

Figure 21. Variation of Specific Radiant Intensity with O/F for O_2/CH_4

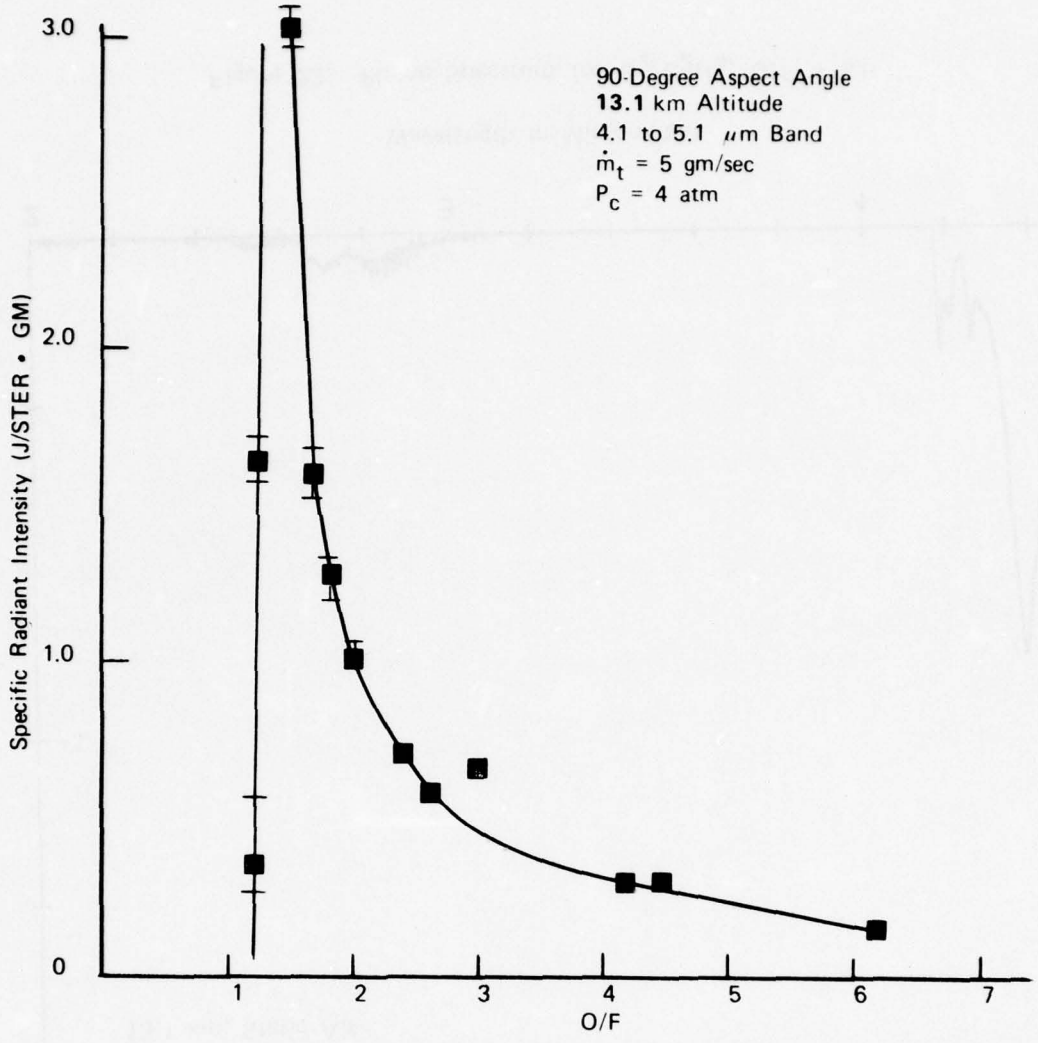

Figure 22. Variation of Specific Radiant Intensity with O/F for O_2/C_6H_6

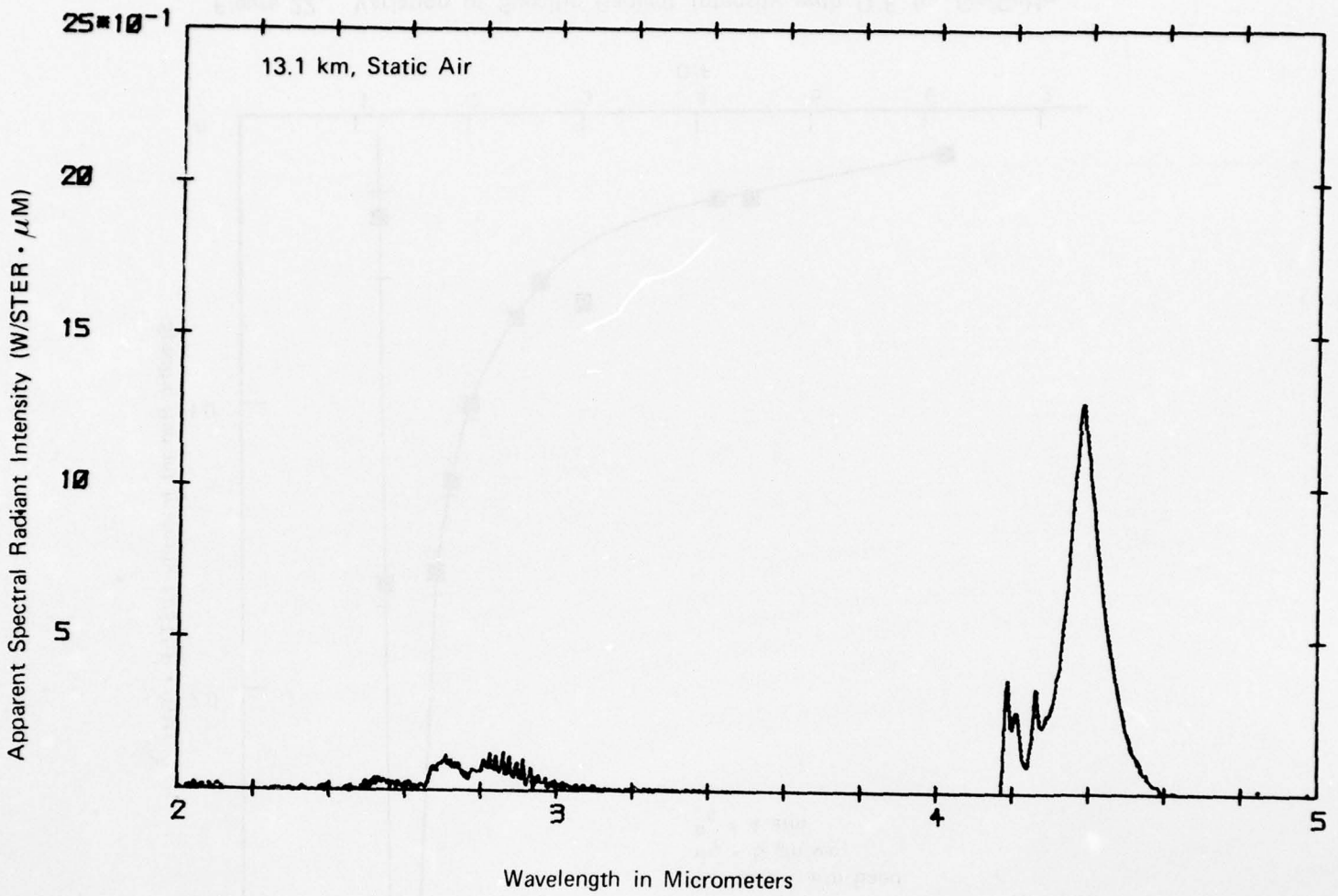

Figure 23. Plume Spectrum for O_2/C_2H_4, O/F = 5.5

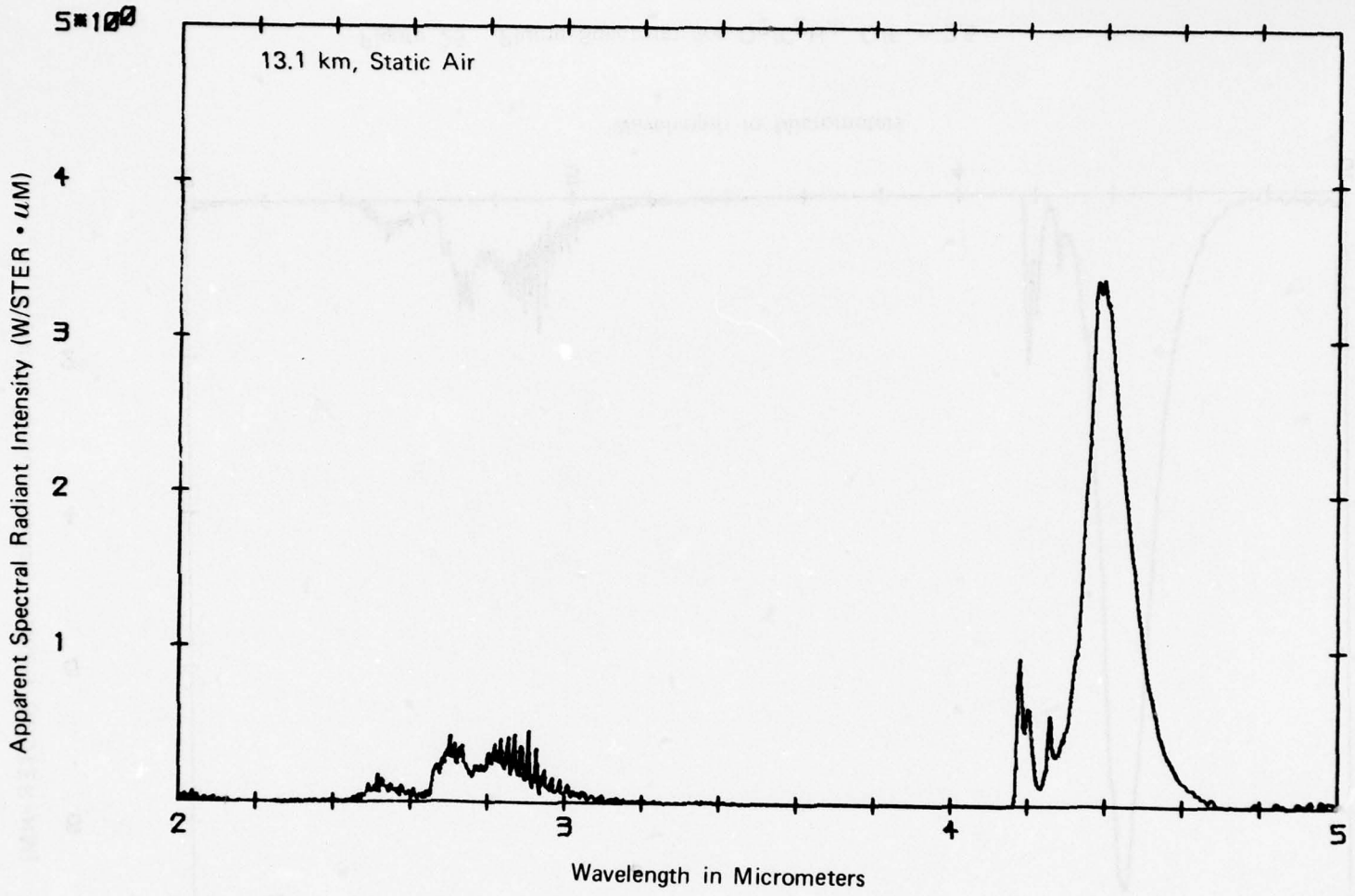

Figure 24. Plume Spectrum for O_2/C_2H_4, O/F = 3.9

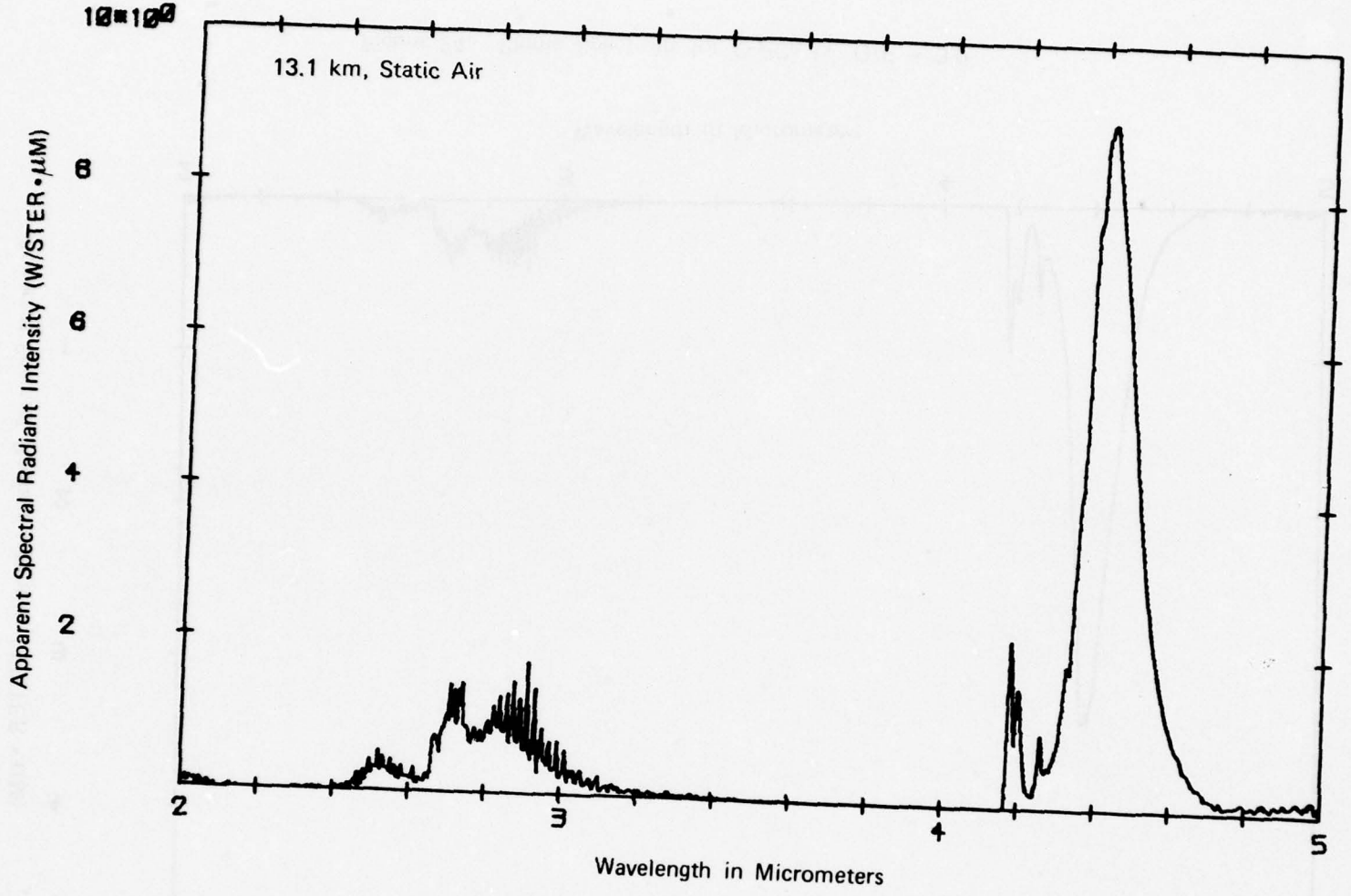

Figure 25. Plume Spectrum for O_2/C_2H_4, O/F = 2.5

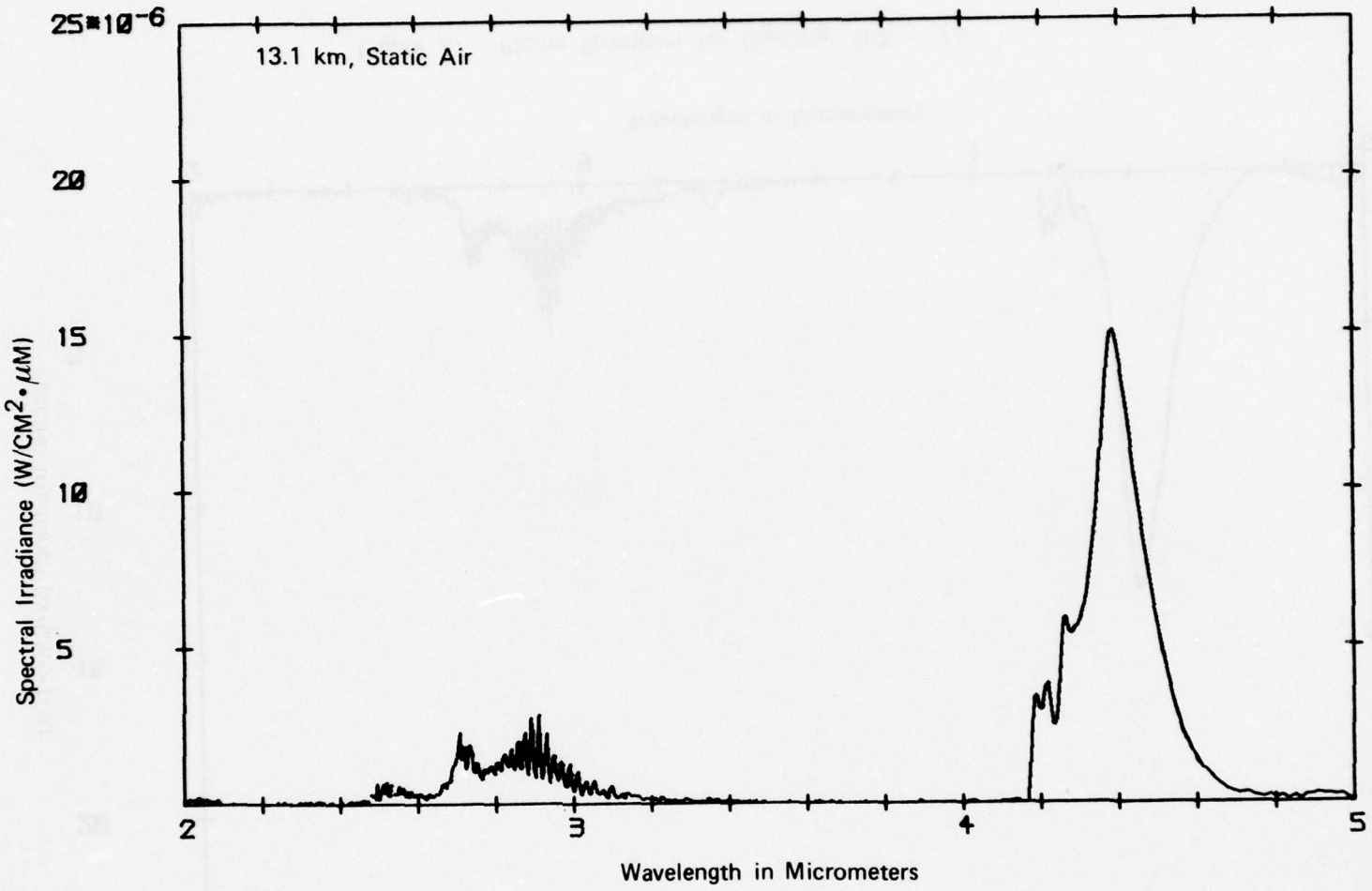

Figure 26. Plume Spectrum for O_2/CH_4, O/F = 5.1

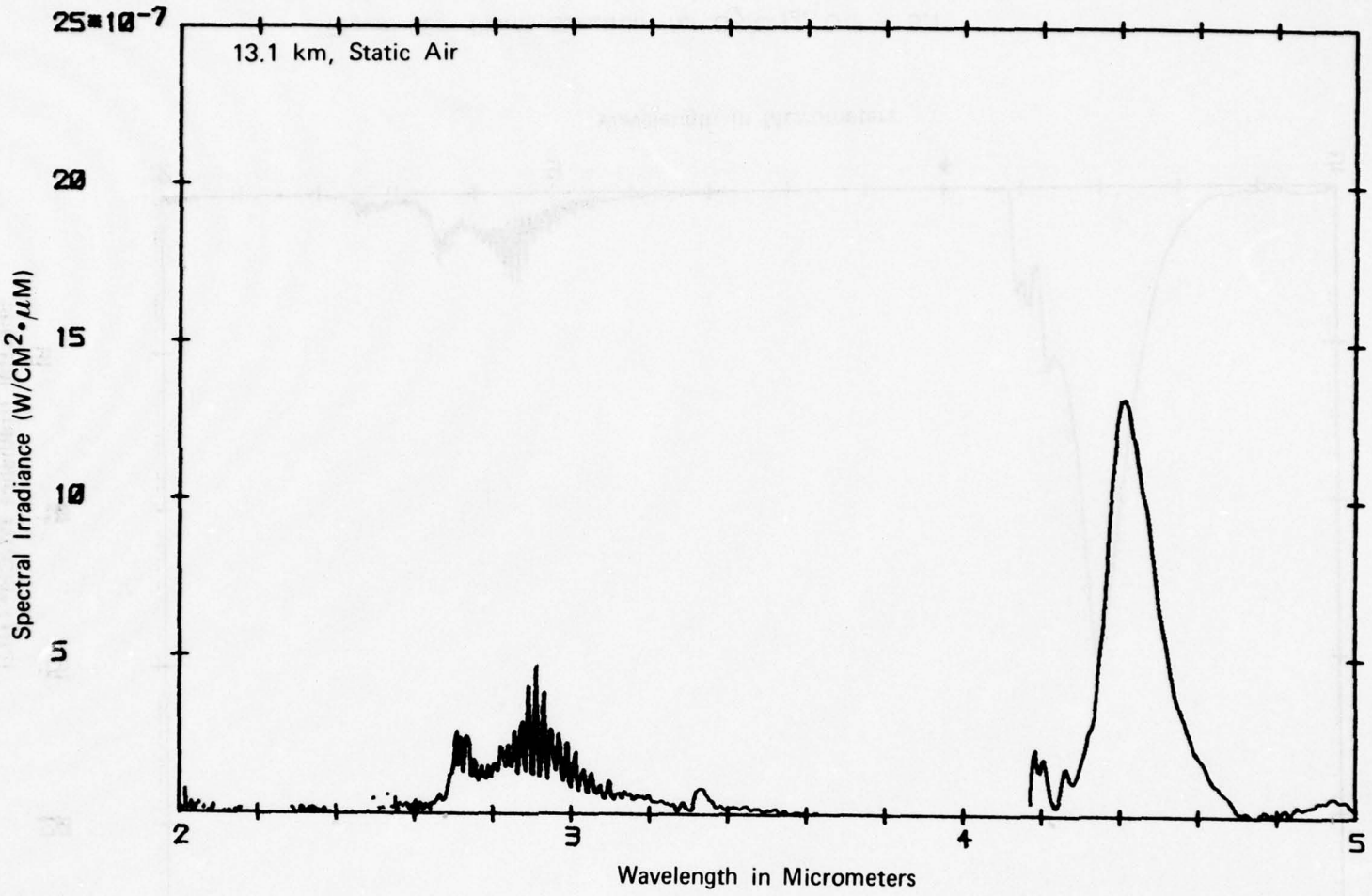

Figure 27. Plume Spectrum for O_2/CH_4, O/F = 2.2

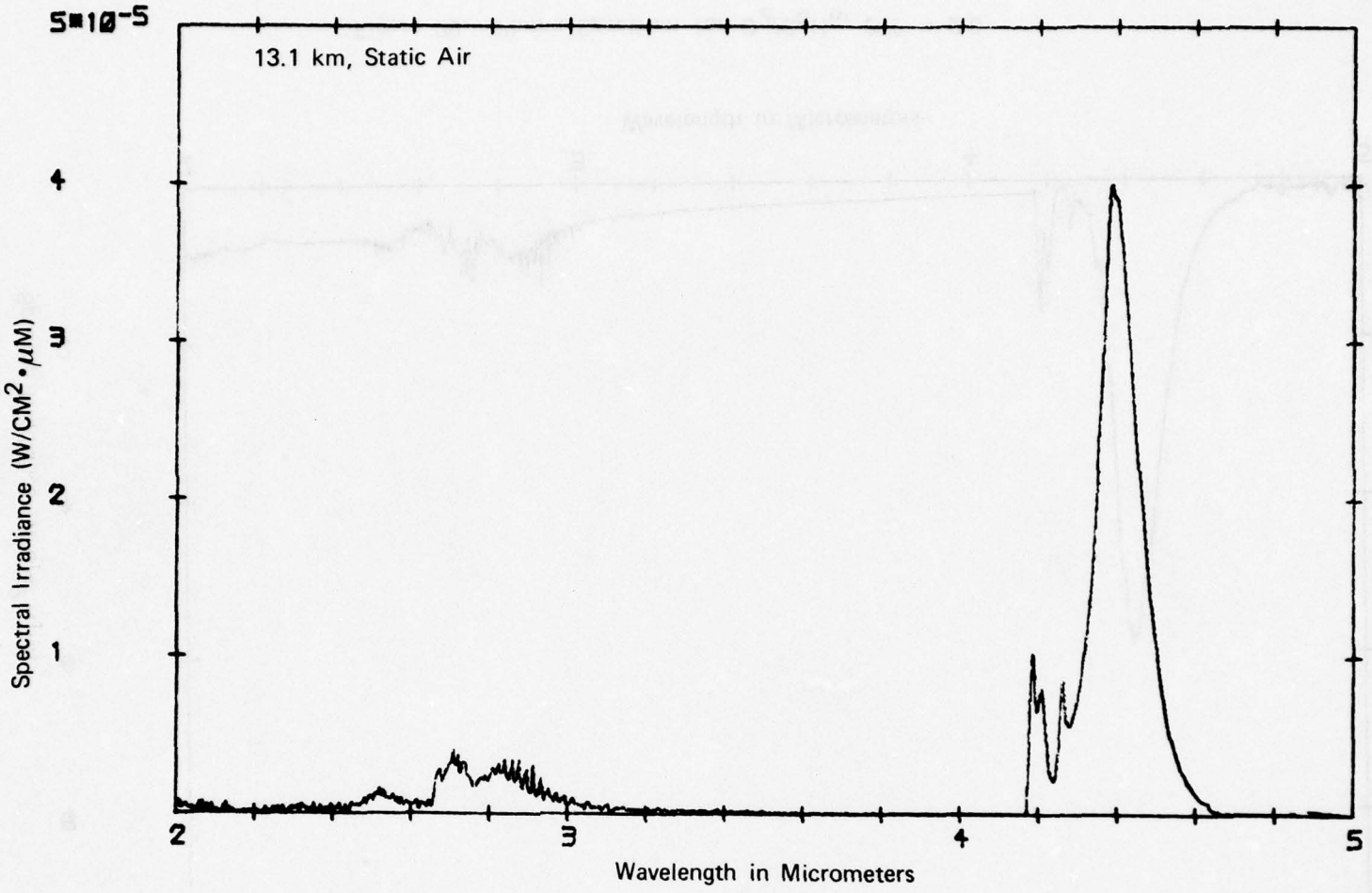

Figure 28. Plume Spectrum for O_2/C_6H_6, O/F = 4.0

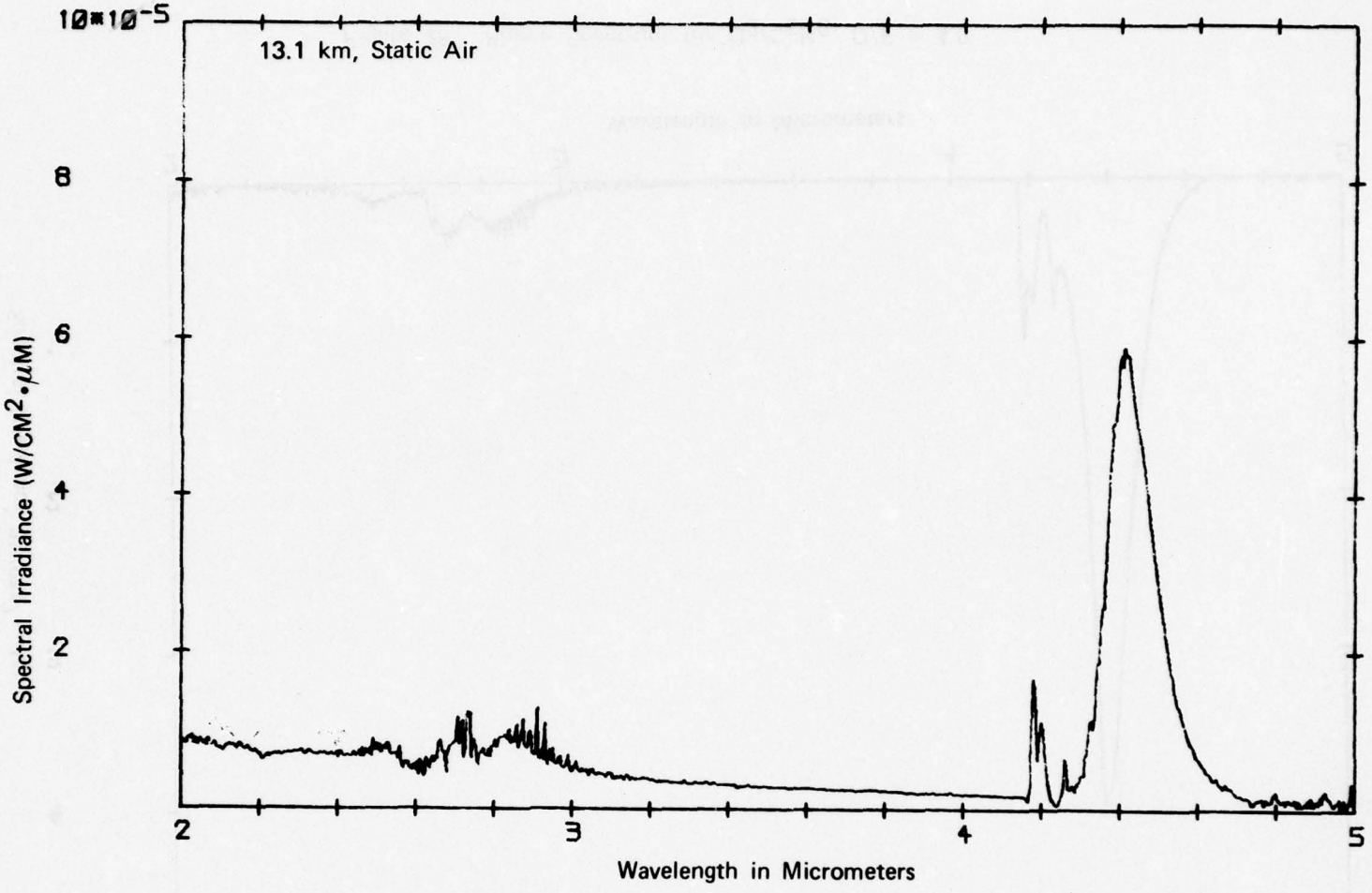

Figure 29. Plume Spectrum for O_2/C_6H_6, O/F = 2.0

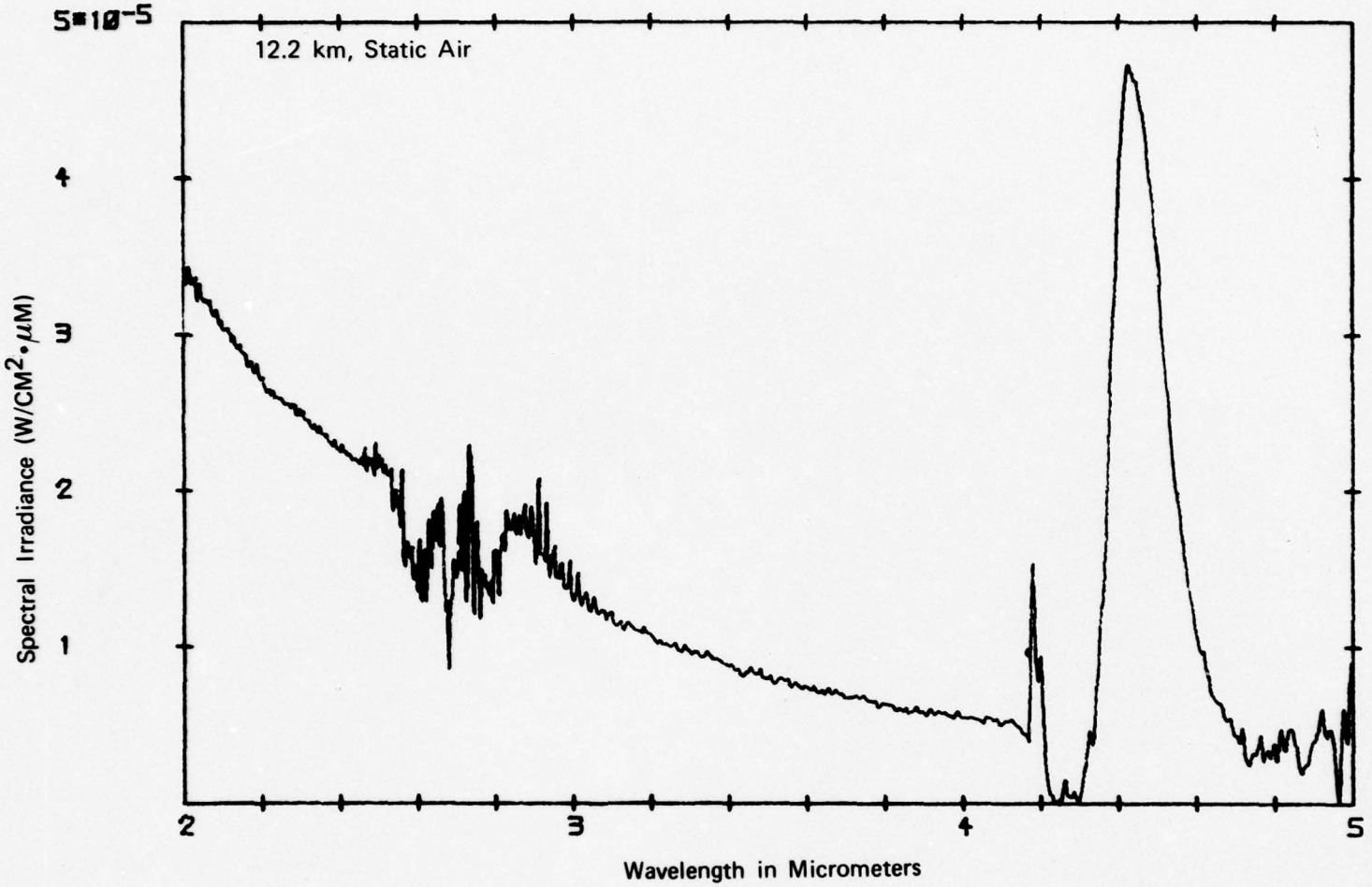

Figure 30. Plume Spectrum for O_2/C_6H_6, O/F = 1.5

(The reverse of this page is blank)

TABLE 1. AFATL ROCKET ENGINE CHARACTERISTICS

Chamber Diameter	1.91 cm
Chamber Length	4.13 cm
Nozzle Convergent Cone Half-Angle	27.6 deg
Nozzle Divergent Cone Half-Angle	15.75 deg
Nozzle Throat Diameter	0.508 cm
Nozzle Exit Diameter	0.787 cm
Nozzle Area Ratio	2.4
L*	58.0 cm
Nominal Chamber Pressure	4 atm
Nominal Mass Flow Rate	5 gm/sec
Calculated Specific Impulse†	216 sec
Calculated Exhaust Velocity†	2280 m/sec
Calculated Characteristic Velocity†	1759 m/sec
Calculated Chamber Temperature†	3274°K
C* Efficiency†	98 percent

†For O_2/RP-1 at O/F = 4

TABLE 2. INFRARED SCANNER COLUMN AND LINE SUM DATA FOR FIGURE 16

Column No.	Sum	Line No.	Sum
1	0	24	4
2	9	25	10
3	3	26	5
4	0	27	4
5	11	28	7
6	19	29	44
7	24	30	13
8	30	31	58
9	35	32	141
10	47	33	112
11	60	34	138
12	67	35	194
13	76	36	211
14	89	37	211
15	106	38	302
16	124	39	399
17	141	40	419
18	151	41	439
19	163	42	462
20	170	43	484
21	167	44	391
22	179	45	309
23	196	46	265
24	186	47	192
25	204	48	132
26	198	49	98
27	195	50	105
28	181	51	62
29	176	52	26
30	159	53	44
31	160	54	23
32	170	55	1
33	161	56	3
34	155	60	1
35	147	61	1
36	147		
37	138	mW/sr•line	
38	130		
39	116		
40	105		
41	93		
42	84		
43	74		
44	65		
45	65		
46	69		
47	65		
48	62		
49	45		
50	27		
51	22		
52	16		
53	8		
54	9		
55	11		
56	0		
mW/sr•col			

TABLE 3. O_2/RP-1 ENGINE CONDITION AND PLUME RADIANT INTENSITY DATA

O/F	$\dot{m}_t$ (gm/sec)	P_c (atm)	C* (m/sec)	J (W/sr) (4.1 to 5.1 μ)	$\bar{J}$ (J/sr/gm)
1.59	5.05	3.65	1600	7.35	1.46
1.68	5.10	3.72	1610	9.65	1.89
1.72	5.38	4.34	1790	10.34	1.92
1.91	5.30	4.20	1750	7.54	1.42
1.96	4.85	a	a	8.33	1.72
2.02	4.92	a	a	7.18	1.46
2.06	4.92	3.88	1620	6.31	1.28
2.18	5.40	4.54	1860	5.71	1.06
2.36	5.38	4.54	1790	5.45	1.01
2.80	5.32	4.54	1890	3.62	0.68
3.15	5.40	4.40	1800	2.24	0.41
3.65	5.35	4.34	1800	1.74	0.33
4.05	5.40	4.20	1720	1.22	0.23
4.28	5.29	4.13	1730	1.06	0.20
4.68	5.40	4.00	1640	0.88	0.16
5.13	5.39	3.86	1580	0.64	0.12
8.42	4.99	3.27	1350	0.34	0.07

[a]This data not available.

TABLE 4. O_2/C_2H_4 ENGINE CONDITION AND PLUME RADIANT INTENSITY DATA

O/F	$\dot{m}_t$ (gm/sec)	P_c (atm)	C* (m/sec)	J (W/sr) (4.1 to 5.1 μ)	$\bar{J}$ (J/sr/gm)
1.68	3.65	2.65	150	0.05	0.01
1.89	3.87	2.86	152	7.02	1.81
2.01	4.19	3.20	157	7.73	1.85
2.10	4.09	2.99	151	4.95	1.21
2.18	4.43	3.33	155	8.17	1.84
2.20	4.92	3.67	154	10.41	2.12
2.35	4.92	3.45	155	10.56	2.15
2.51	4.75	3.40	147	4.16	0.88
2.60	5.12	3.65	158	7.63	1.49
2.73	4.63	3.33	148	2.80	0.60
2.73	4.94	3.59	161	7.64	1.55
3.24	5.08	3.31	141	3.76	0.74
3.97	5.20	3.65	155	1.86	0.36
4.85	5.19	3.31	141	0.92	0.18
7.30	5.00	2.70	120	0.26	0.05

TABLE 5. O_2/CH_4 ENGINE CONDITION AND PLUME RADIANT INTENSITY DATA

O/F	$\dot{m}_t$ (gm/sec)	P_c (atm)	C* (m/sec)	$\overline{J}$ (W/sr) (4.1 to 5.1μ)	$\overline{J}$ (J/sr/gm)
1.81	5.47	3.93	159	0.01	~ 0
2.07	5.42	3.59	146	0.04	0.01
2.09	4.73	a	a	3.24	0.69
2.13	4.47	3.47	145	2.00	0.45
2.26	5.31	3.65	152	8.02	1.51
2.32	4.56	a	a	2.32	0.51
2.36	4.70	3.33	146	2.32	0.49
2.36	5.48	4.27	172	4.35	0.79
2.37	4.65	a	a	3.39	0.73
2.40	4.59	3.33	149	2.00	0.44
2.58	4.91	3.47	145	2.37	0.48
2.69	5.14	4.06	175	4.64	0.90
2.71	5.27	3.52	148	a	0.71
2.93	5.30	4.34	181	3.98	0.75
3.79	5.27	4.06	170	1.43	0.27
4.24	4.82	3.59	165	1.04	0.22
5.37	5.22	3.86	164	0.65	0.12
6.82	5.08	3.24	141	0.32	0.06
7.00	5.20	3.52	150	0.34	0.07

[a]This data not available.

TABLE 6. O_2/C_6H_6 ENGINE CONDITION AND PLUME RADIANT INTENSITY DATA

O/F	$\dot{m}_t$ (gm/sec)	P_c (atm)	C* (m/sec)	$\overline{J}$ (W/sr) (4.1 to 5.1μ)	$\overline{J}$ (J/sr/gm)
1.18	4.44	3.38	169	1.65	0.37
1.21	5.30	3.52	147	8.74	1.65
1.46	4.80	3.31	153	14.54	3.03
1.65	5.03	3.52	155	8.04	1.60
1.80	5.16	3.52	151	6.64	1.29
1.98	5.09	3.59	156	5.13	1.01
2.35	5.13	2.84	122	3.47	0.68
2.55	5.15	2.97	128	2.83	0.55
2.95	5.05	3.59	157	3.39	0.67
4.15	5.15	3.38	145	1.62	0.31
4.42	5.15	3.31	142	1.54	0.30
6.14	5.00	3.72	165	0.73	0.15

APPENDIX A

CENTERLINE RADIATION DISTRIBUTIONS

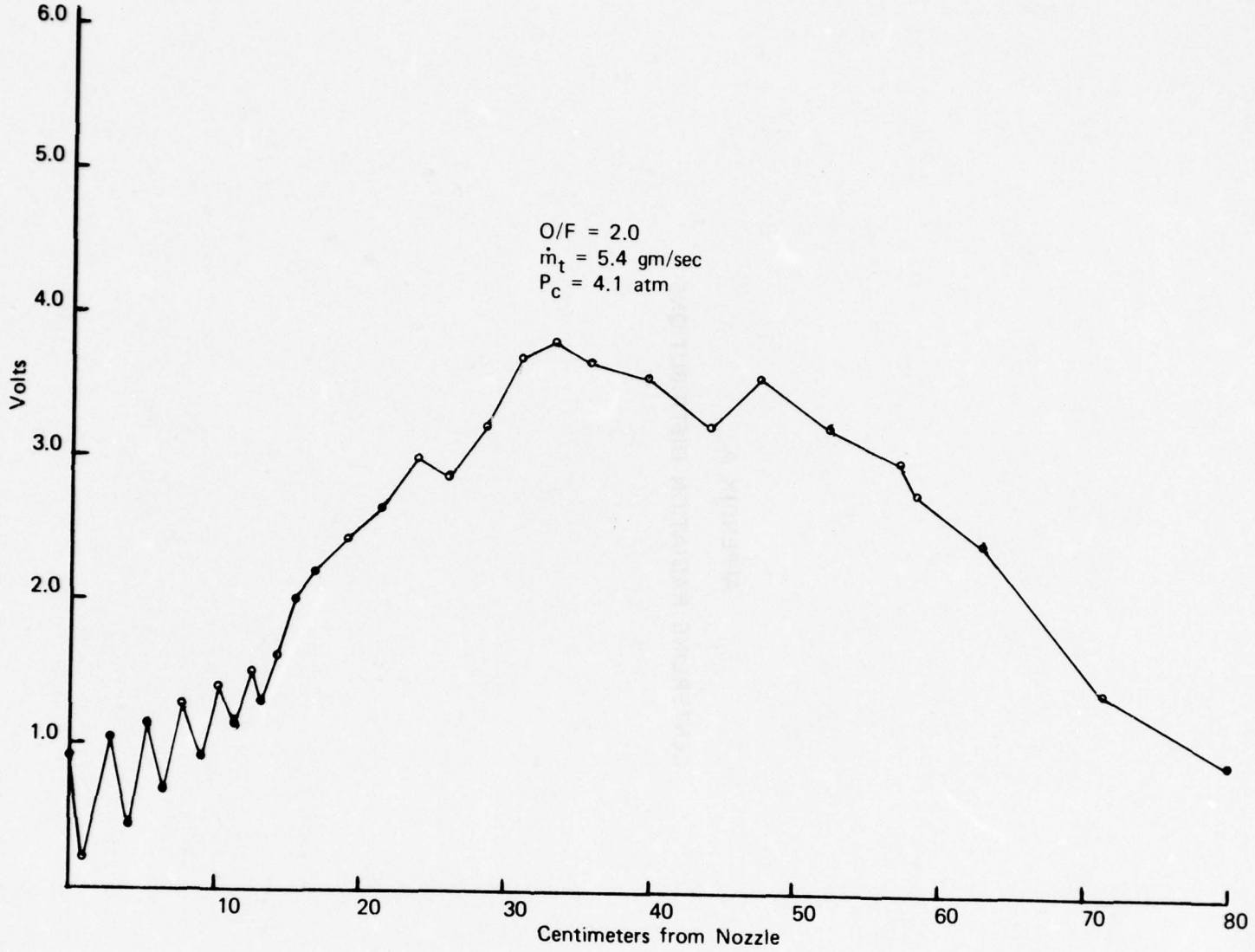

Figure A-1. Plume Centerline Radiation Distribution for O_2/RP-1/GOX, O/F = 2.0

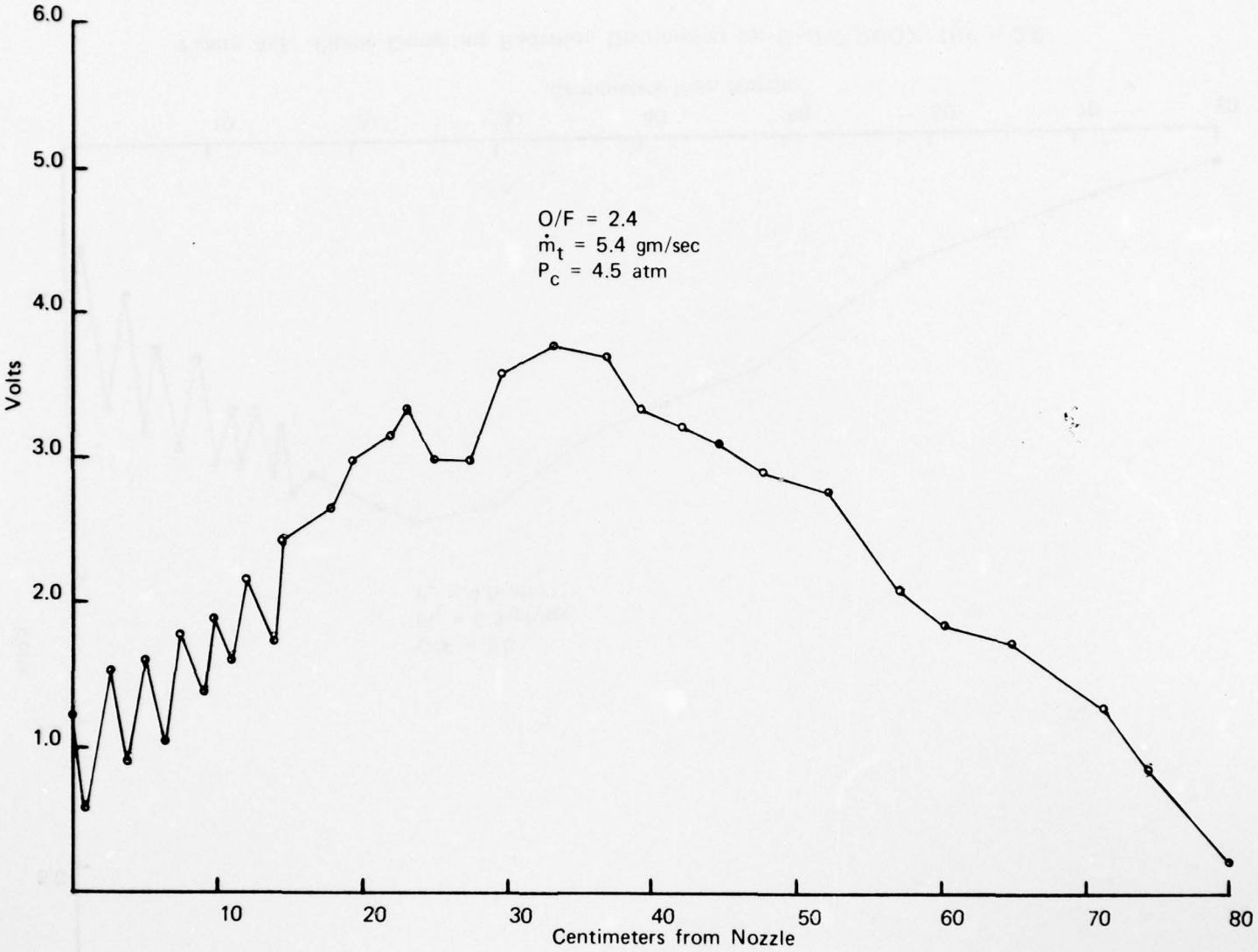

Figure A-2. Plume Centerline Radiation Distribution for O_2/RP-1/GOX, O/F = 2.4

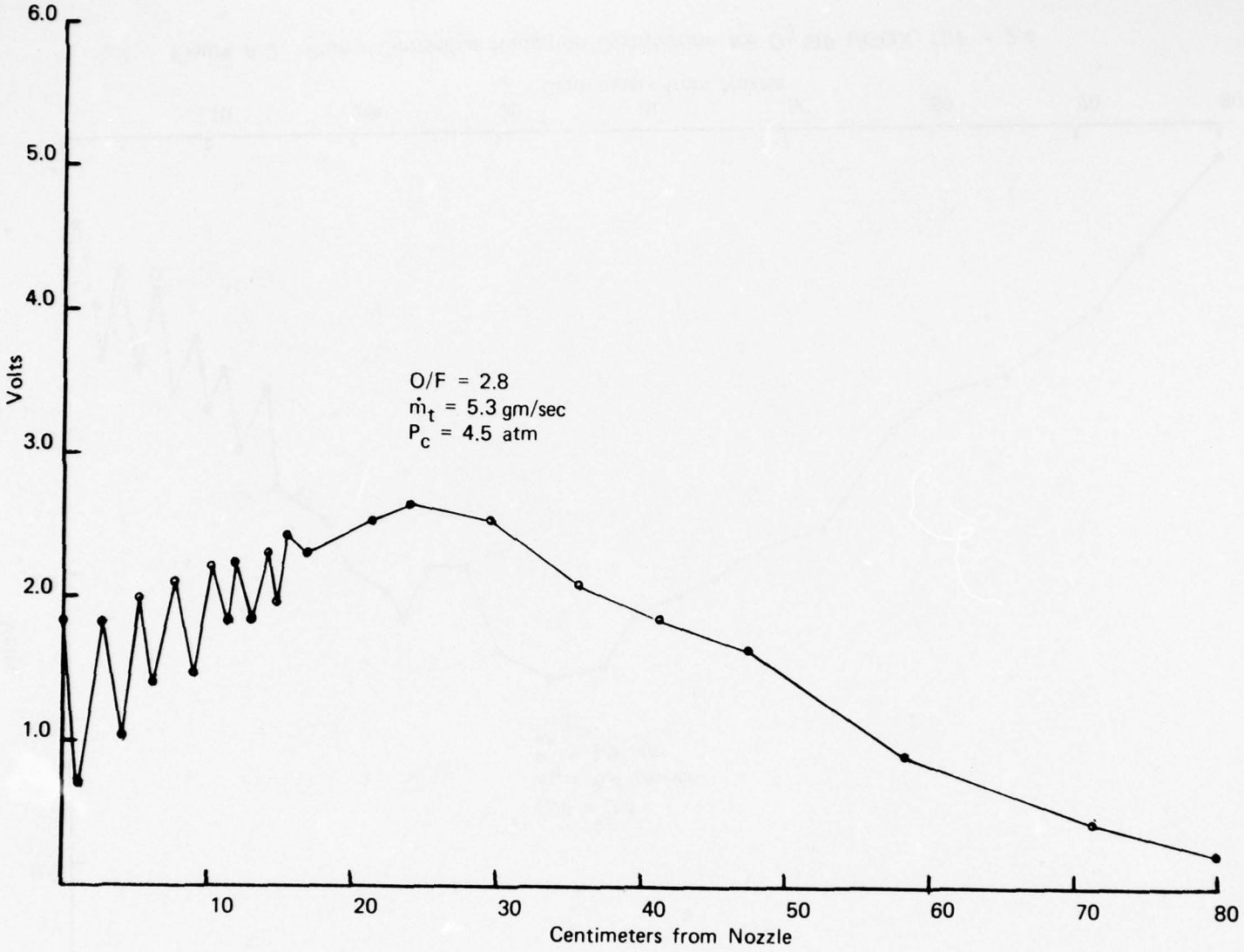

Figure A-3. Plume Centerline Radiation Distribution for O_2/RP-1/GOX, O/F = 2.8

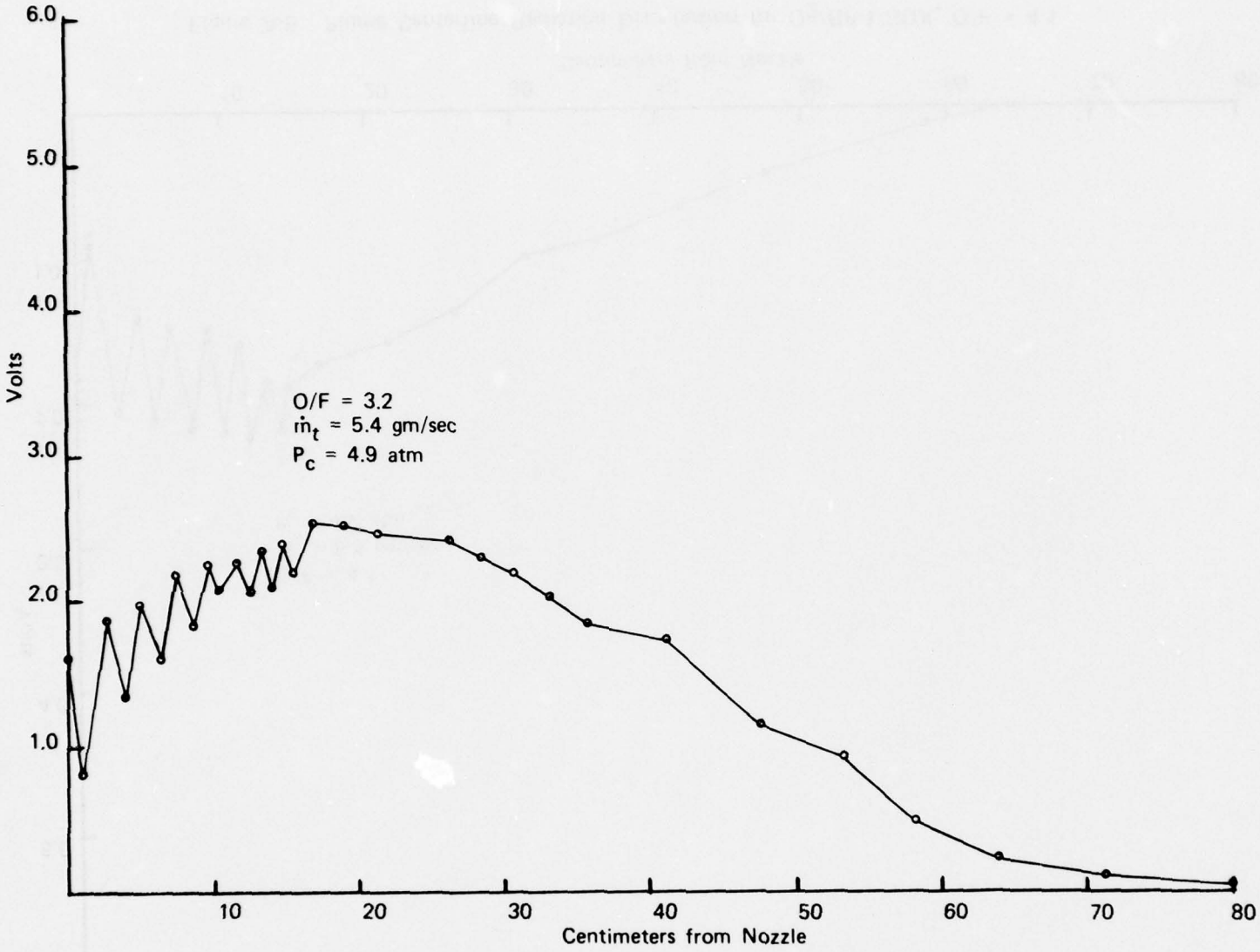

Figure A-4. Plume Centerline Radiation Distribution for O_2/RP-1/GOX, O/F = 3.2

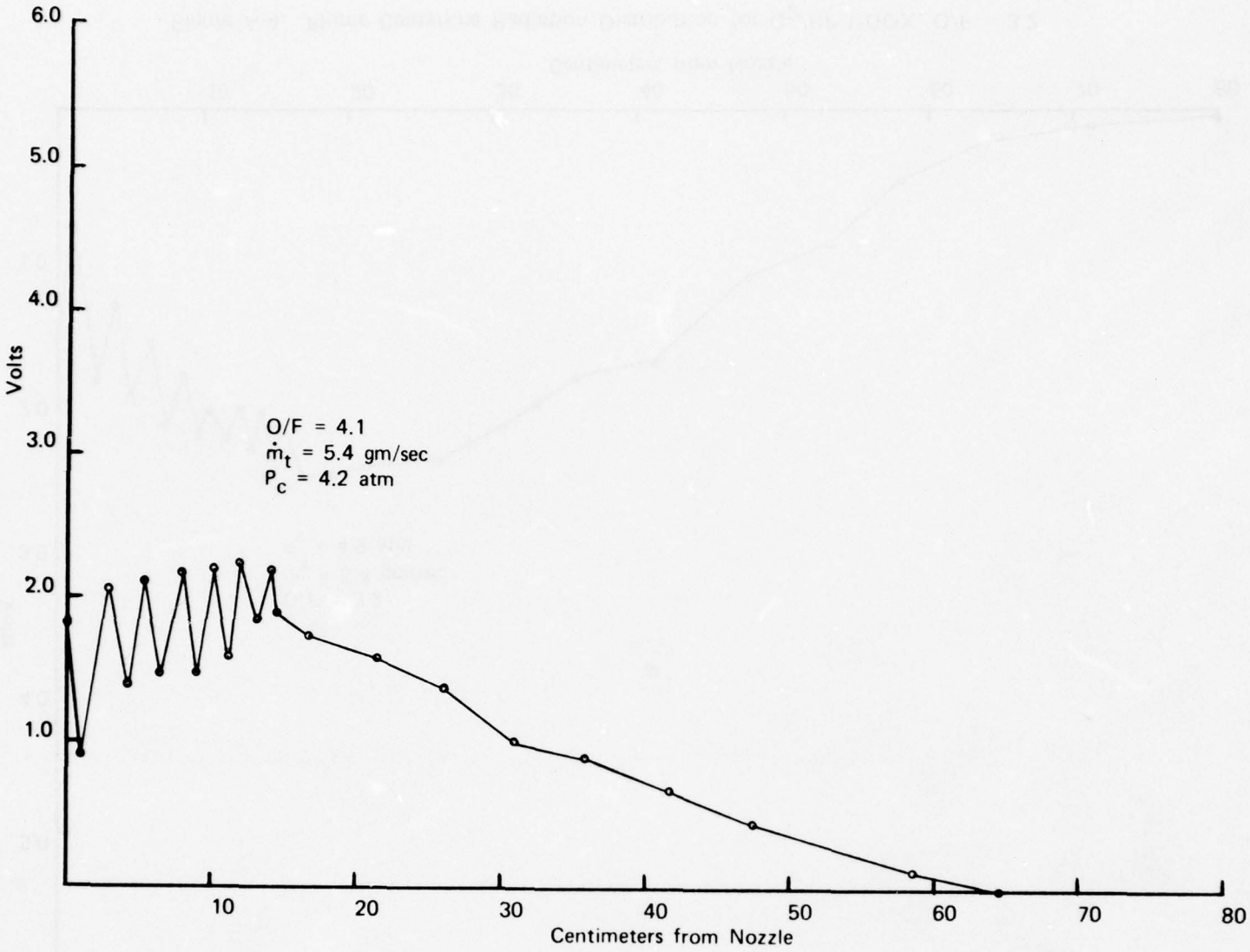

Figure A-5. Plume Centerline Radiation Distribution for O_2/RP-1/GOX, O/F = 4.1

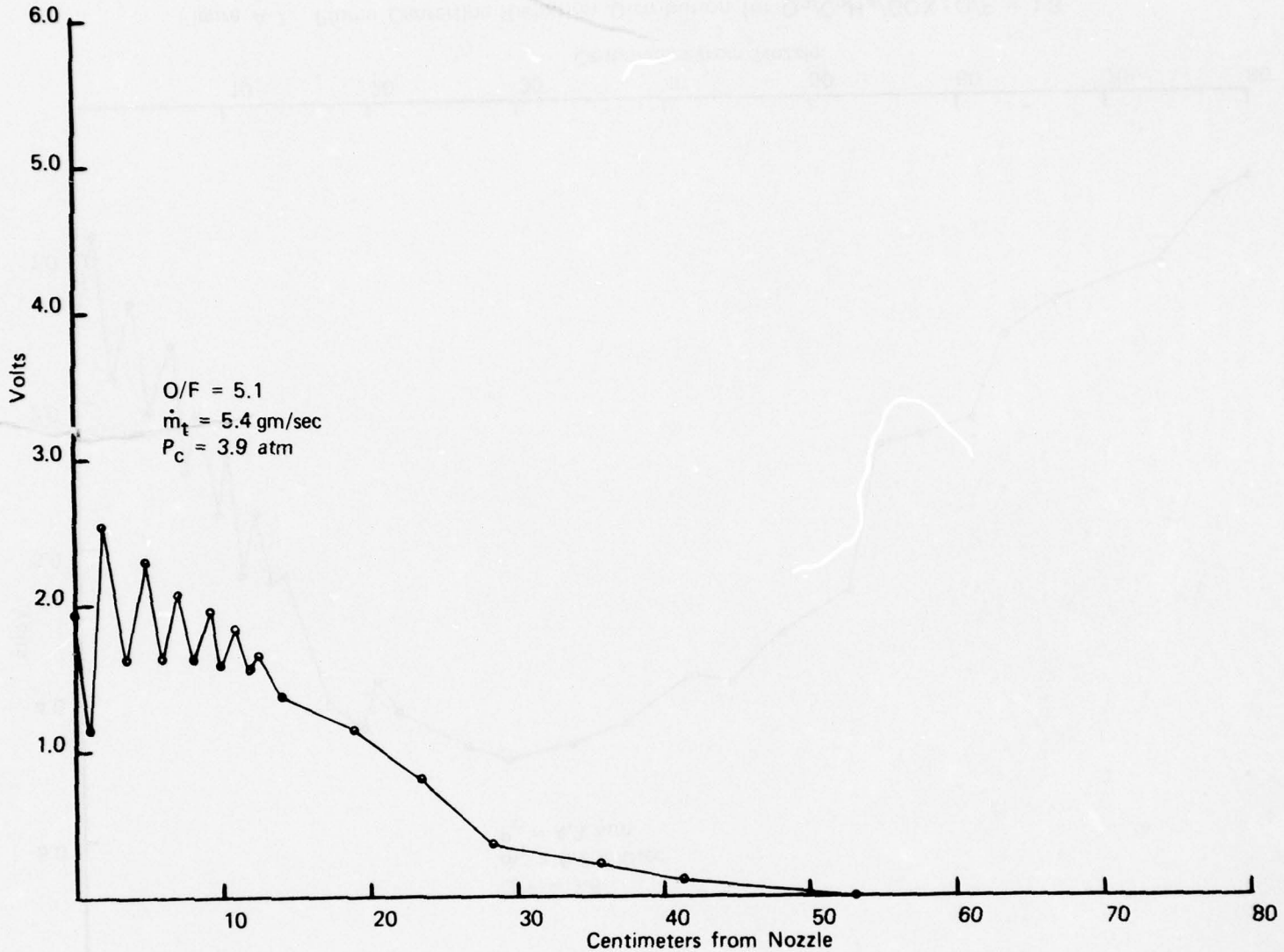

Figure A-6. Plume Centerline Radiation Distribution for O_2/RP-1/GOX, O/F = 5.1

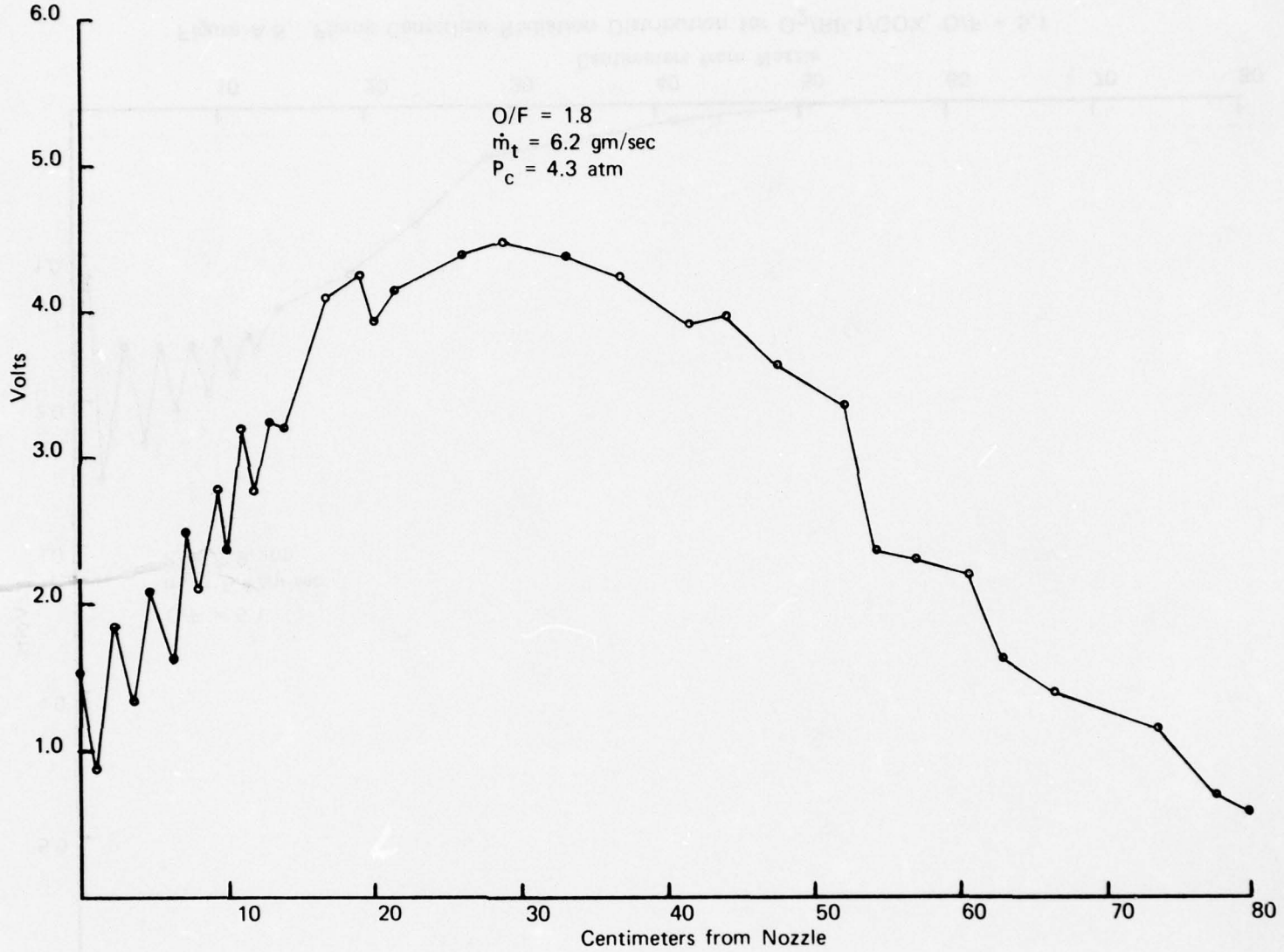

Figure A-7. Plume Centerline Radiation Distribution for O_2/C_2H_4/GOX, O/F = 1.8

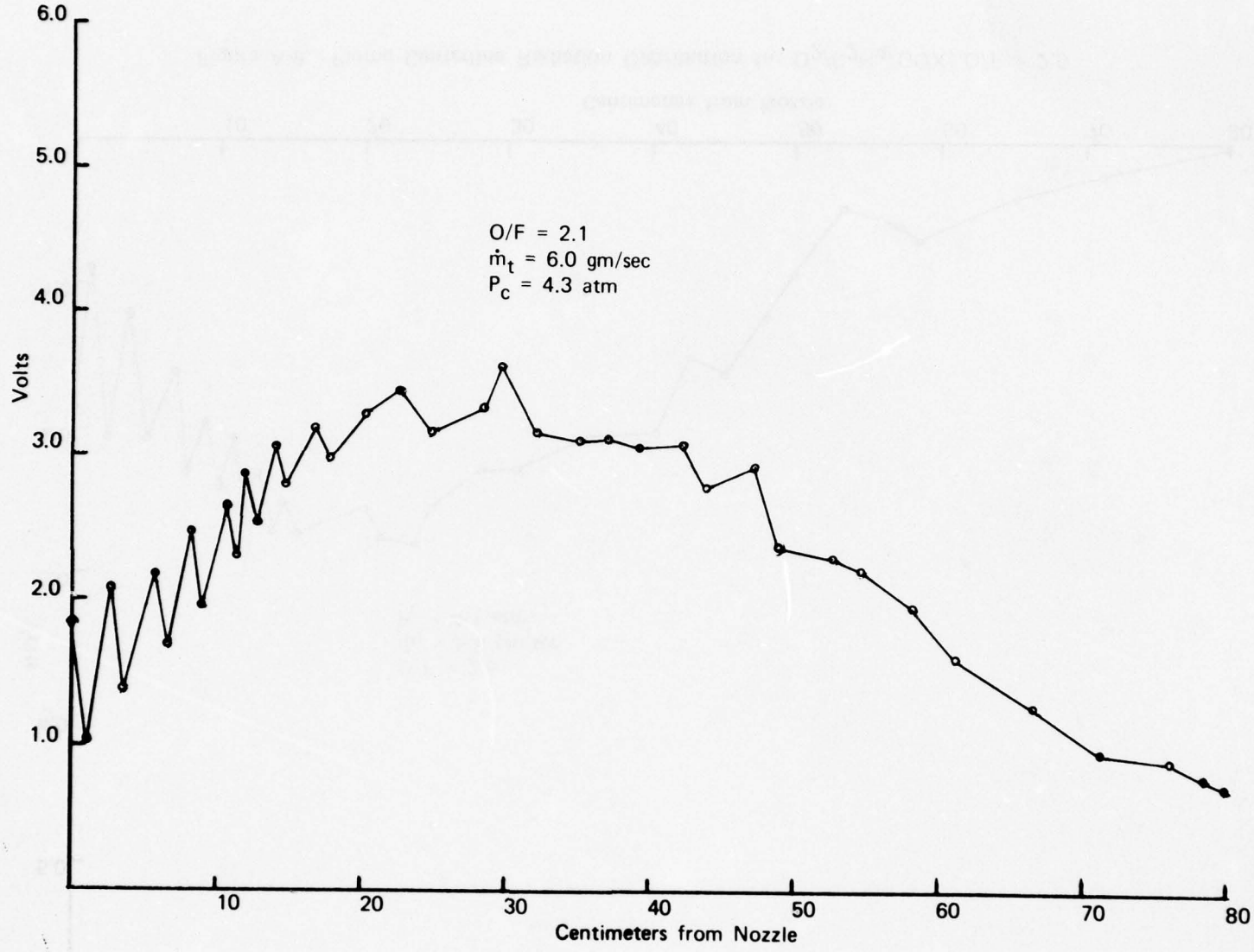

Figure A-8. Plume Centerline Radiation Distribution for O_2/C_2H_4/GOX, O/F = 2.1

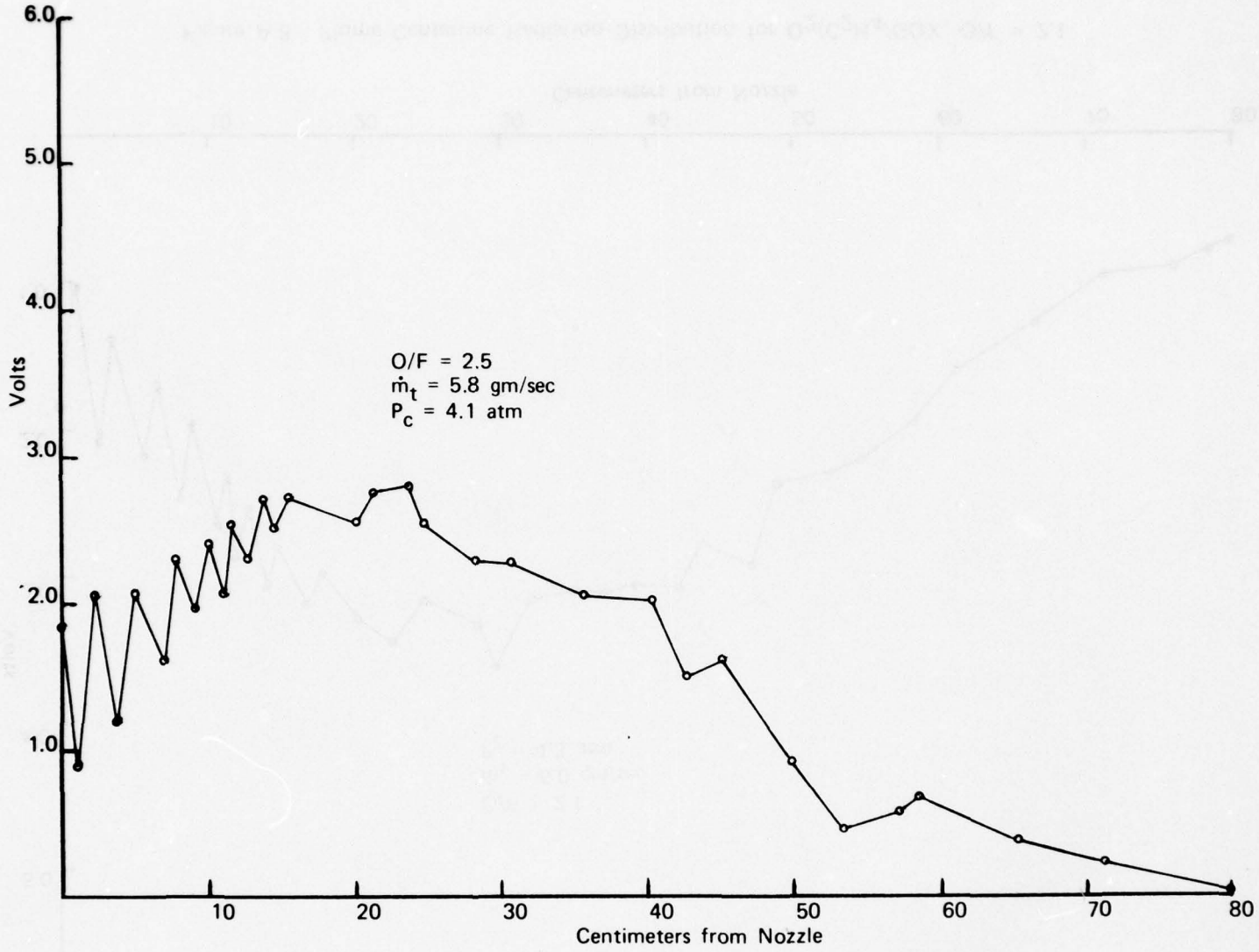

Figure A-9. Plume Centerline Radiation Distribution for O_2/C_2H_4/GOX, O/F = 2.5

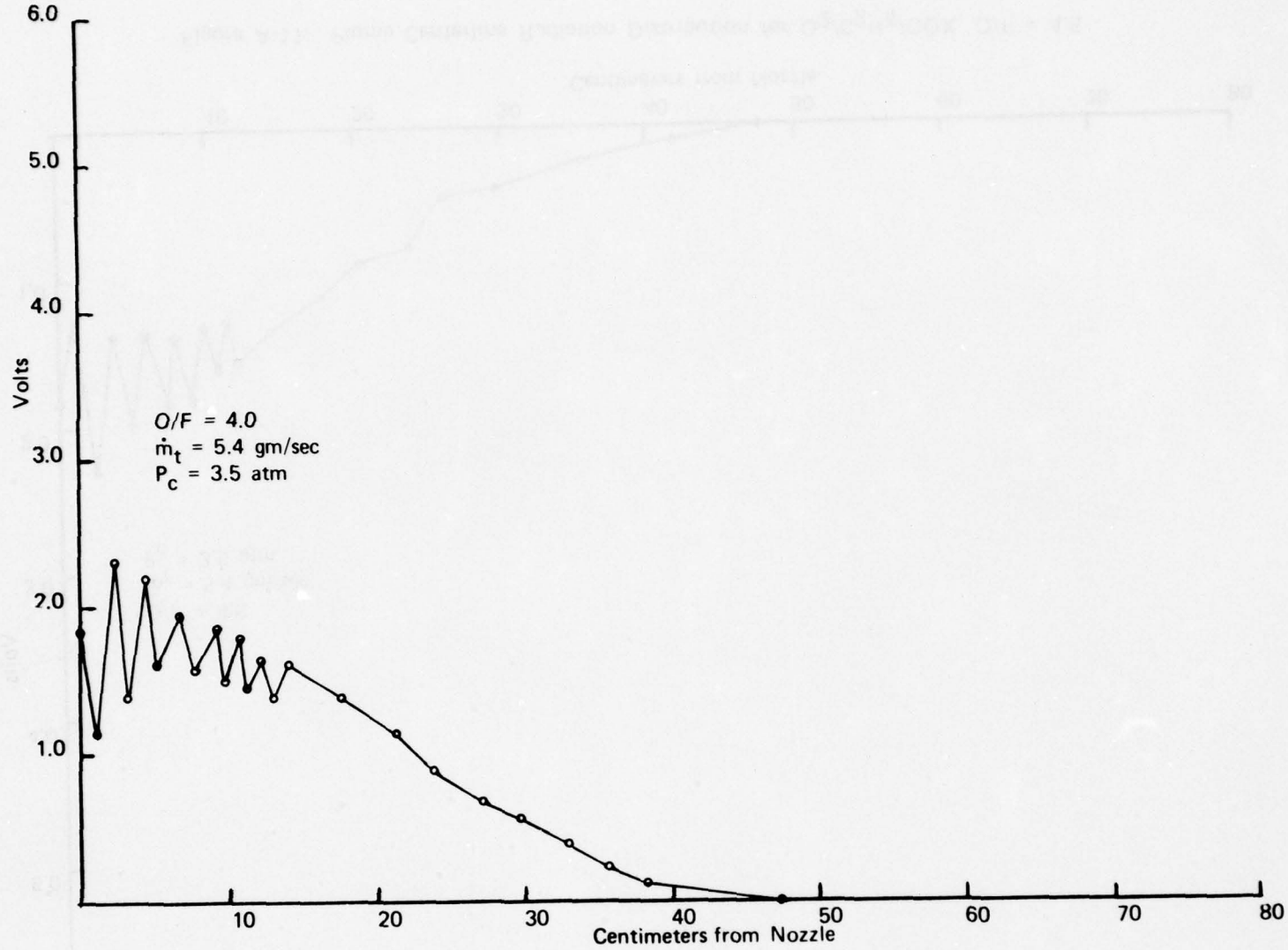

Figure A-10. Plume Centerline Radiation Distribution for O_2/C_2H_4/GOX, O/F = 4.0

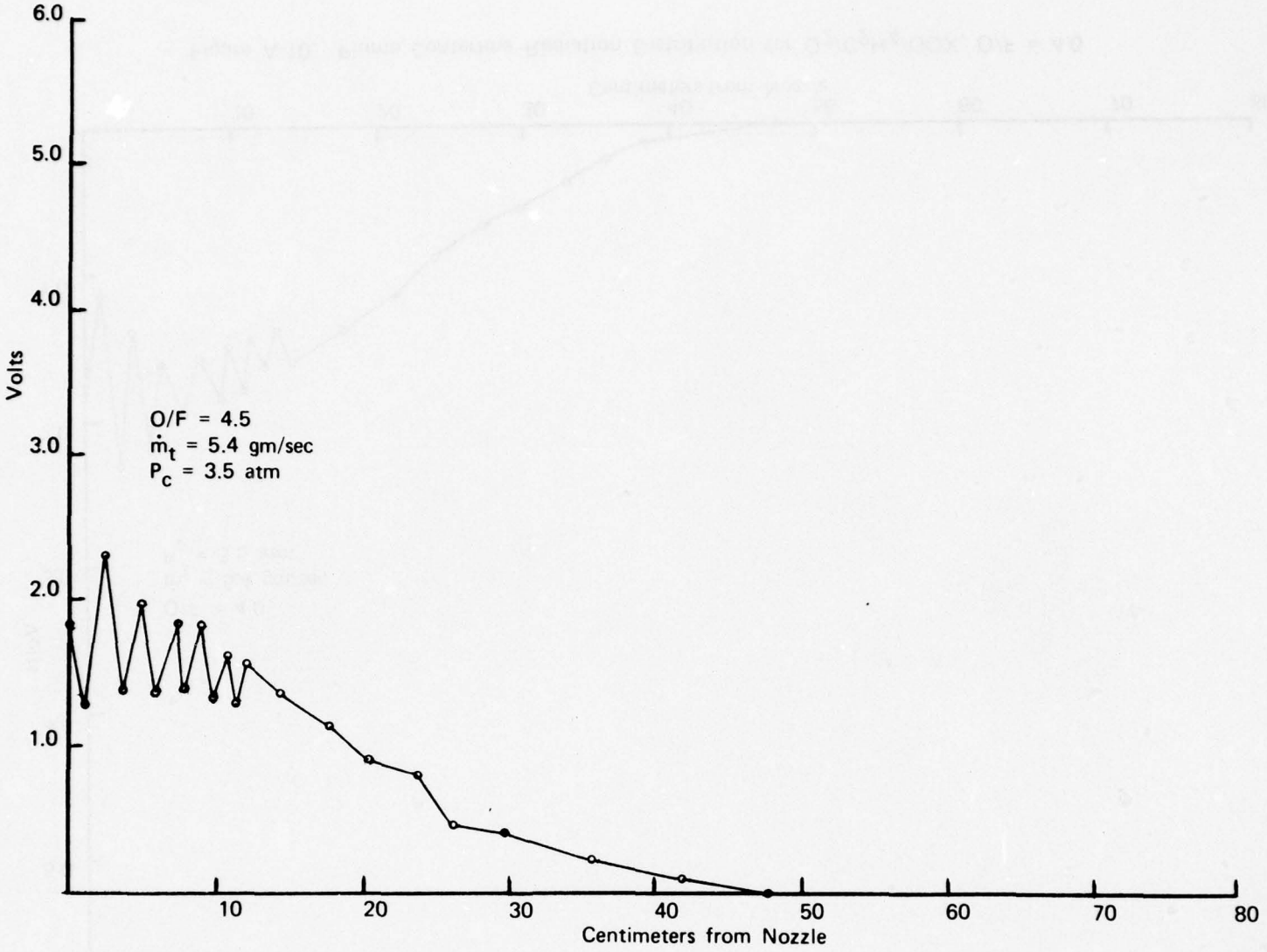

Figure A-11. Plume Centerline Radiation Distribution for O_2/C_2H_4/GOX, O/F = 4.5

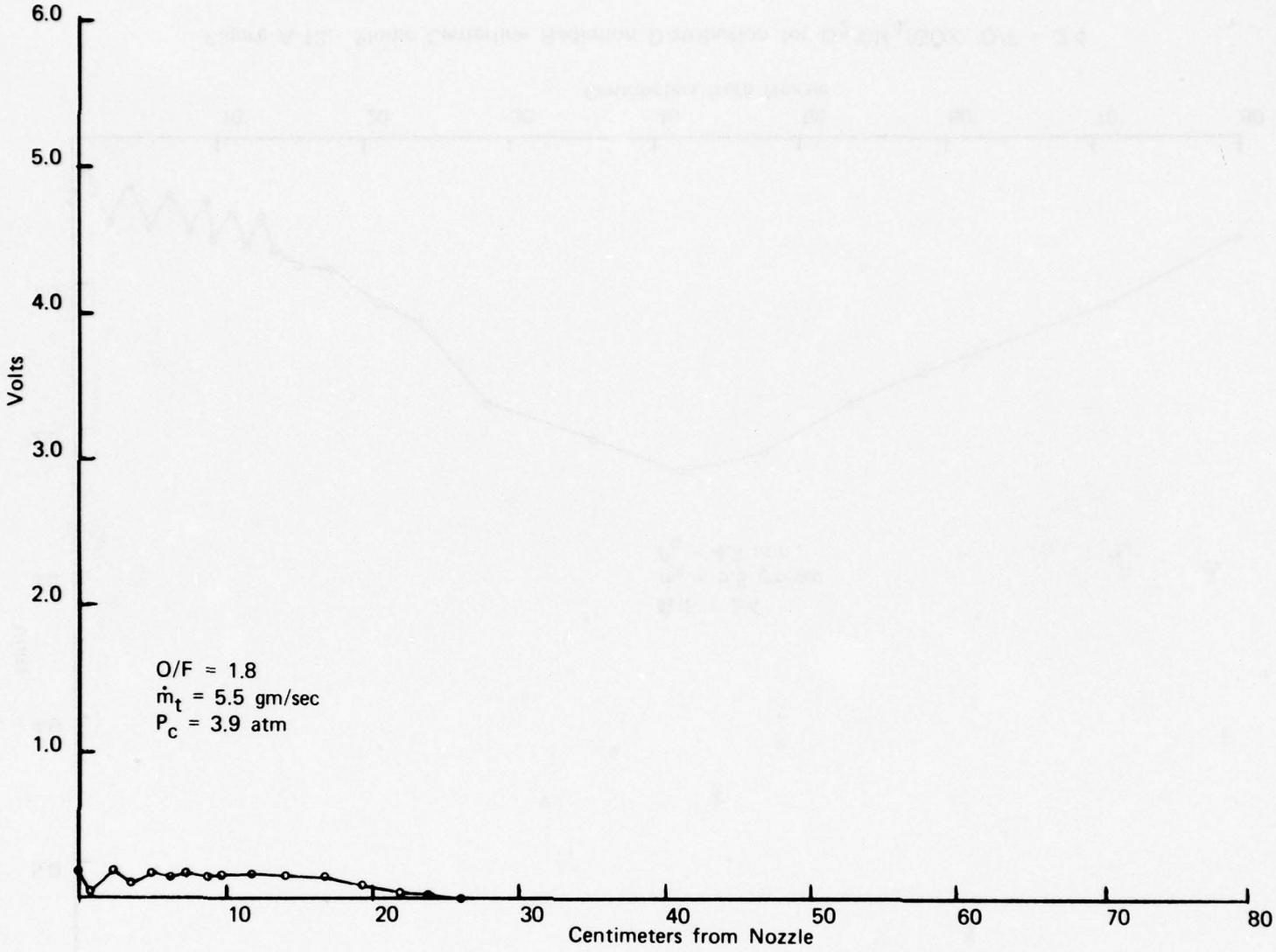

Figure A-12. Plume Centerline Radiation Distribution for O_2/CH_4/GOX, O/F = 1.8

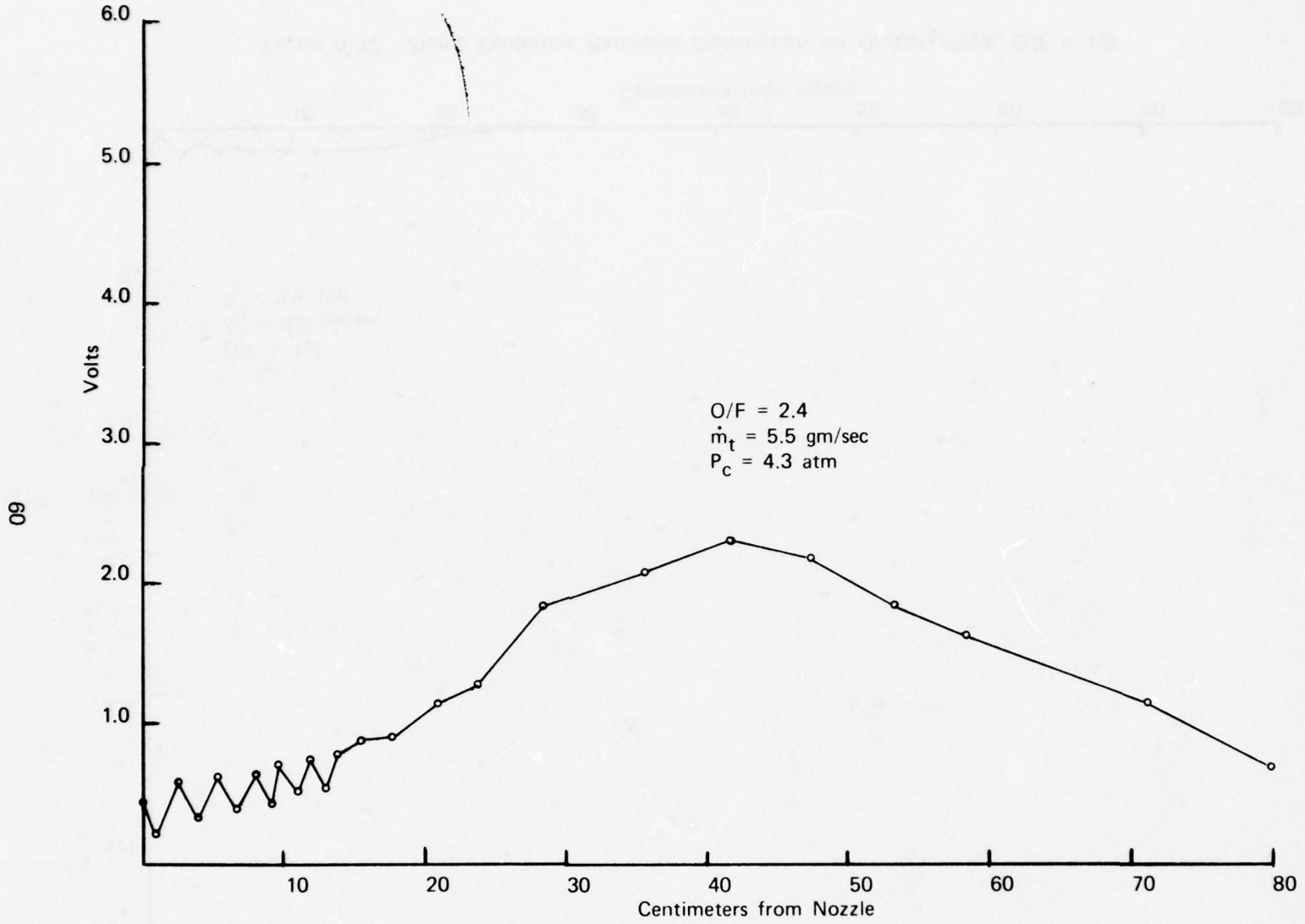

Figure A-13. Plume Centerline Radiation Distribution for O_2/CH_4/GOX, O/F = 2.4

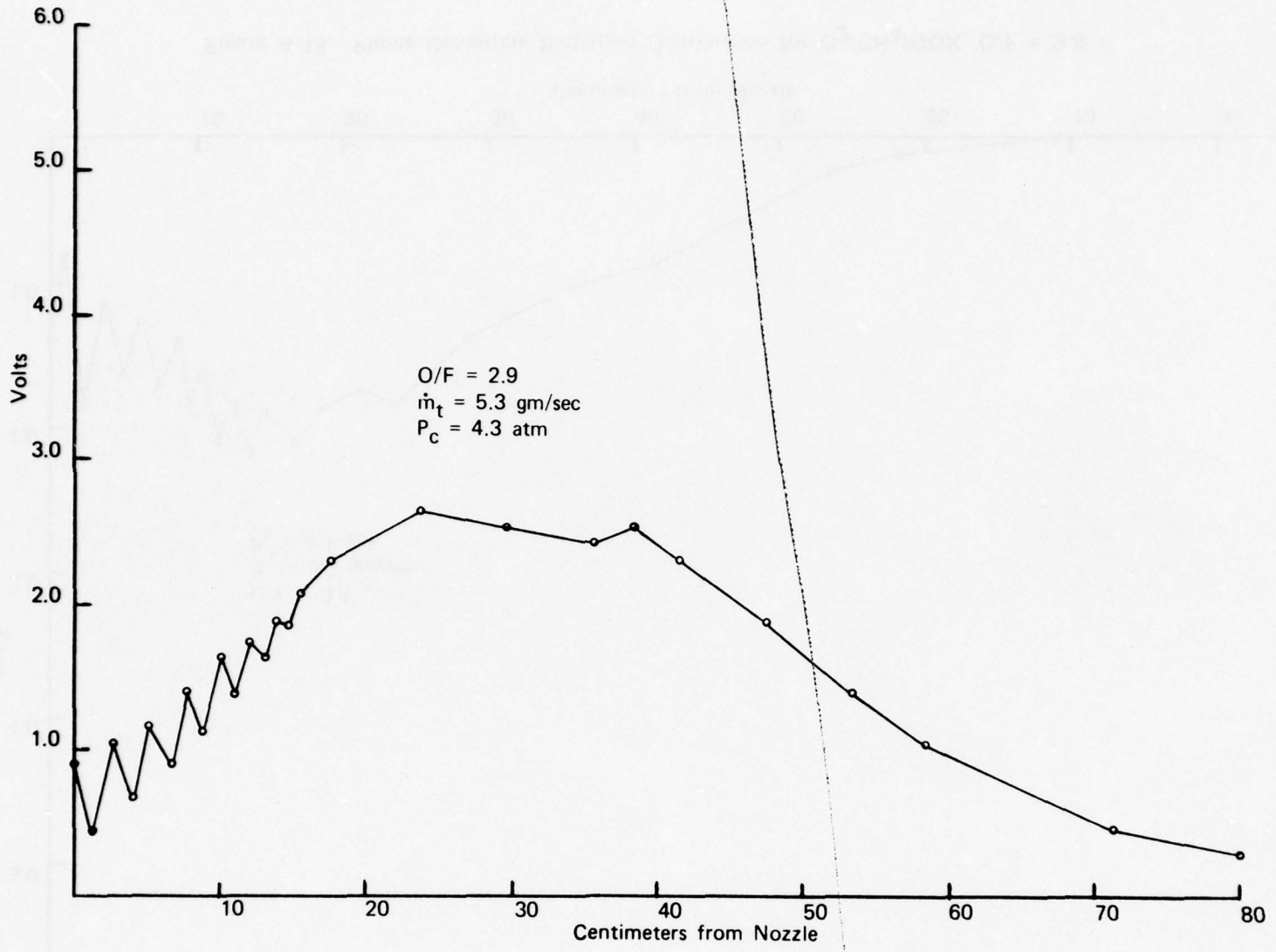

Figure A-14. Plume Centerline Radiation Distribution for O_2/CH_4/GOX, O/F = 2.9

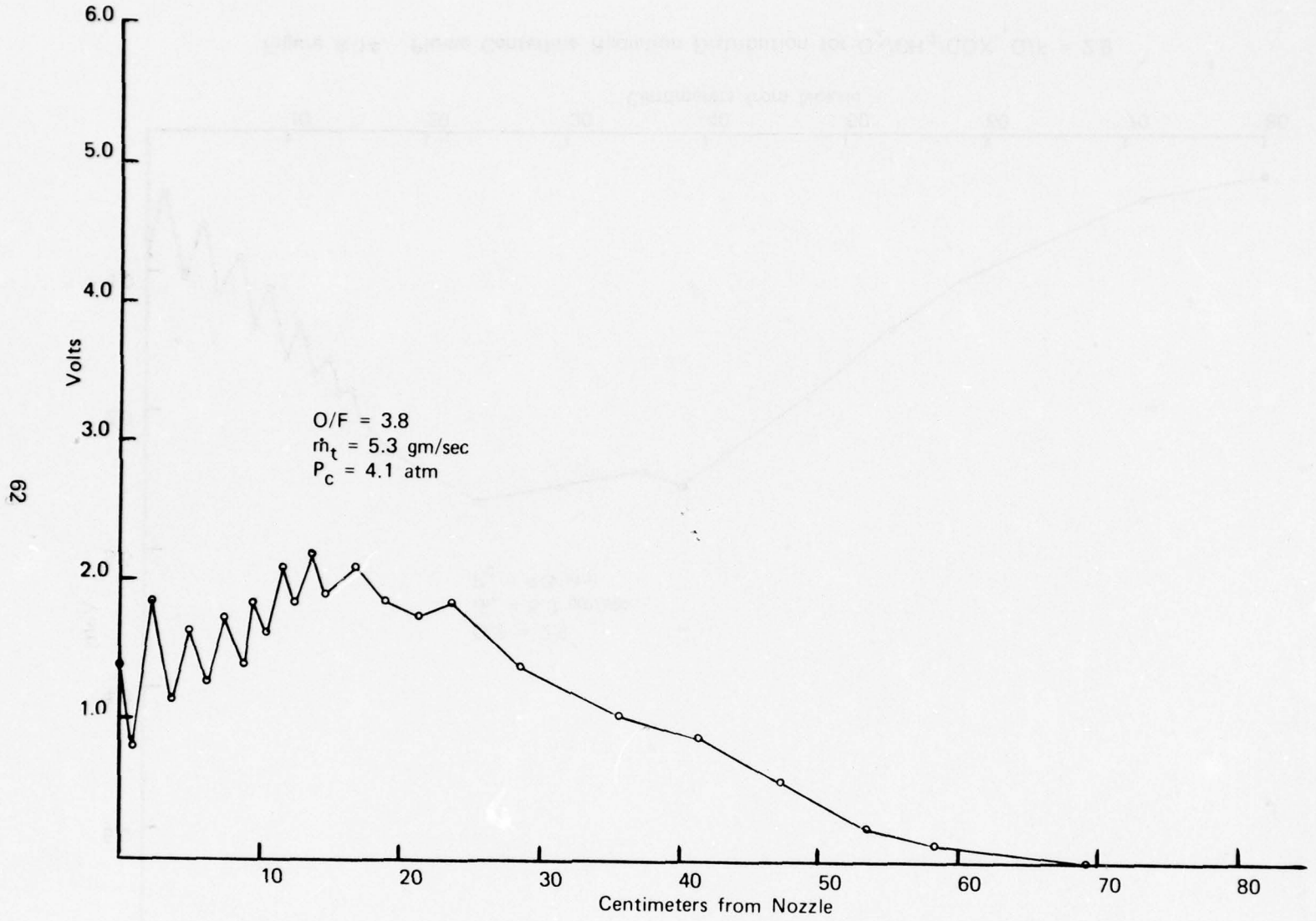

Figure A-15. Plume Centerline Radiation Distribution for O_2/CH_4/GOX, O/F = 3.8

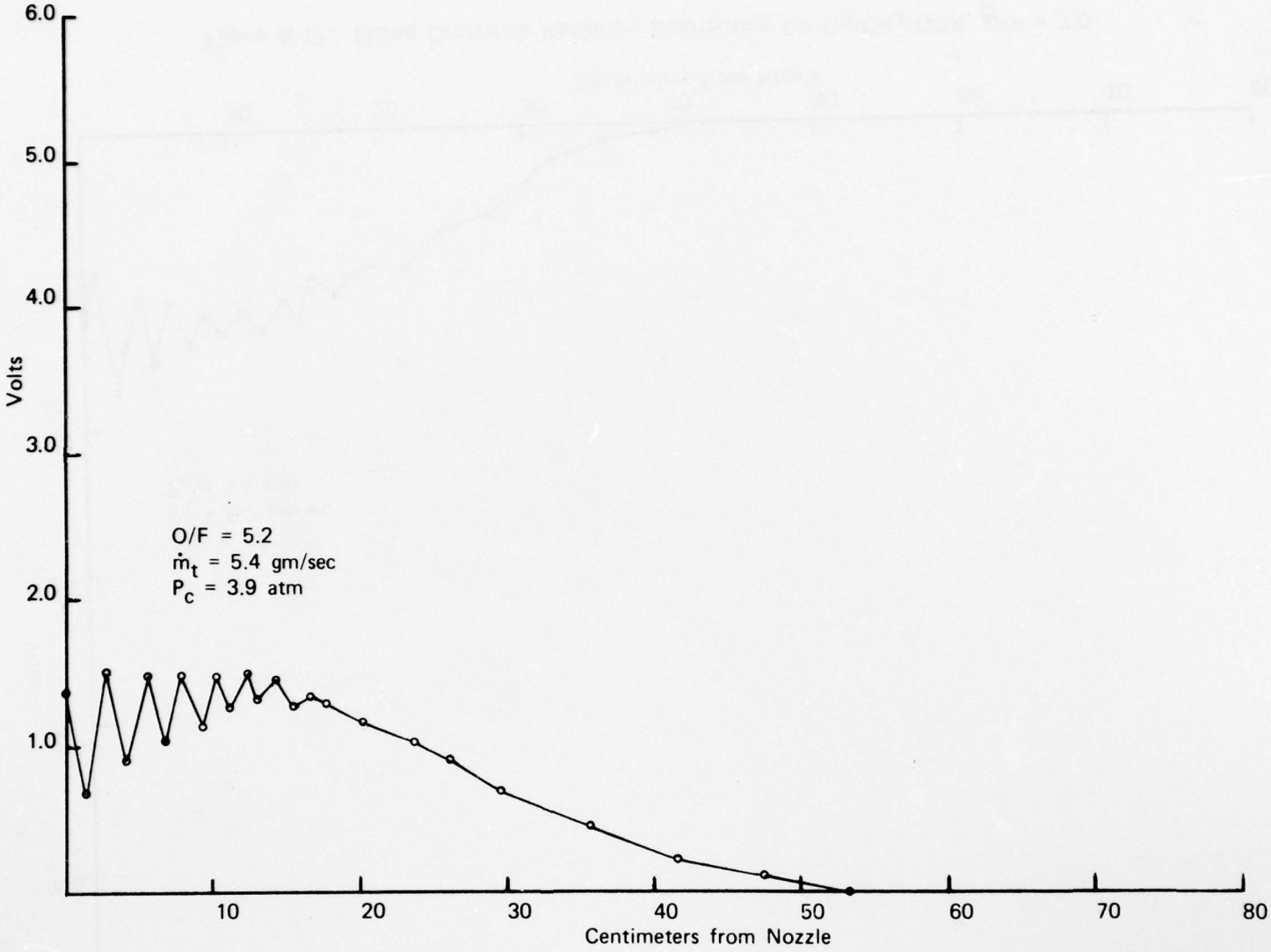

Figure A-16. Plume Centerline Radiation Distribution for O_2/CH_4/GOX, O/F = 5.2

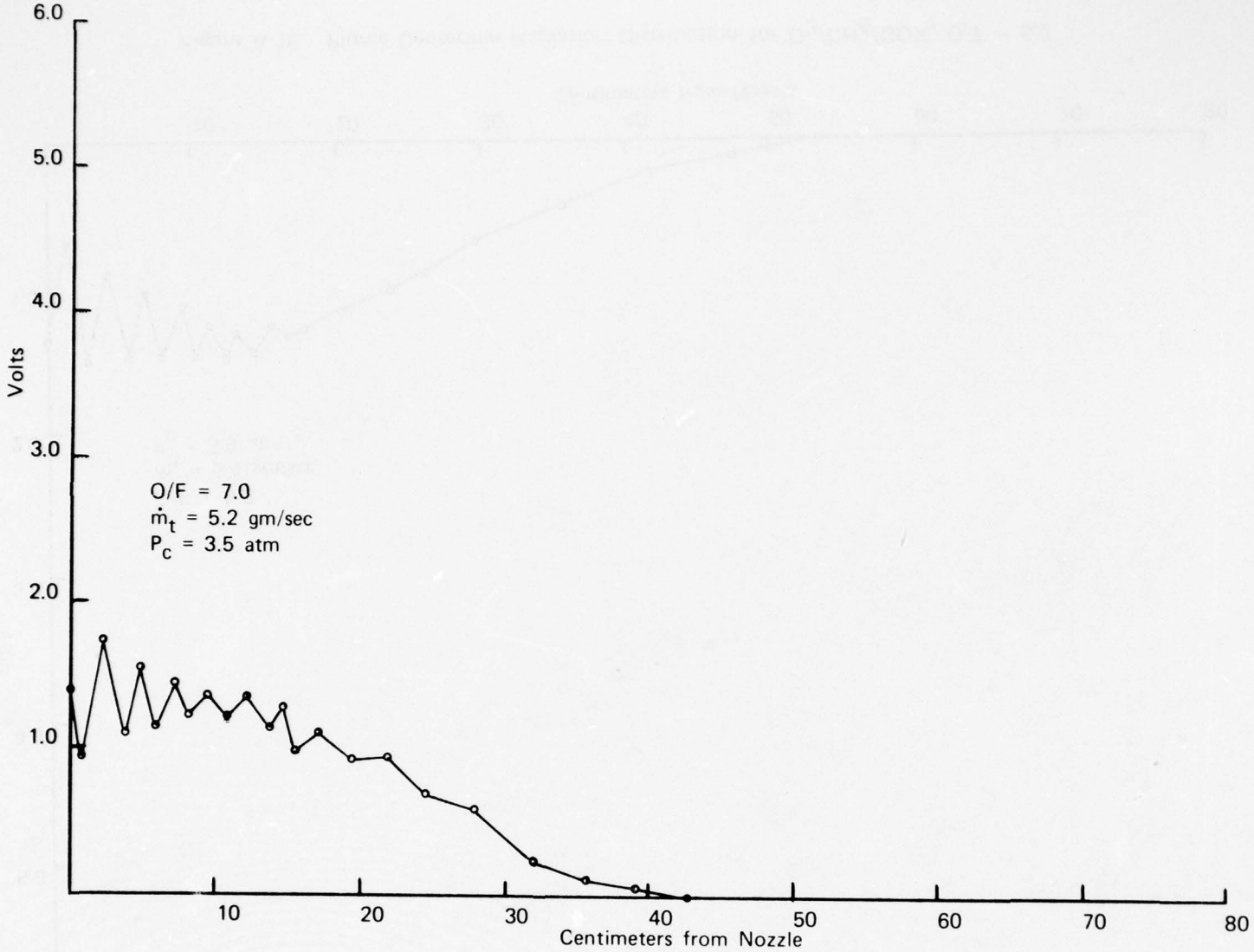

Figure A-17. Plume Centerline Radiation Distribution for O_2/CH_4/GOX, O/F = 7.0

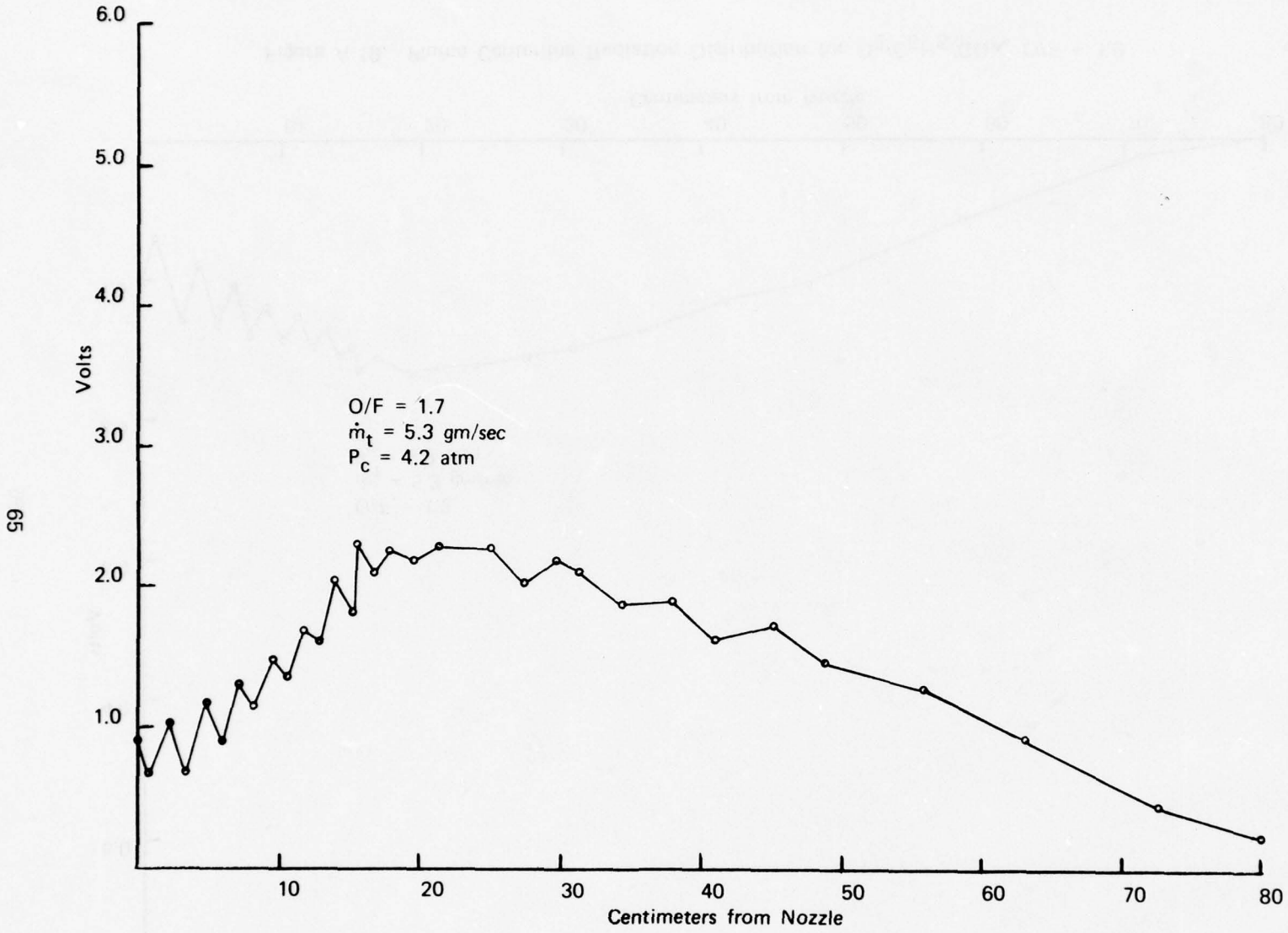

Figure A-18. Plume Centerline Radiation Distribution for O_2/C_6H_6/GOX, O/F = 1.7

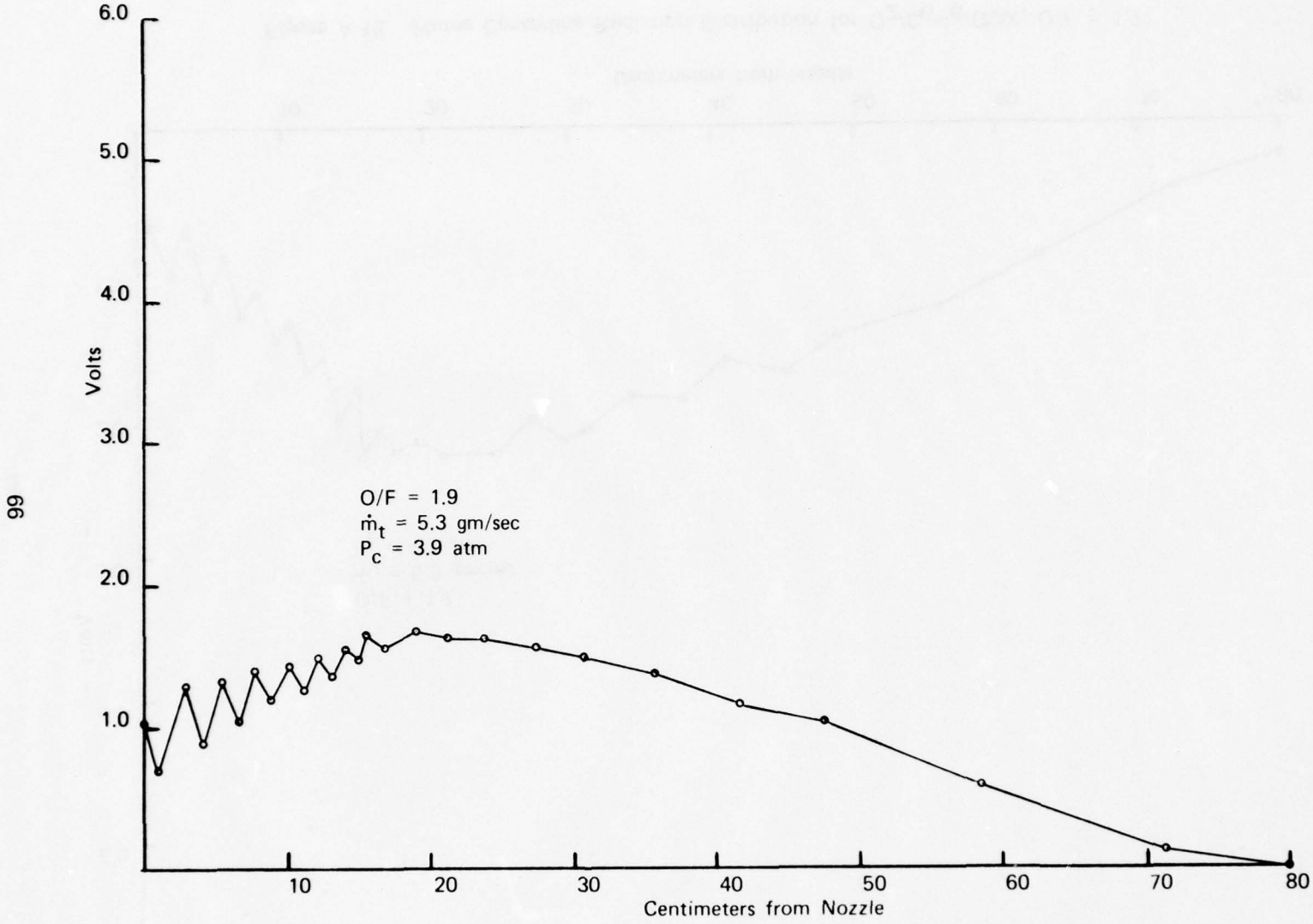

Figure A-19. Plume Centerline Radiation Distribution for O_2/C_6H_6/GOX, O/F = 1.9

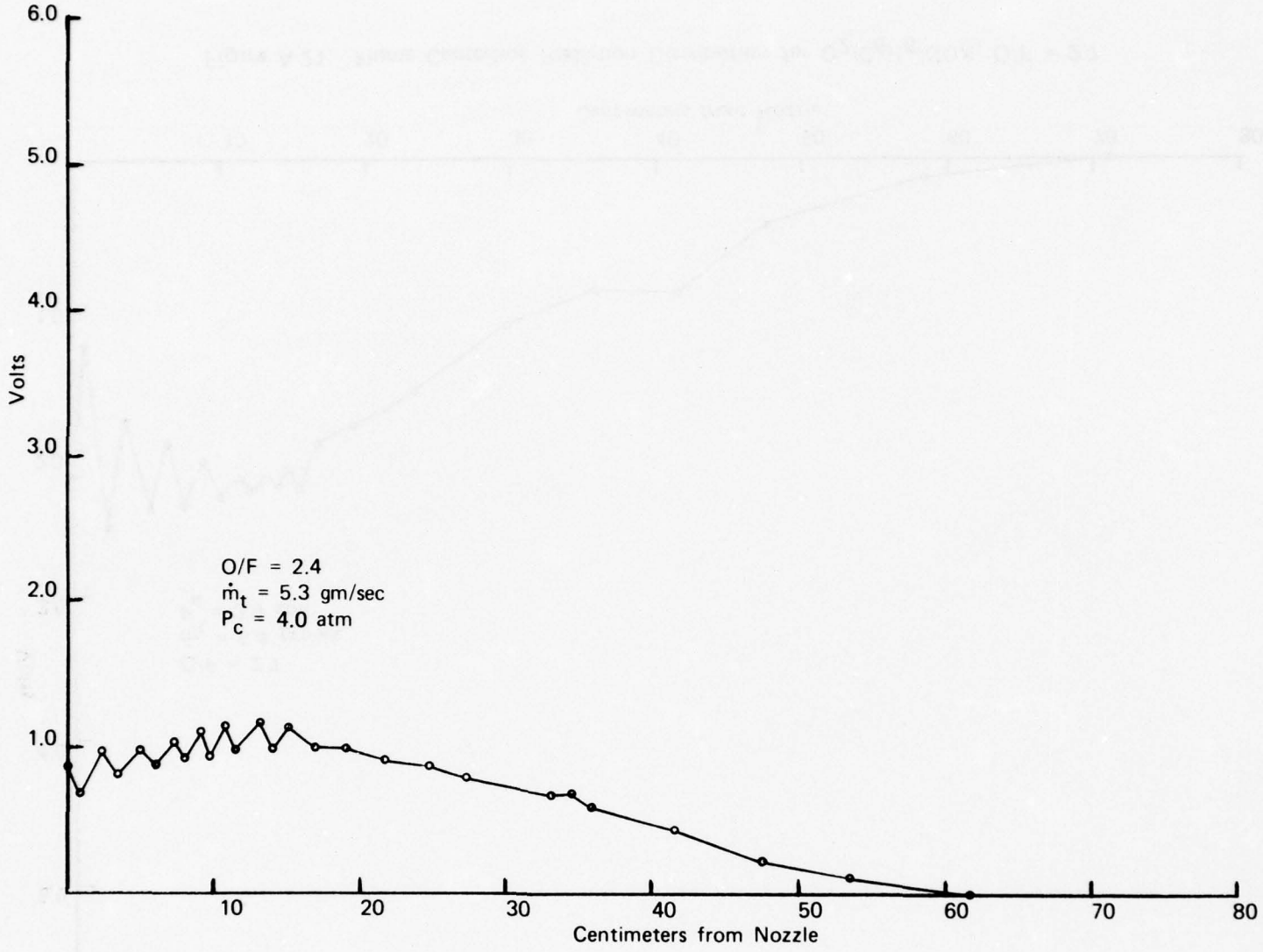

Figure A-20. Plume Centerline Radiation Distribution for O_2/C_6H_6/GOX, O/F = 2.4

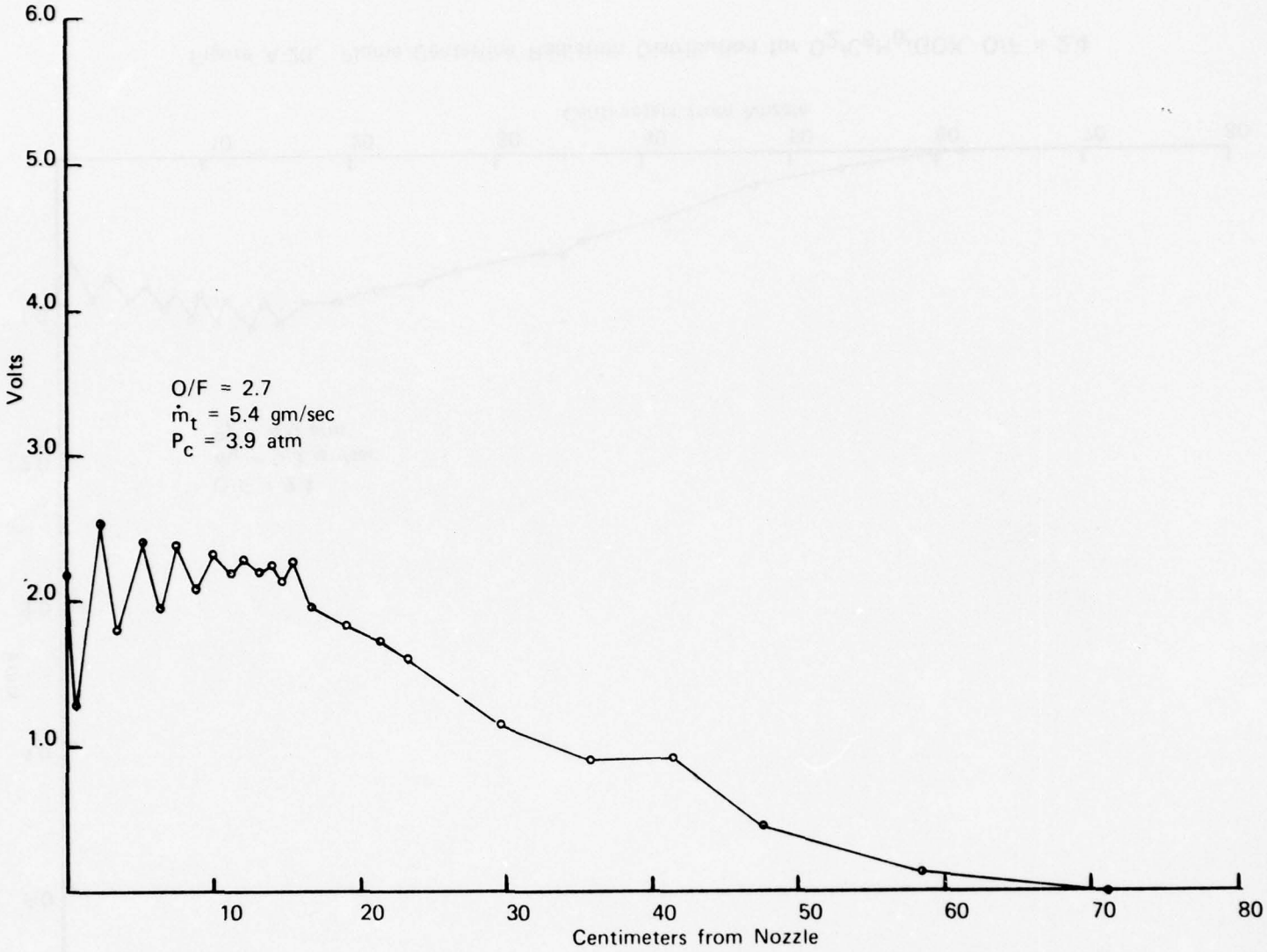

Figure A-21. Plume Centerline Radiation Distribution for O_2/C_6H_6/GOX, O/F = 2.7

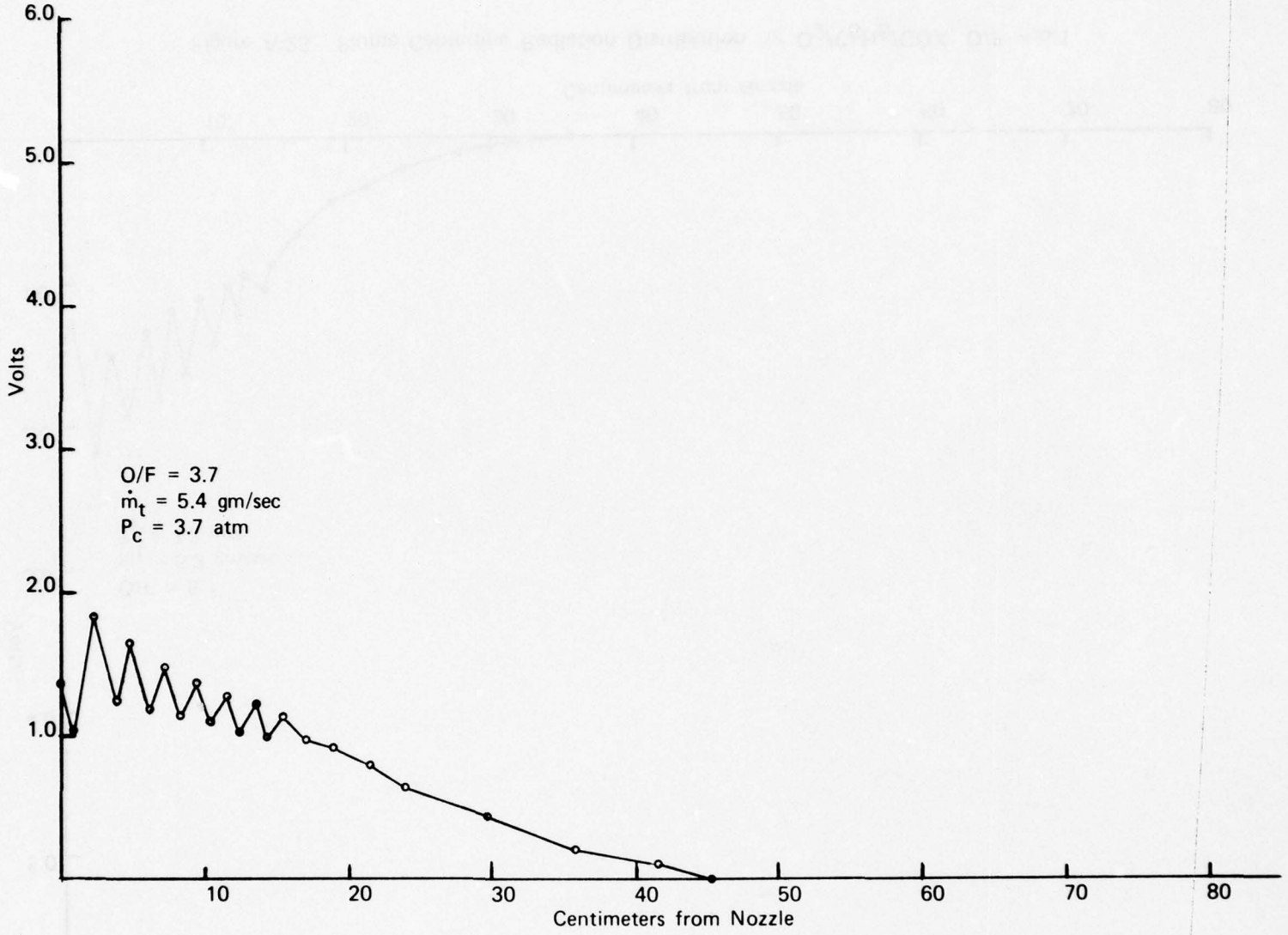

Figure A-22. Plume Centerline Radiation Distribution for O_2/C_6H_6/GOX, O/F = 3.7

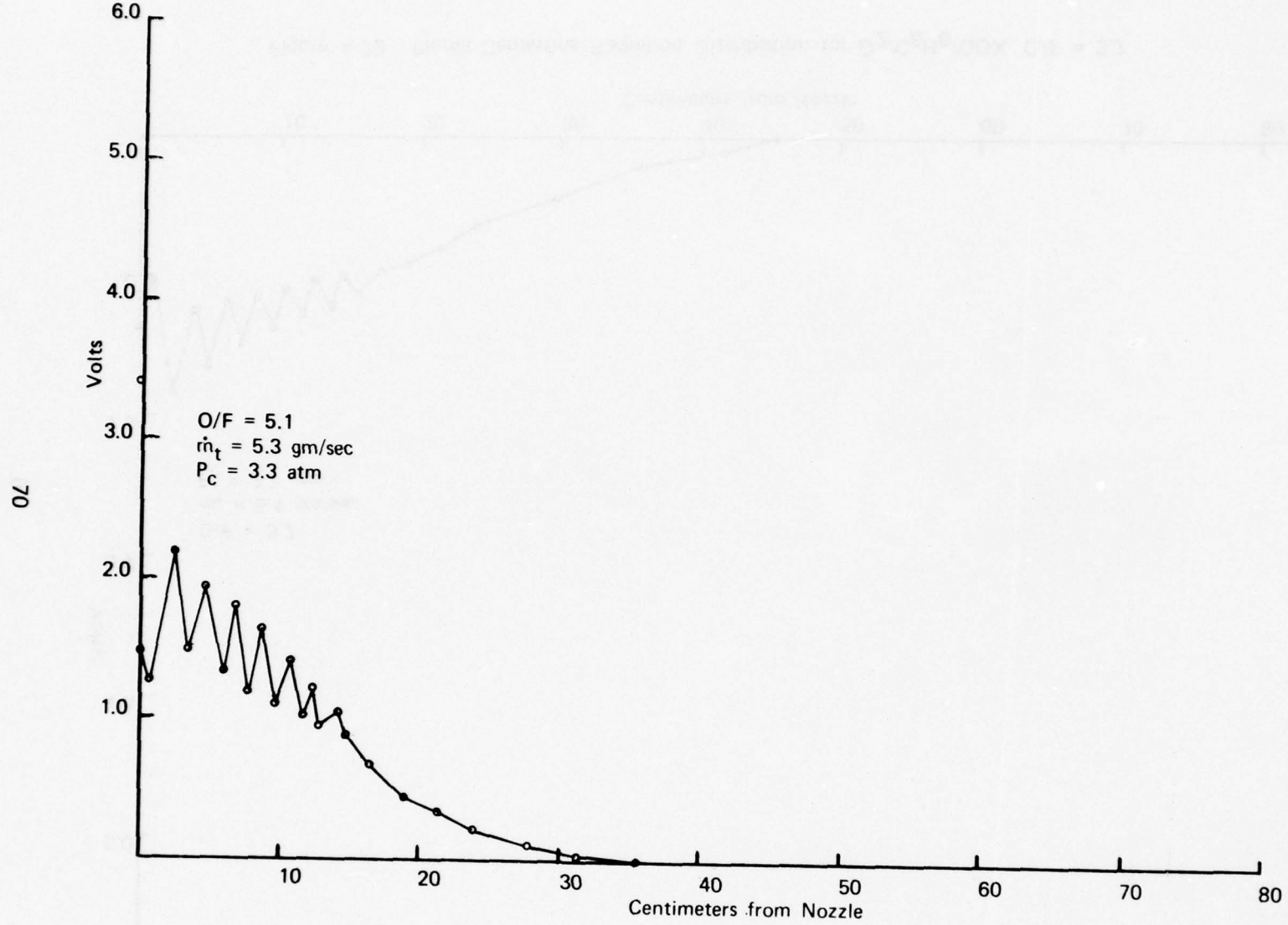

Figure A-23. Plume Centerline Radiation Distribution for O_2/C_6H_6/GOX, O/F = 5.1

APPENDIX B

STATION RADIATION DISTRIBUTIONS

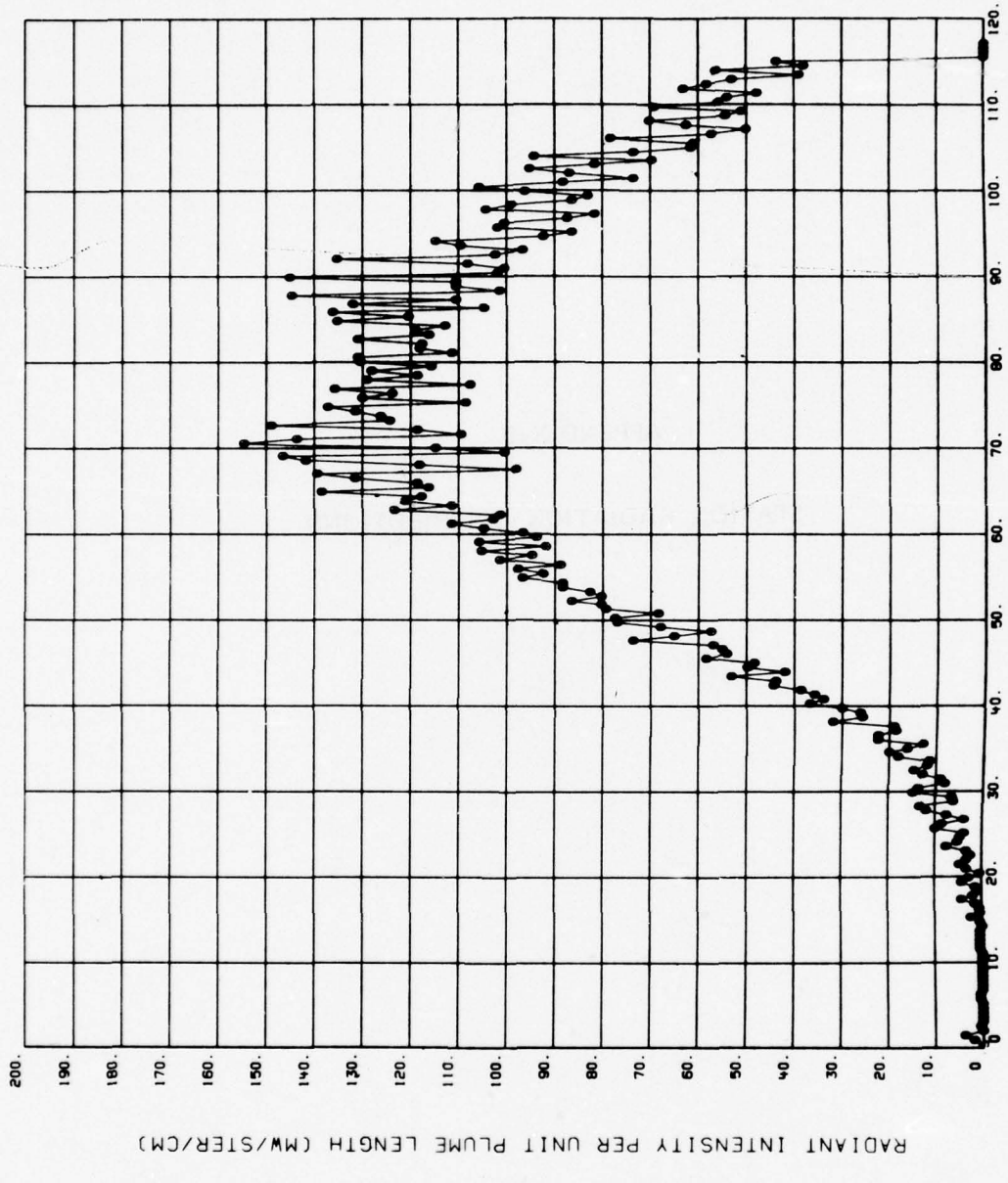

Figure B-1. Station Radiation Data for O_2/RP-1, O/F = 1.6

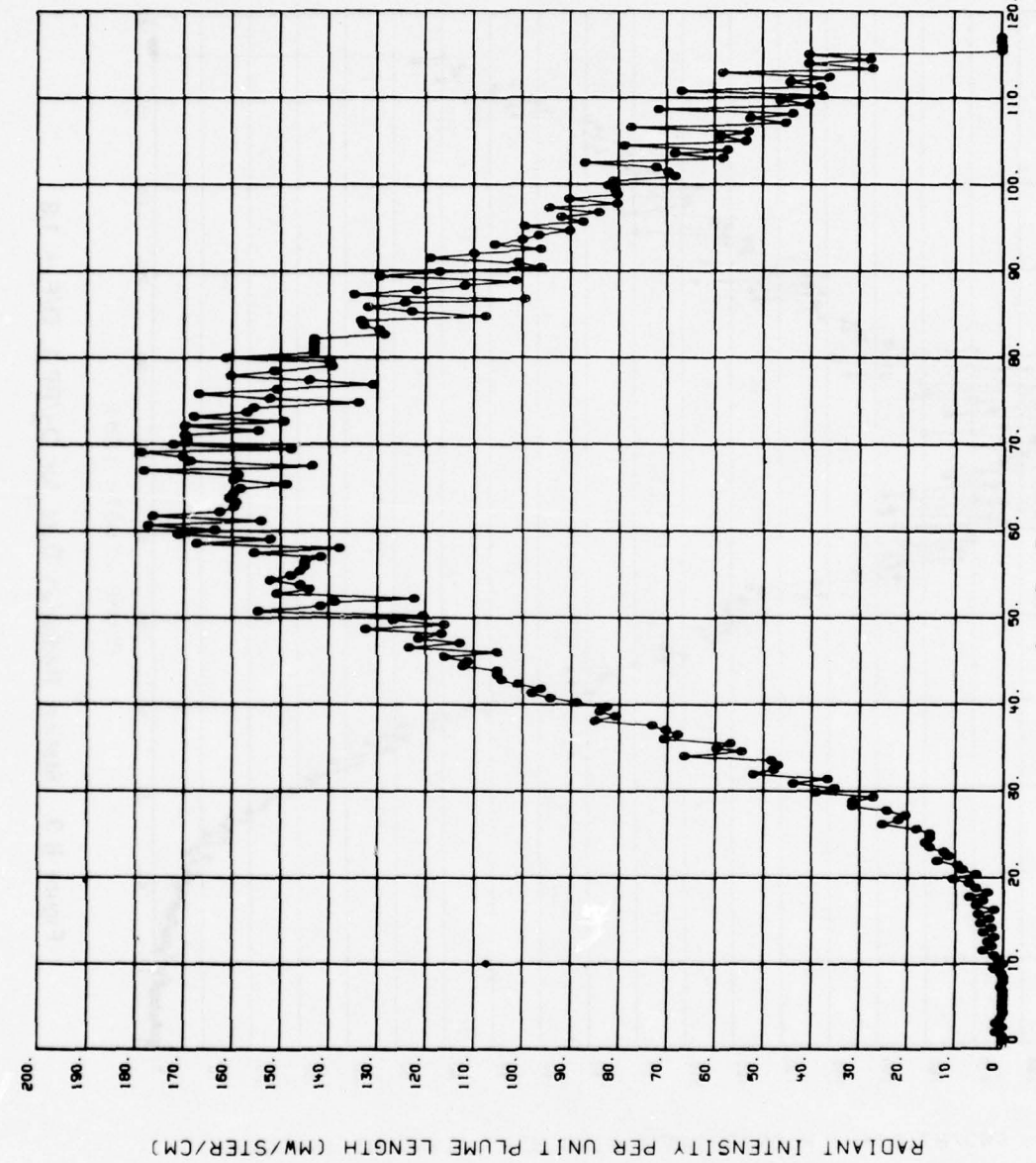

Figure B-2. Station Radiation Data for O_2/RP-1, O/F = 1.7

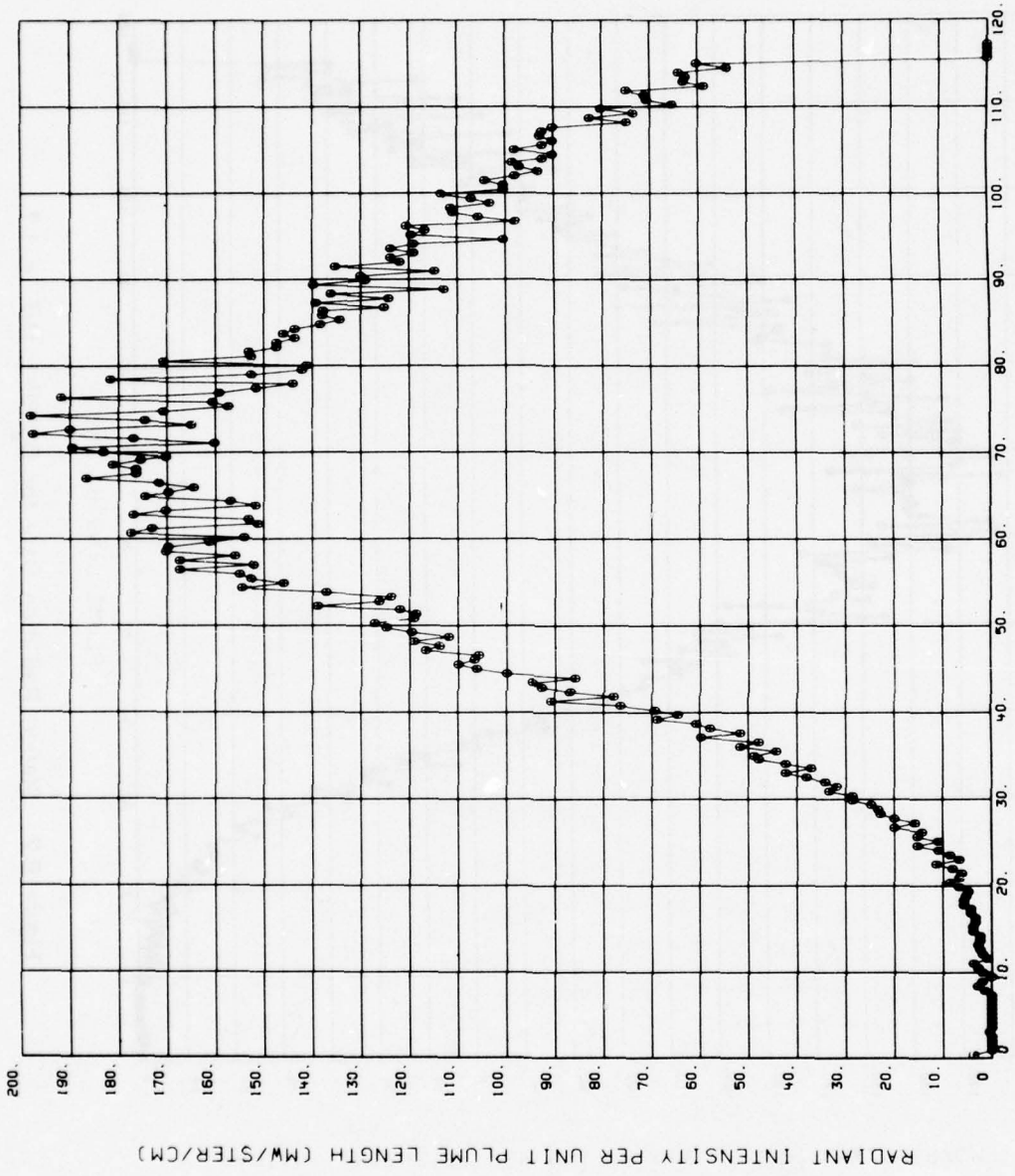

Figure B-3. Station Radiation Data for O_2/RP-1, O/F = 1.8

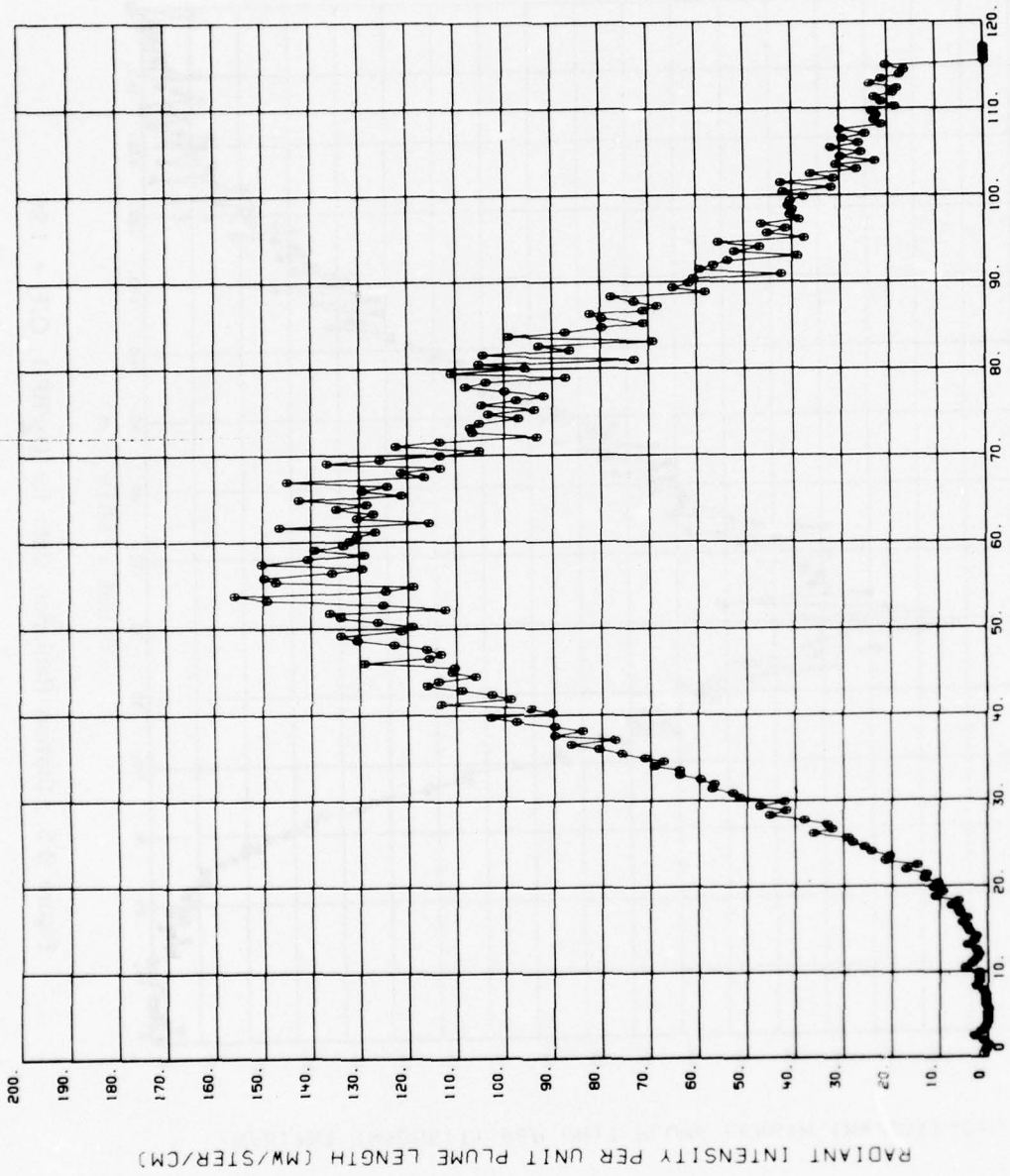

Figure B-4. Station Radiation Data for O_2/RP-1, O/F = 1.91

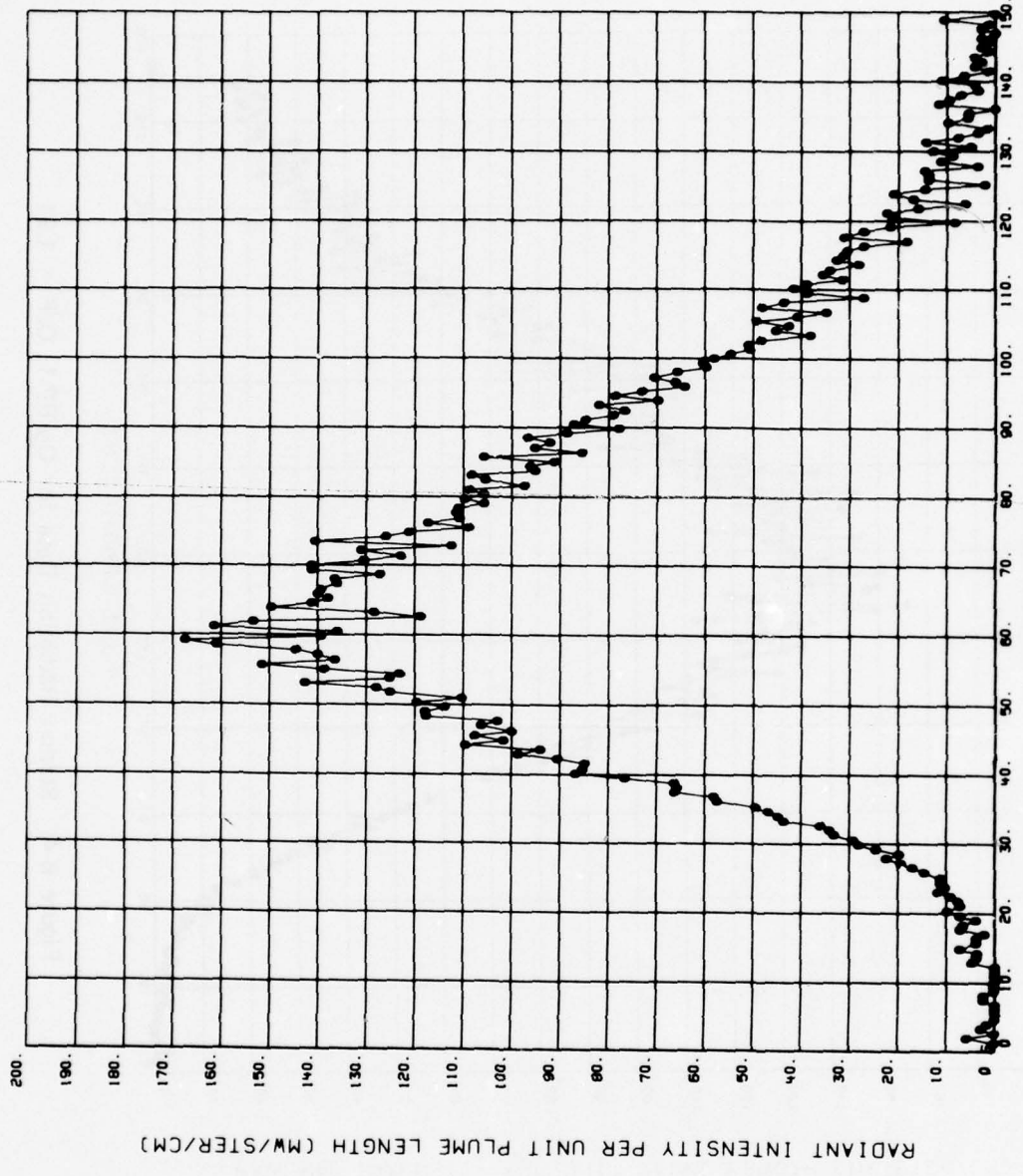

Figure B-5. Station Radiation Data for O_2/RP-1, O/F = 1.96

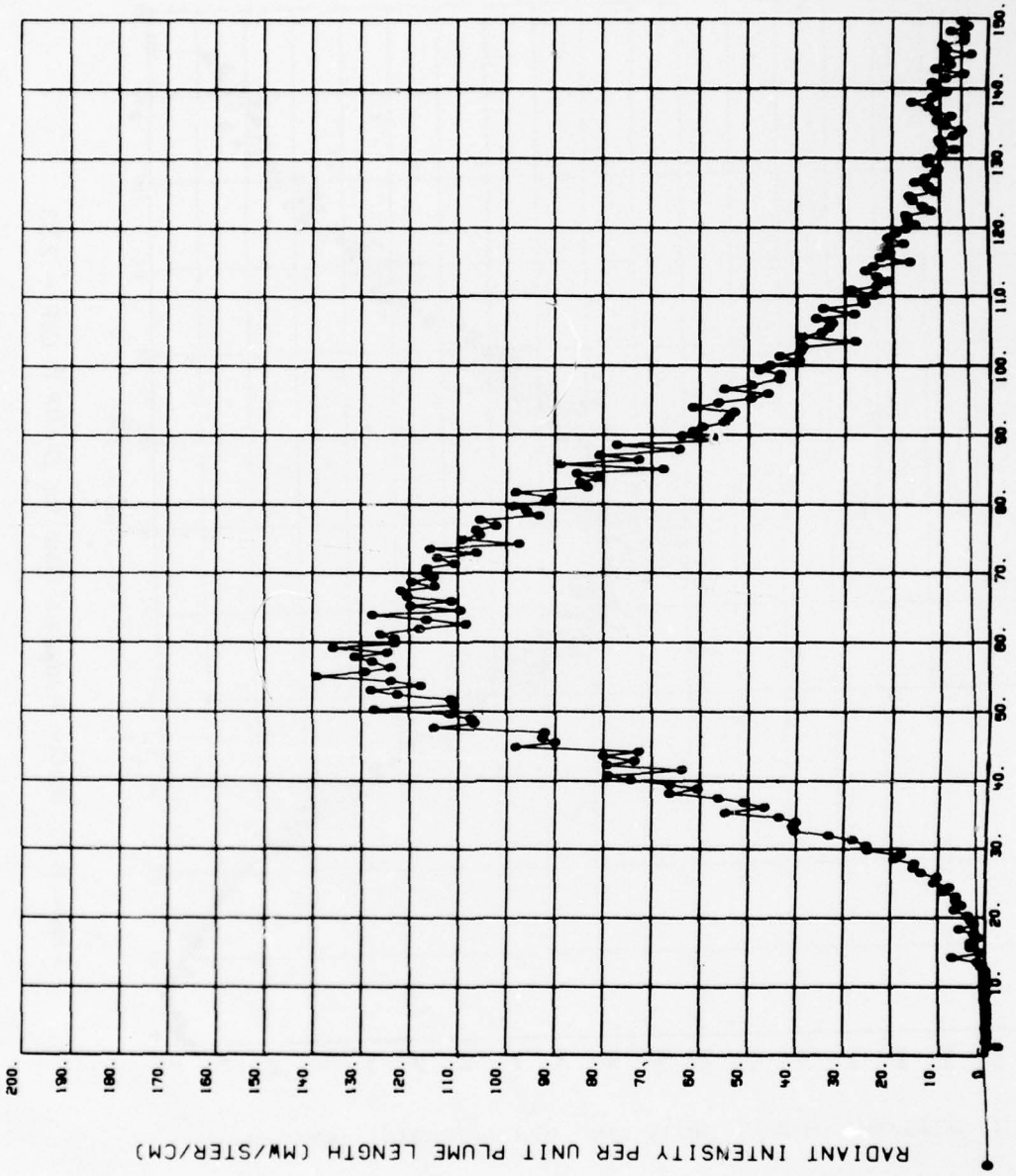

Figure B-6. Station Radiation Data for O_2/RP-1, O/F = 2.02

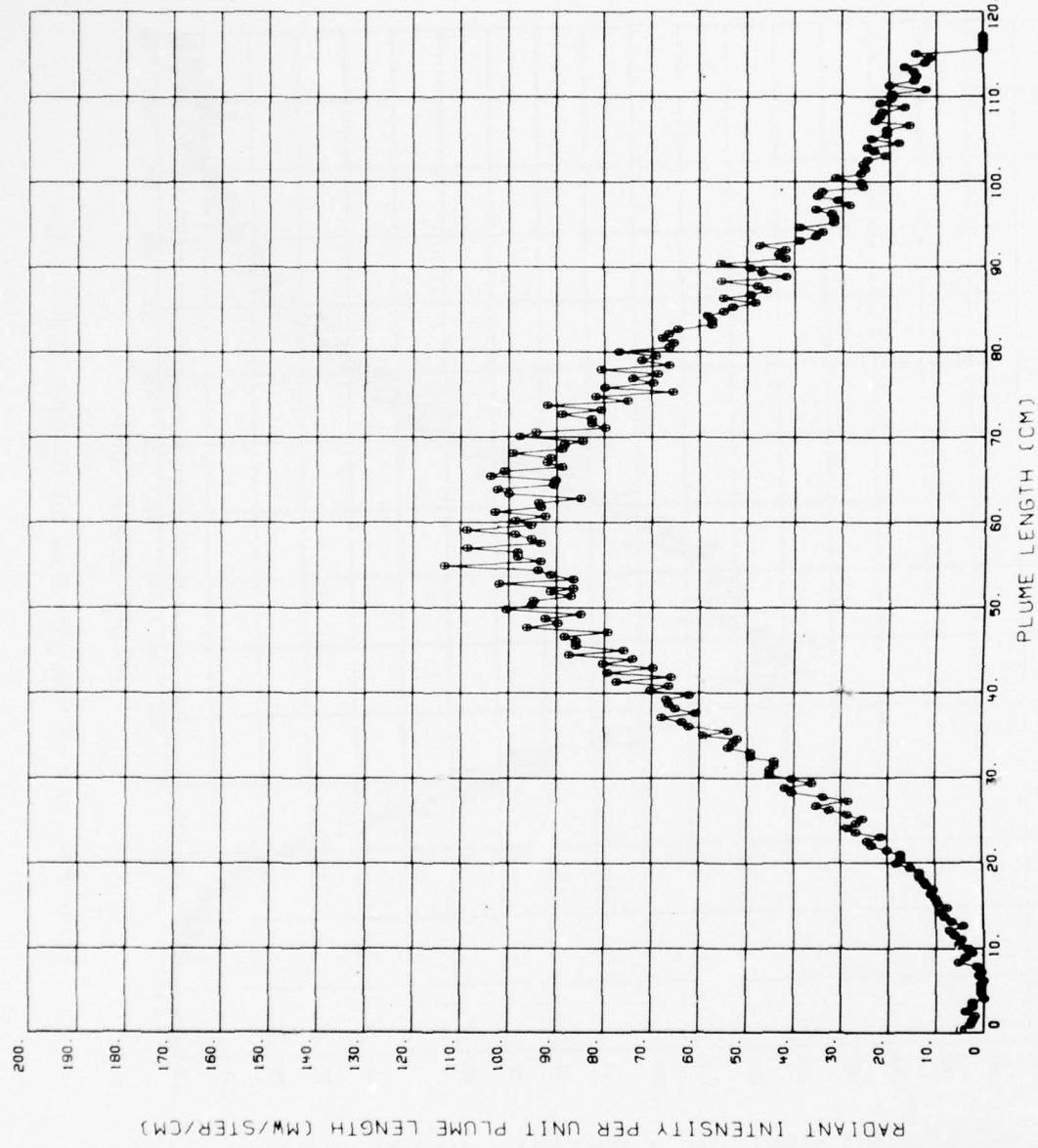

Figure B-7. Station Radiation Data for O_2/RP-1, O/F = 2.33

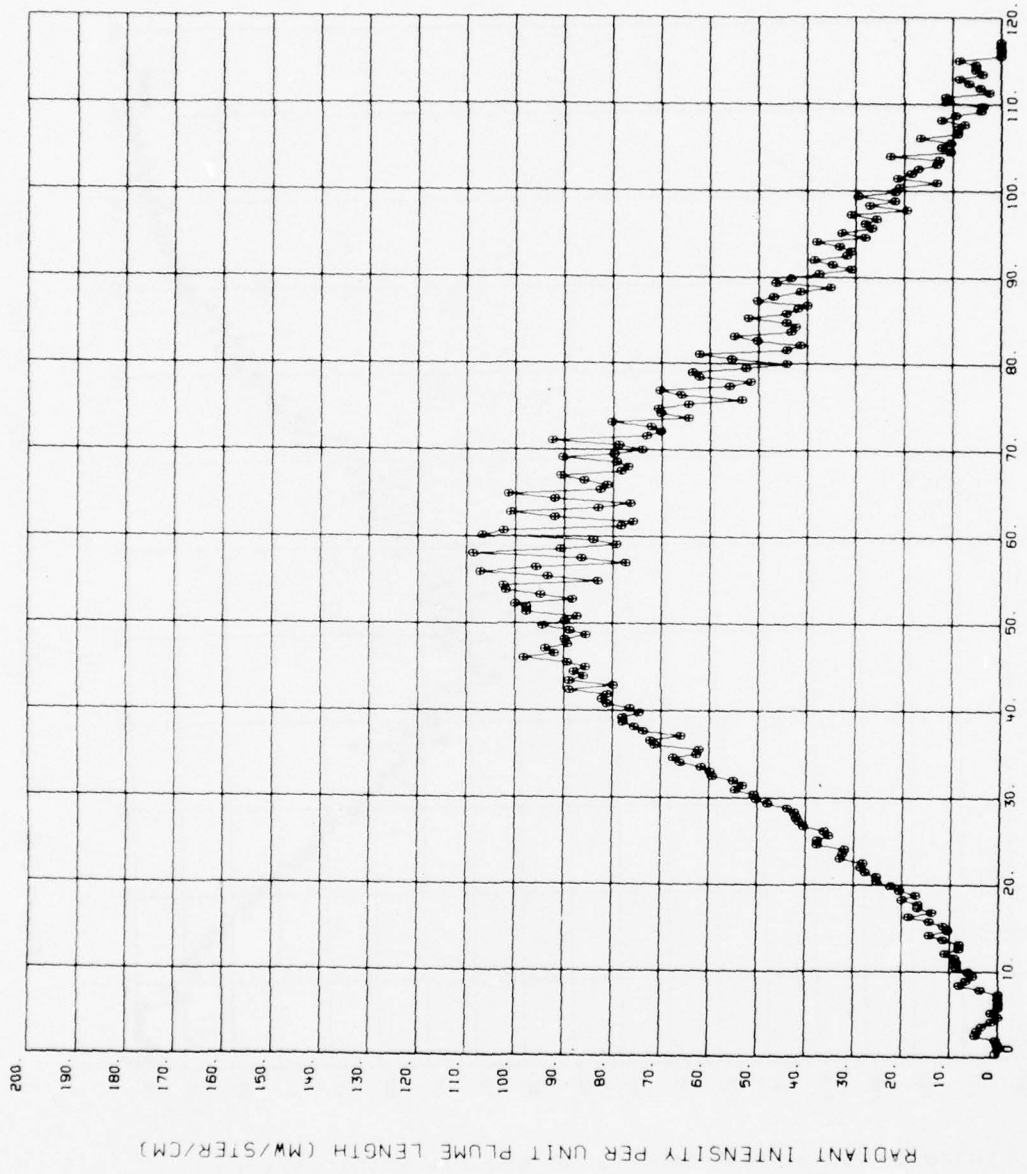

Figure B-8. Station Radiation Data for O_2/RP-1, O/F = 2.5

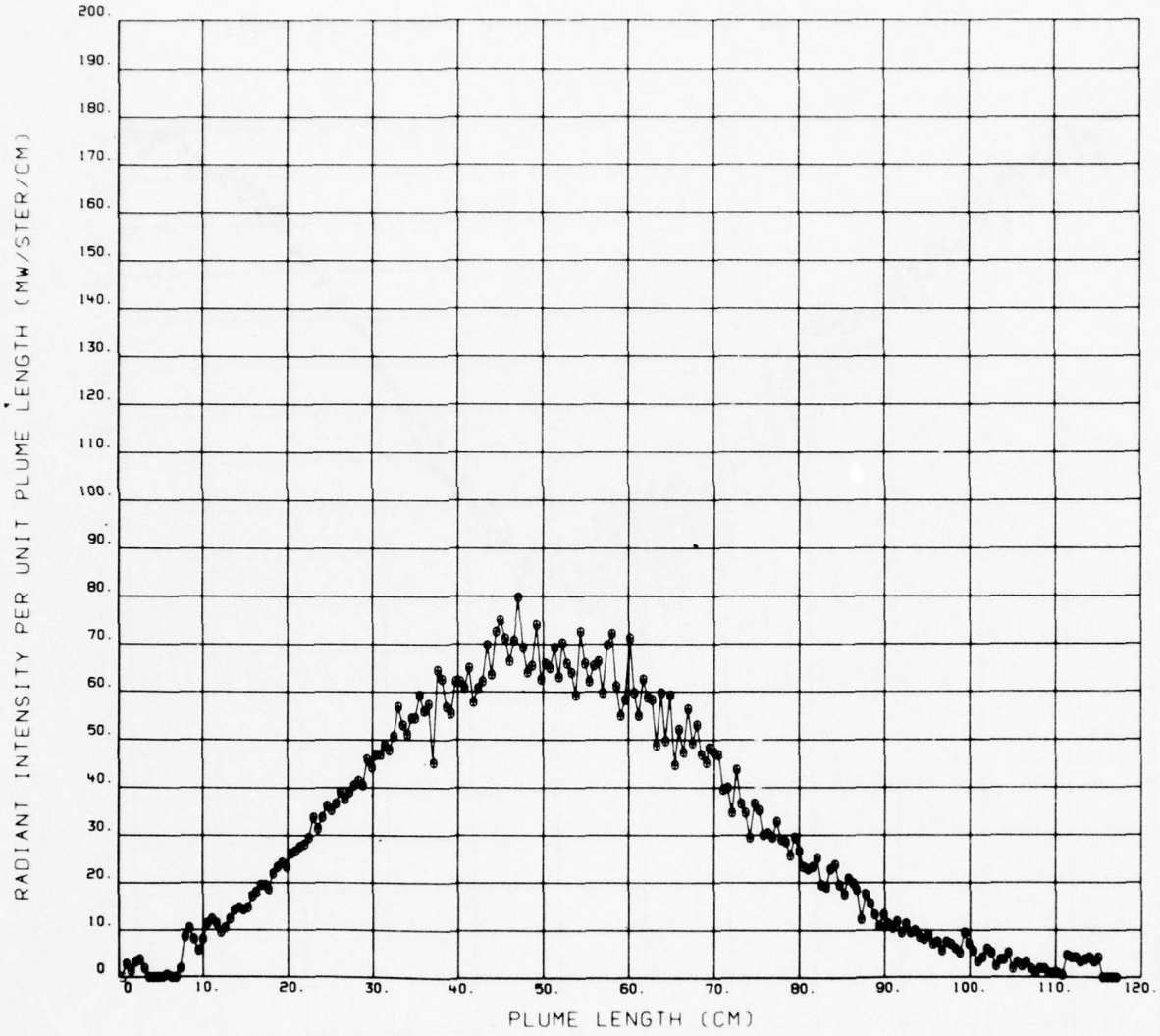

Figure B-9. Station Radiation Data for O_2/RP-1, O/F = 3.0

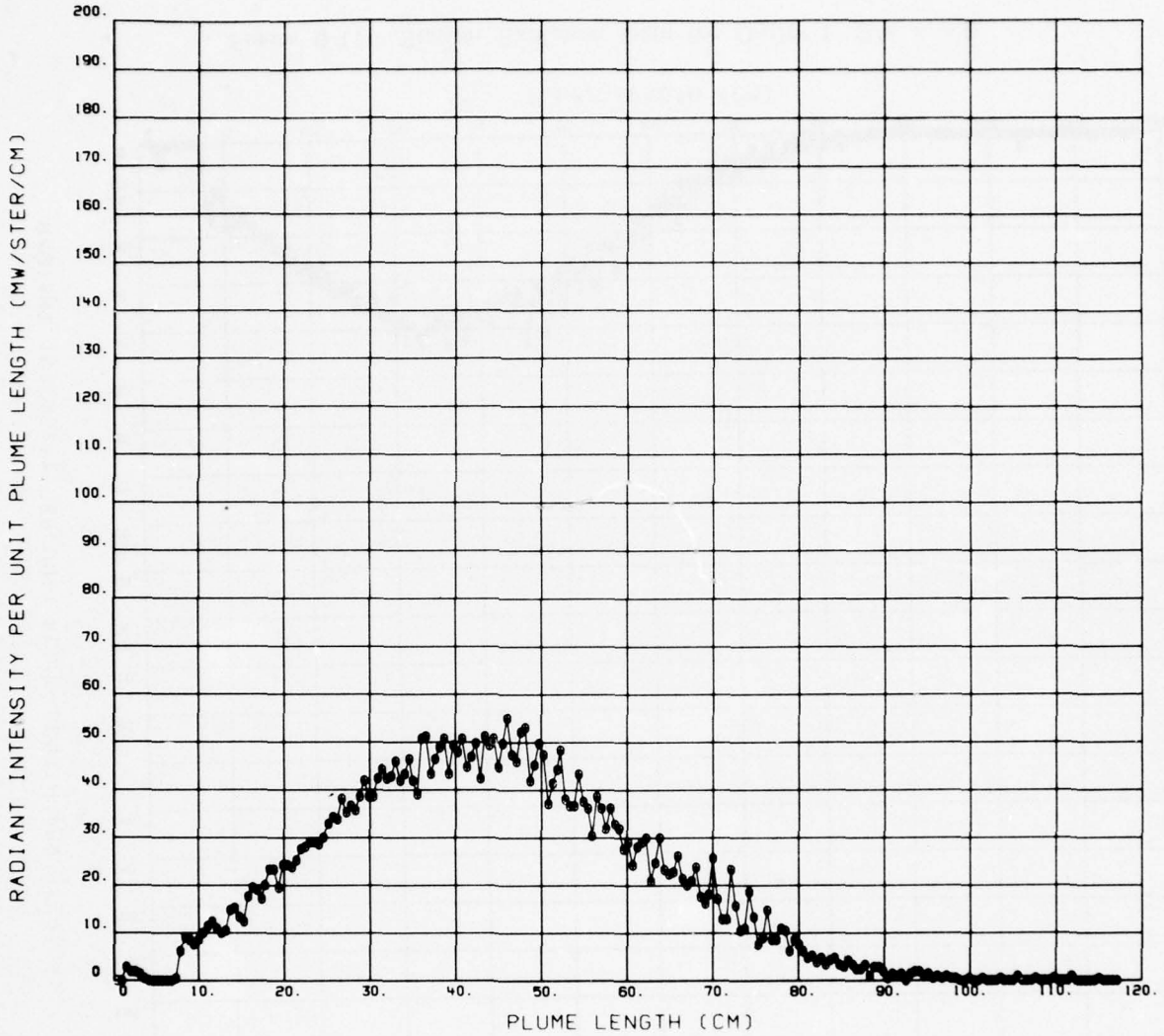

Figure B-10. Station Radiation Data for O_2/RP-1, O/F = 3.5

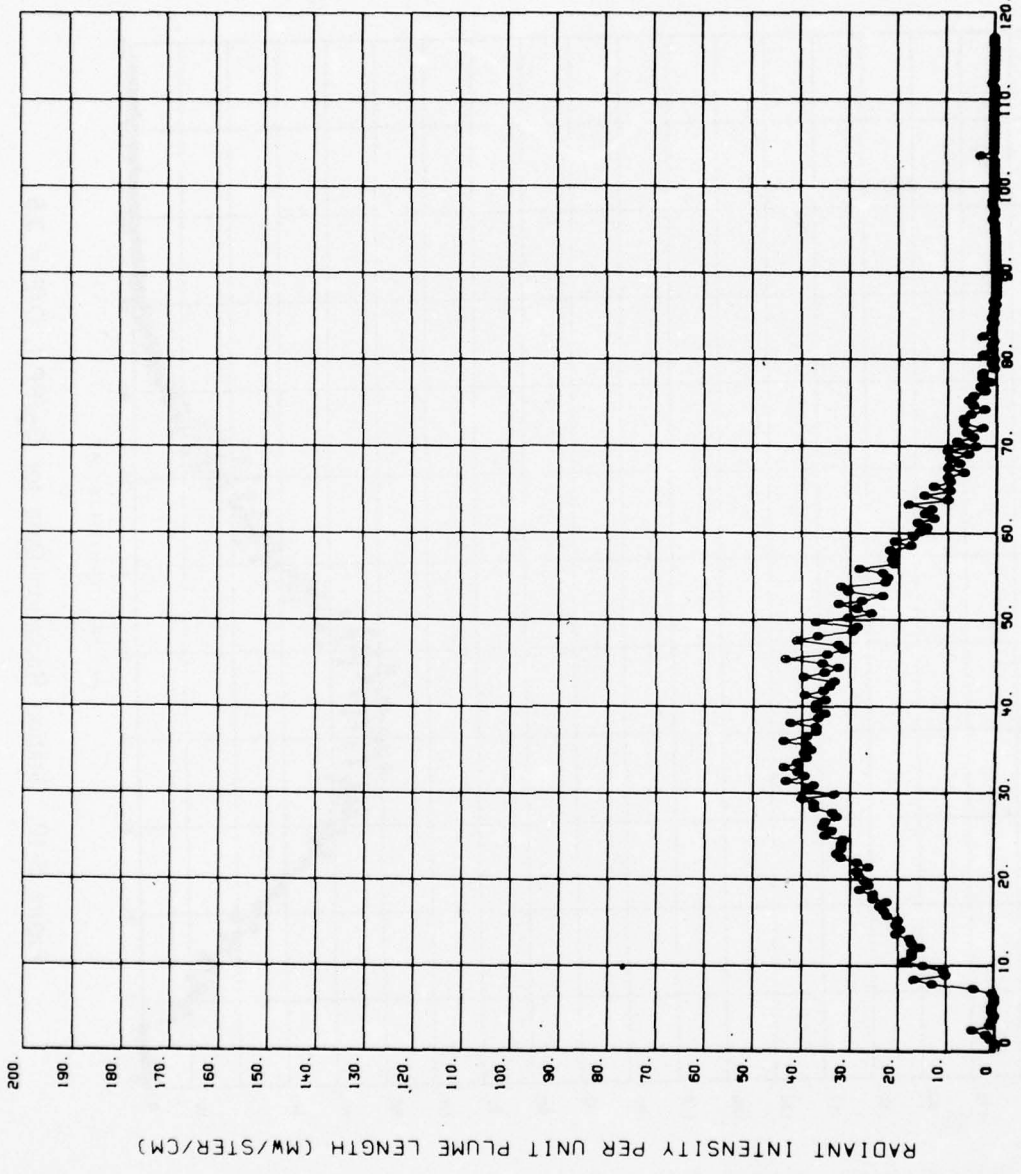

Figure B-11. Station Radiation Data for O_2/RP-1, O/F = 4.0

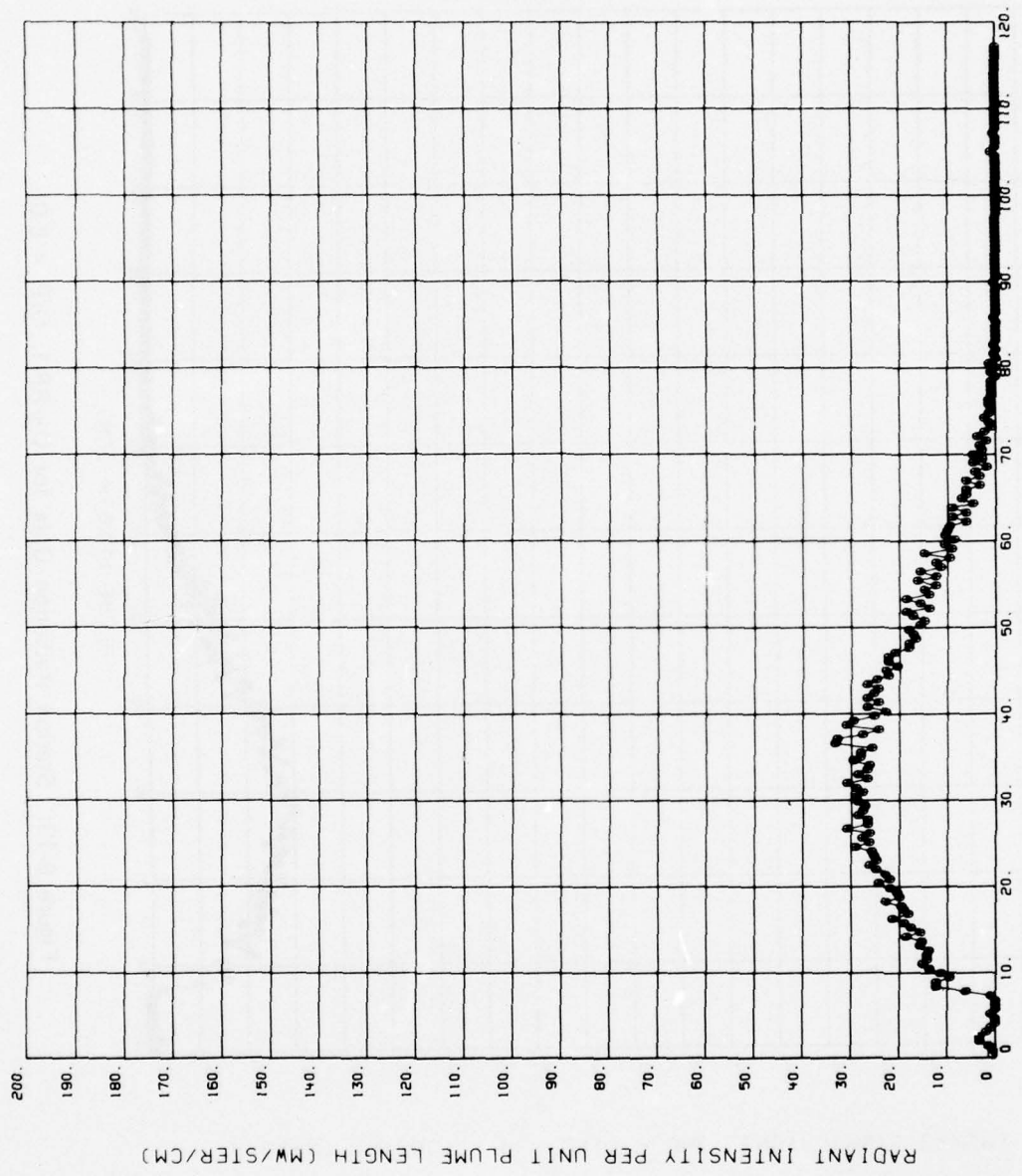

Figure B-12. Station Radiation Data for O_2/RP-1, O/F = 4.5

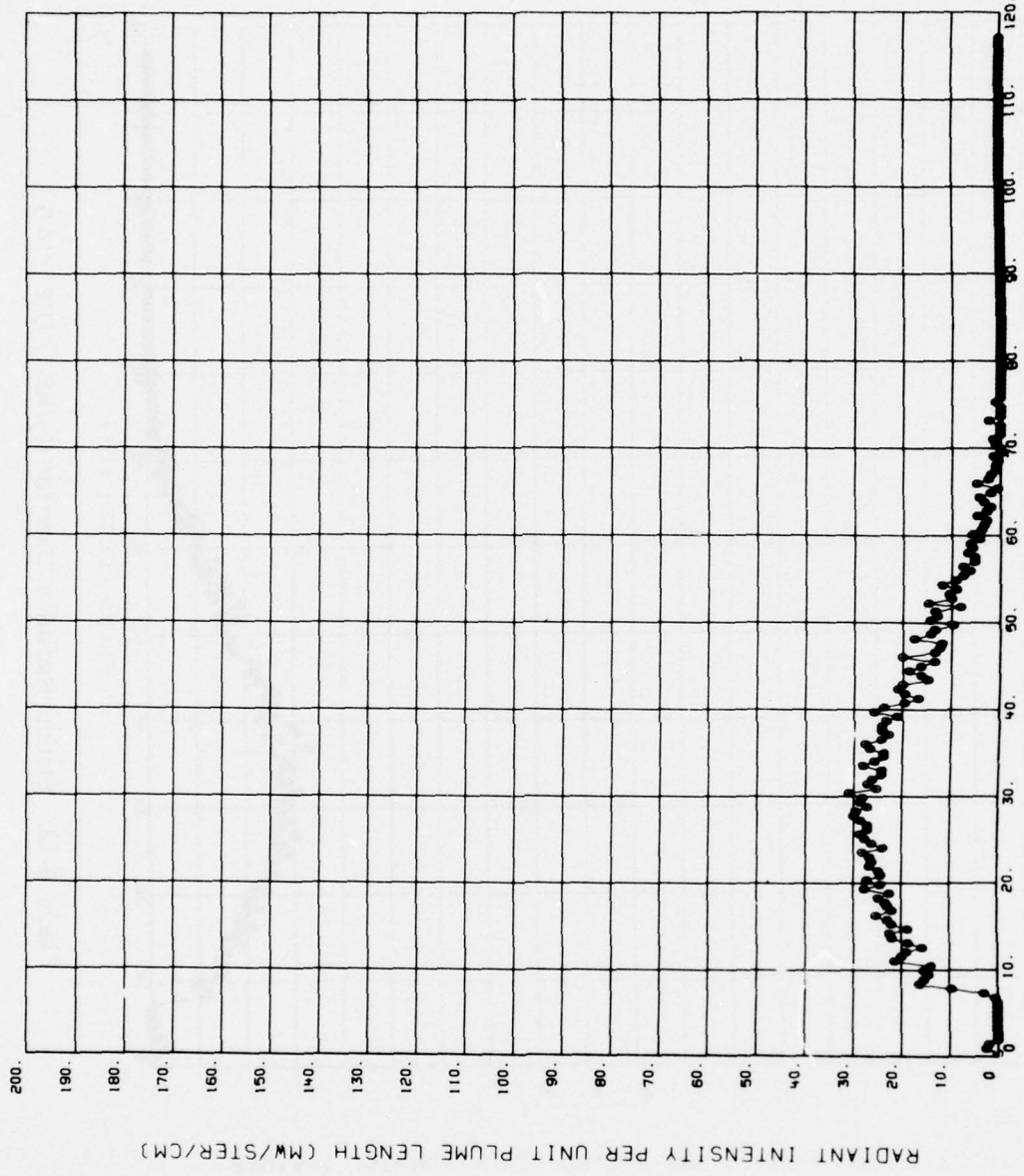

Figure B-13. Station Radiation Data for O_2/RP-1, O/F = 5.0

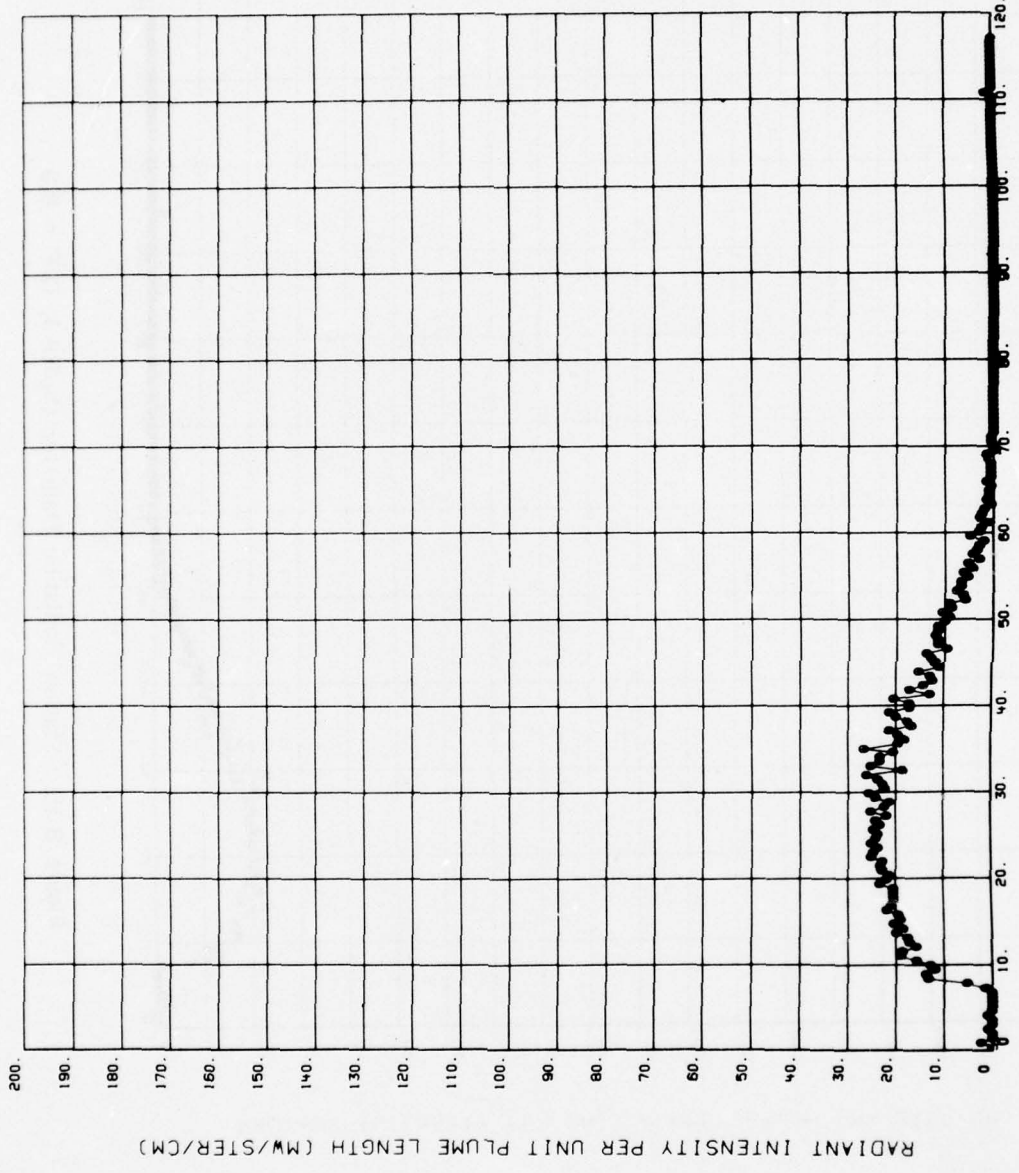

Figure B-14. Station Radiation Data for O_2/RP-1, O/F = 5.5

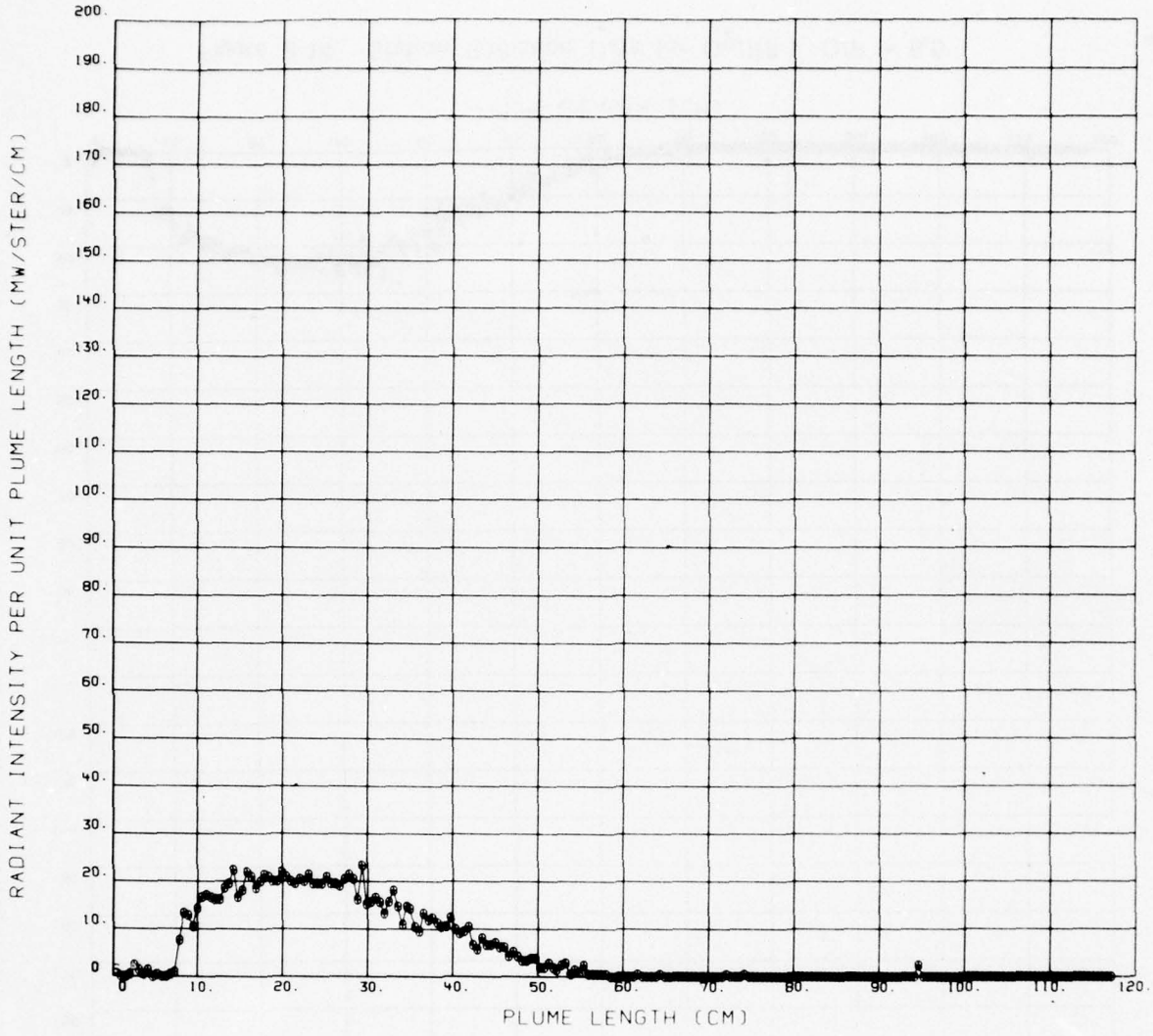

Figure B-15. Station Radiation Data for O_2/RP-1, O/F = 6.0

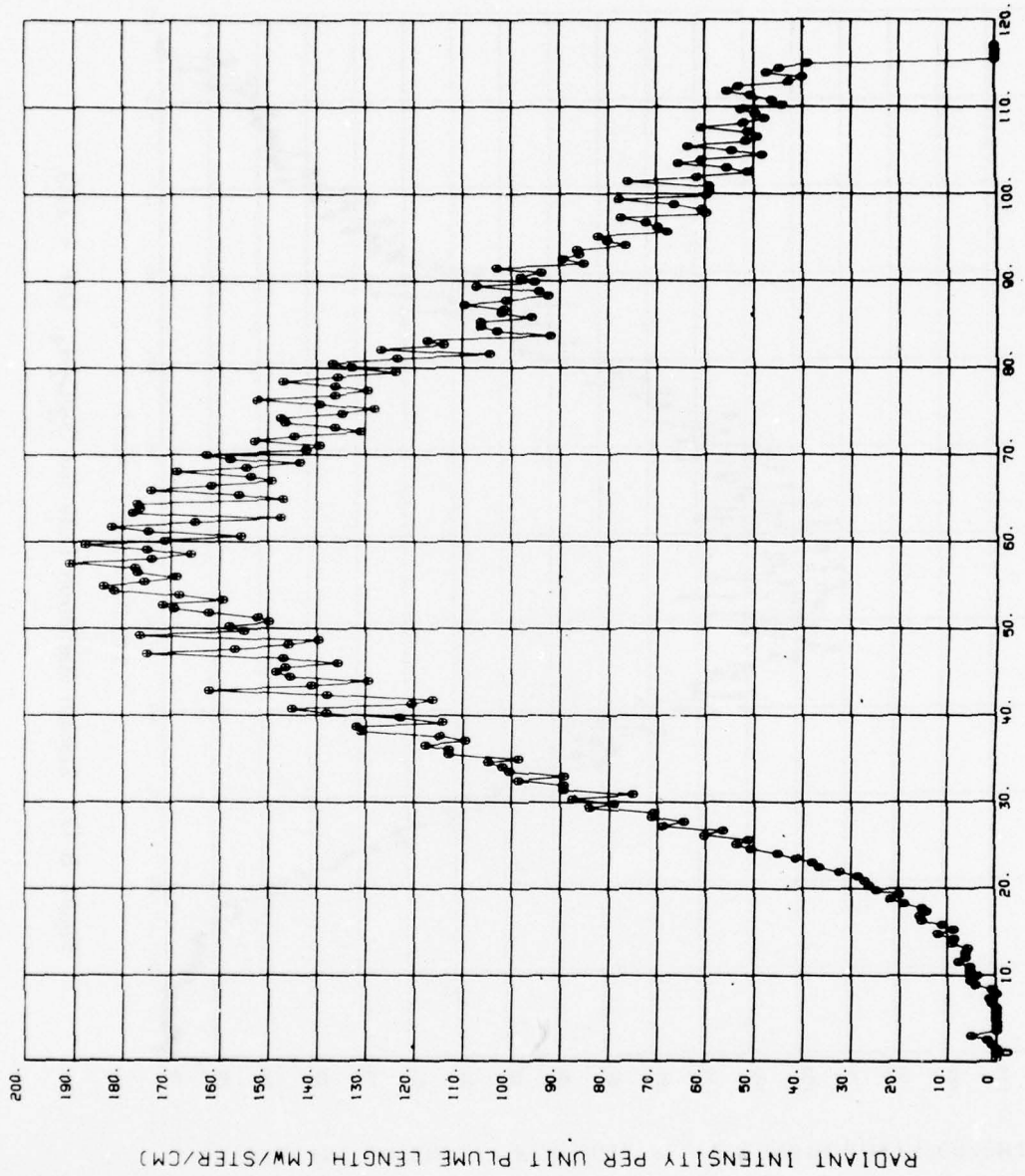

Figure B-16. Station Radiation Data for O_2/C_2H_4, O/F = 2.0

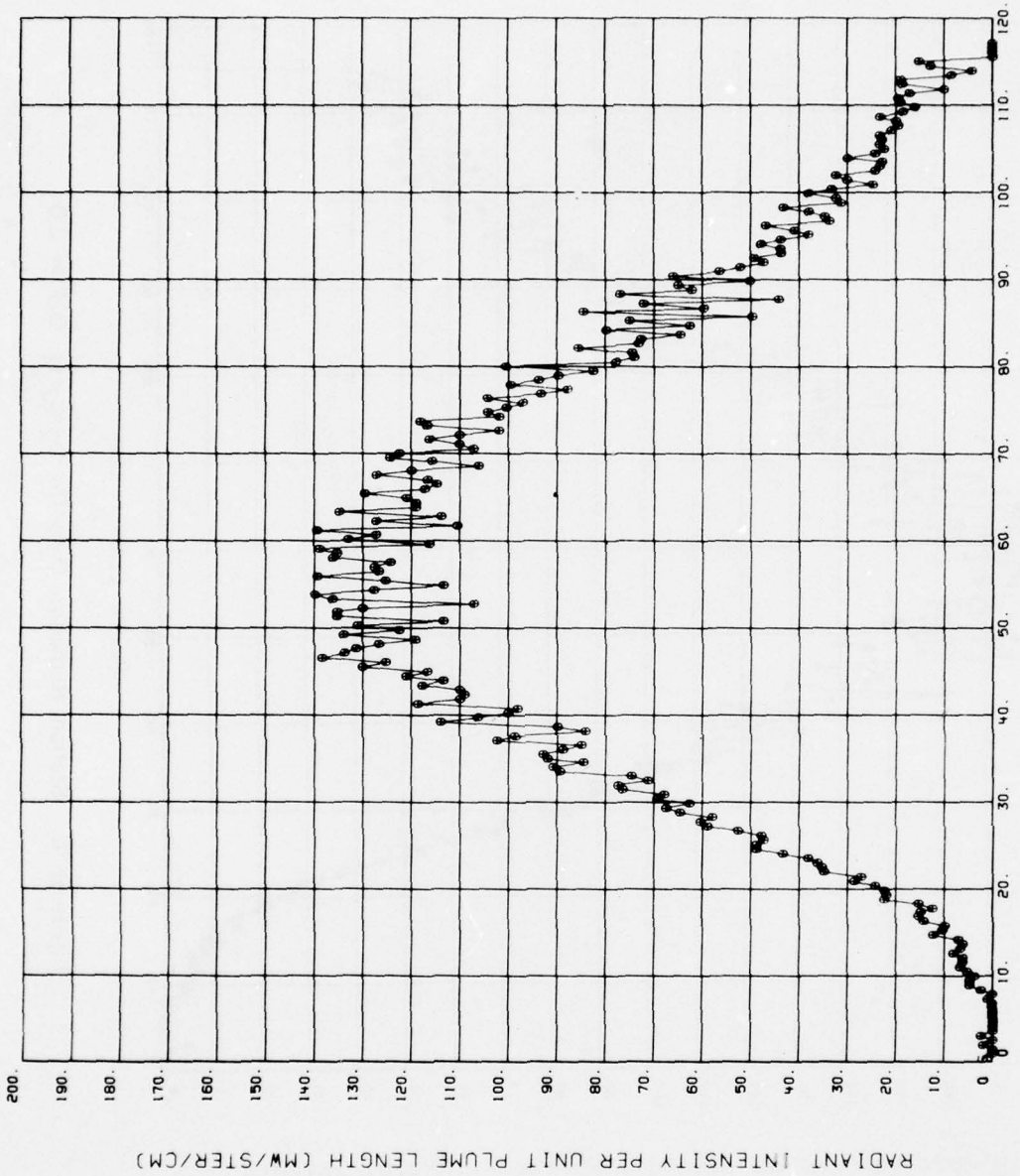

Figure B-17. Station Radiation Data for O_2/C_2H_4, O/F = 2.33

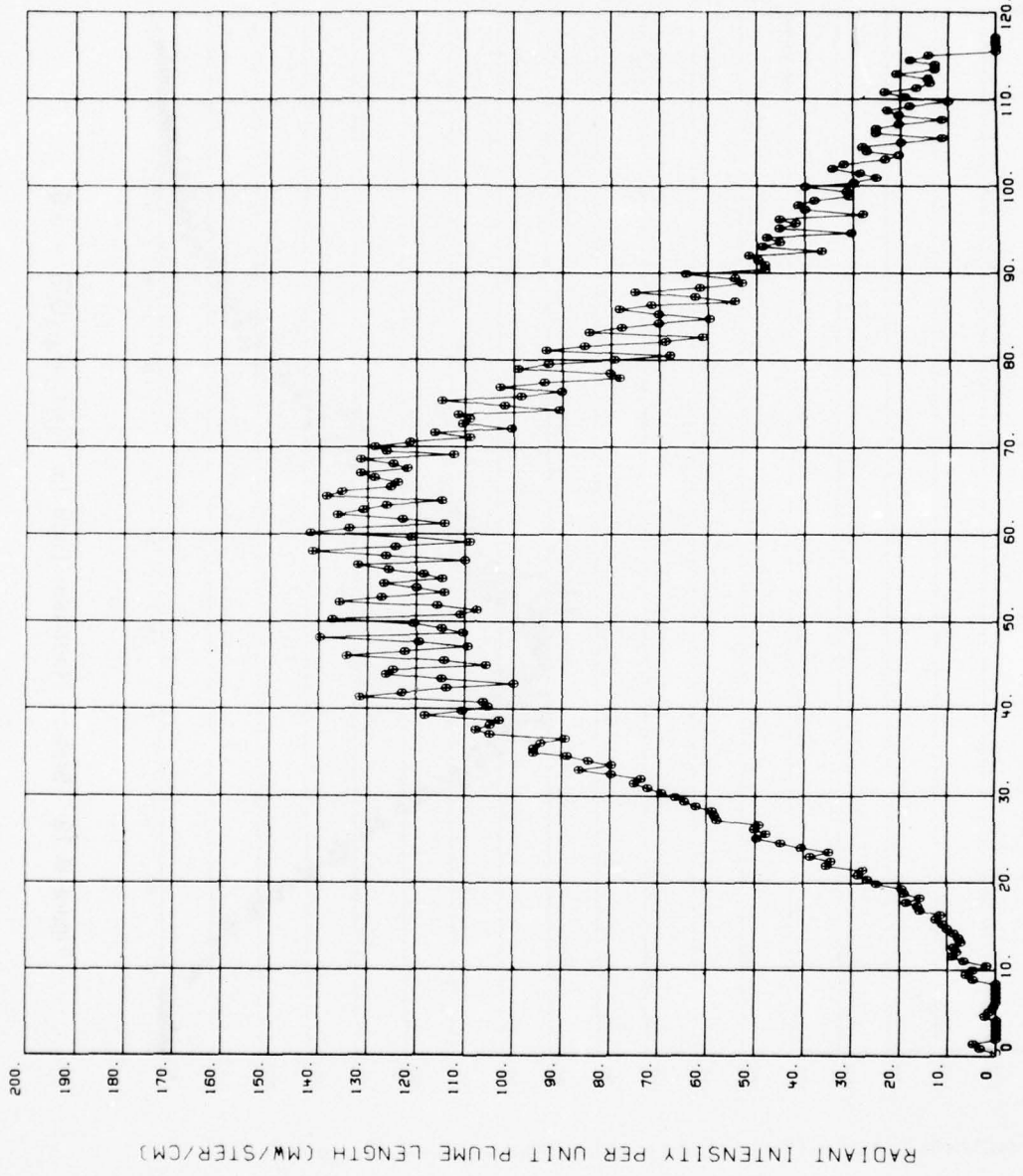

Figure B-18. Station Radiation Data for O_2/C_2H_4, O/F = 2.5

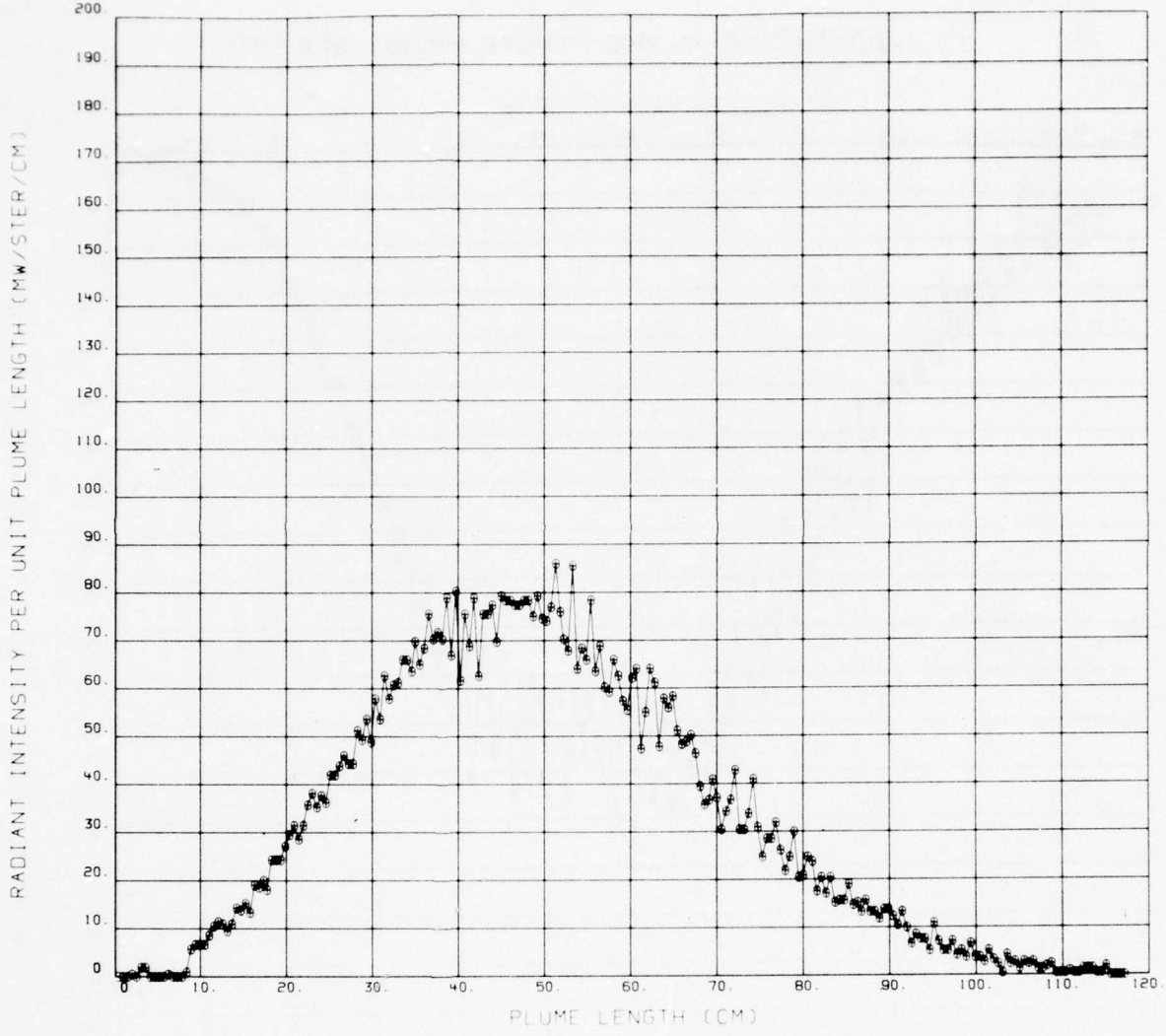

Figure B-19. Station Radiation Data for O_2/C_2H_4, O/F = 3.0

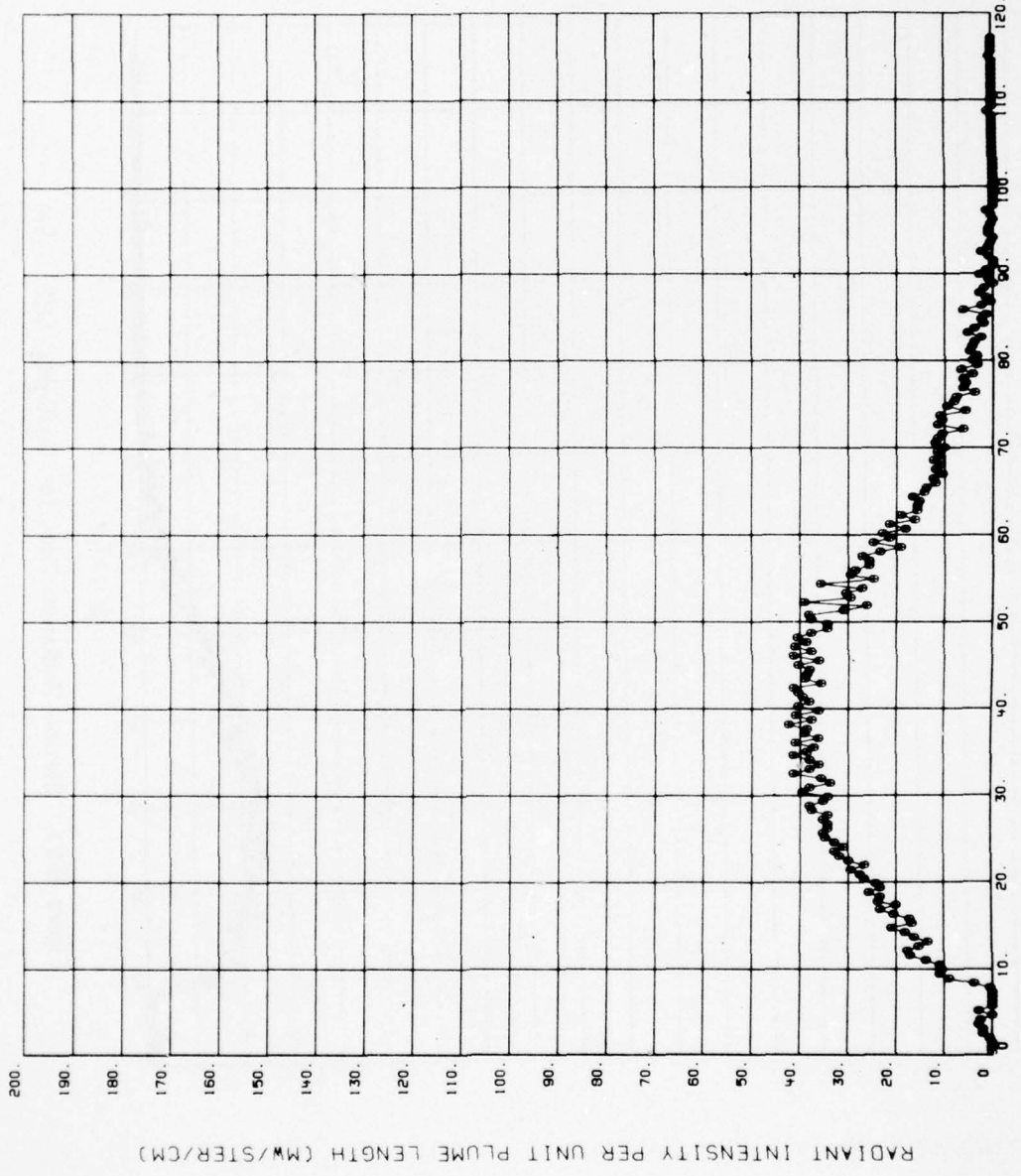

Figure B-20. Station Radiation Data for O_2/C_2H_4, O/F = 4.0

AD-A037 252 AIR FORCE ARMAMENT LAB EGLIN AFB FLA F/G 17/5
EXPERIMENTAL RESULTS FOR HYDROCARBON EXHAUST INFRARED MODEL VER--ETC(U)
JUL 76 W J ROTHSCHILD, C W MARTIN
AFATL-TR-76-74

UNCLASSIFIED NL

2 OF 2
AD A037252

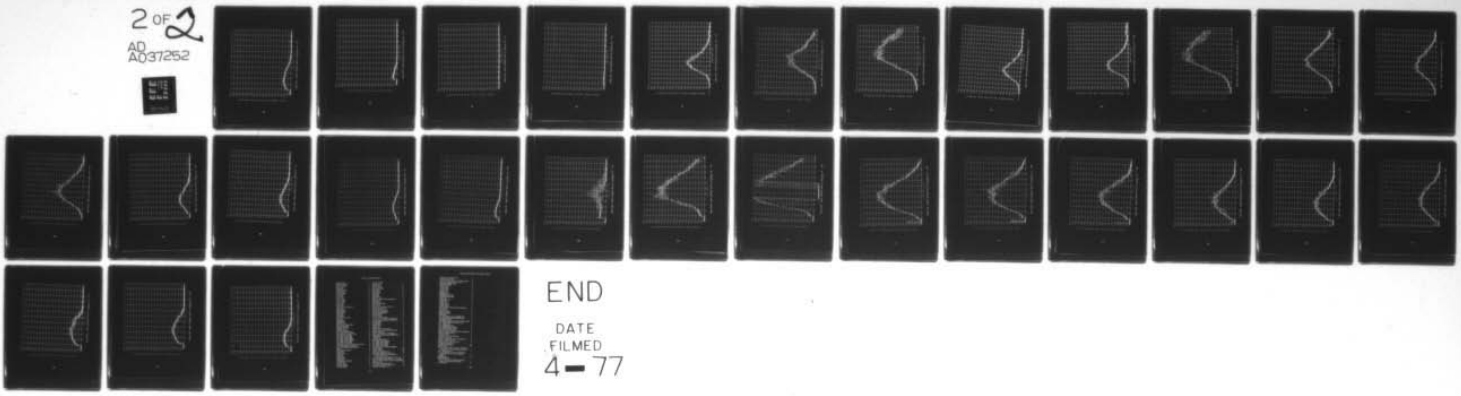

END

DATE FILMED
4-77

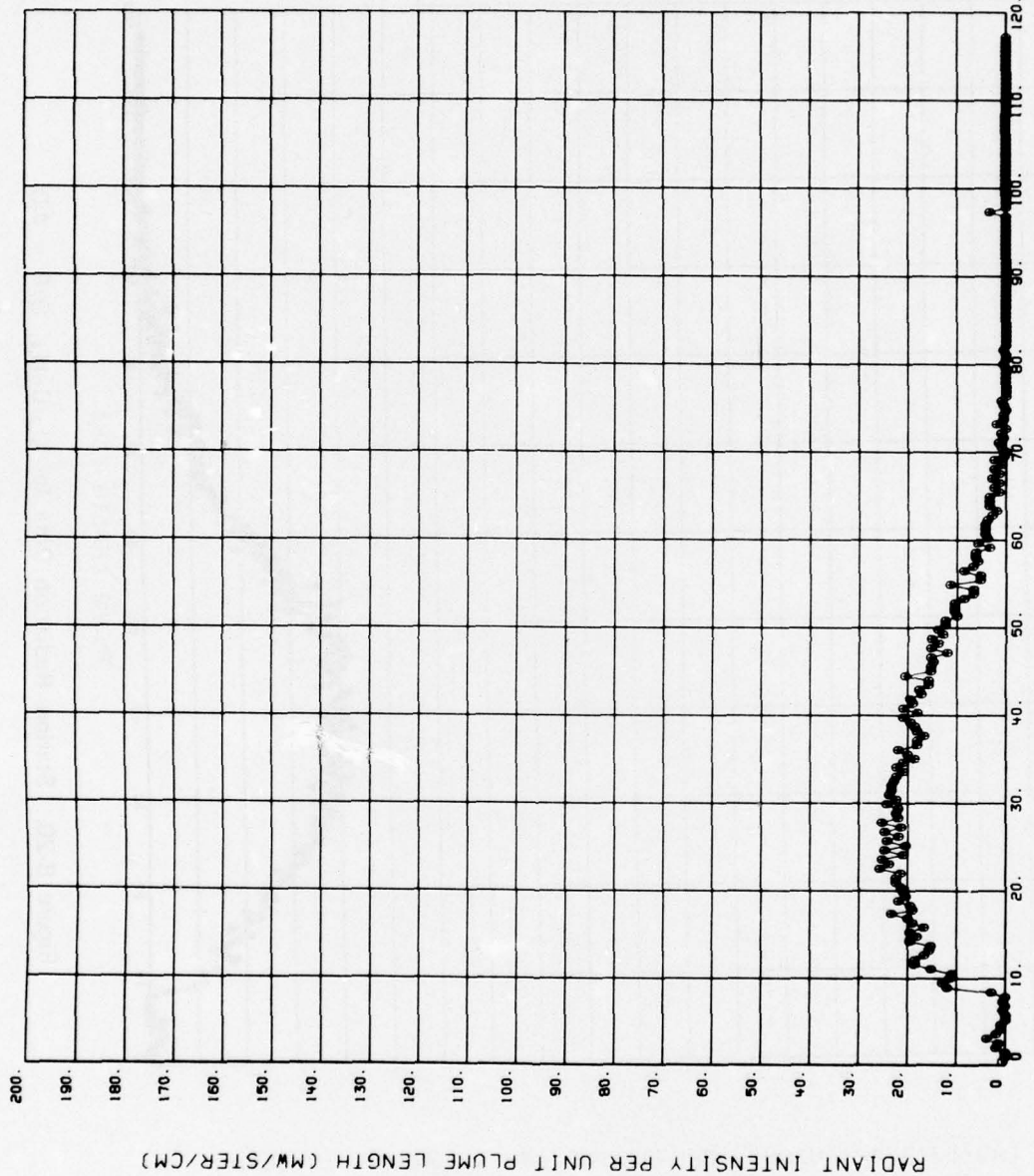

Figure B-21. Station Radiation Data for O_2/C_2H_4, O/F = 5.0

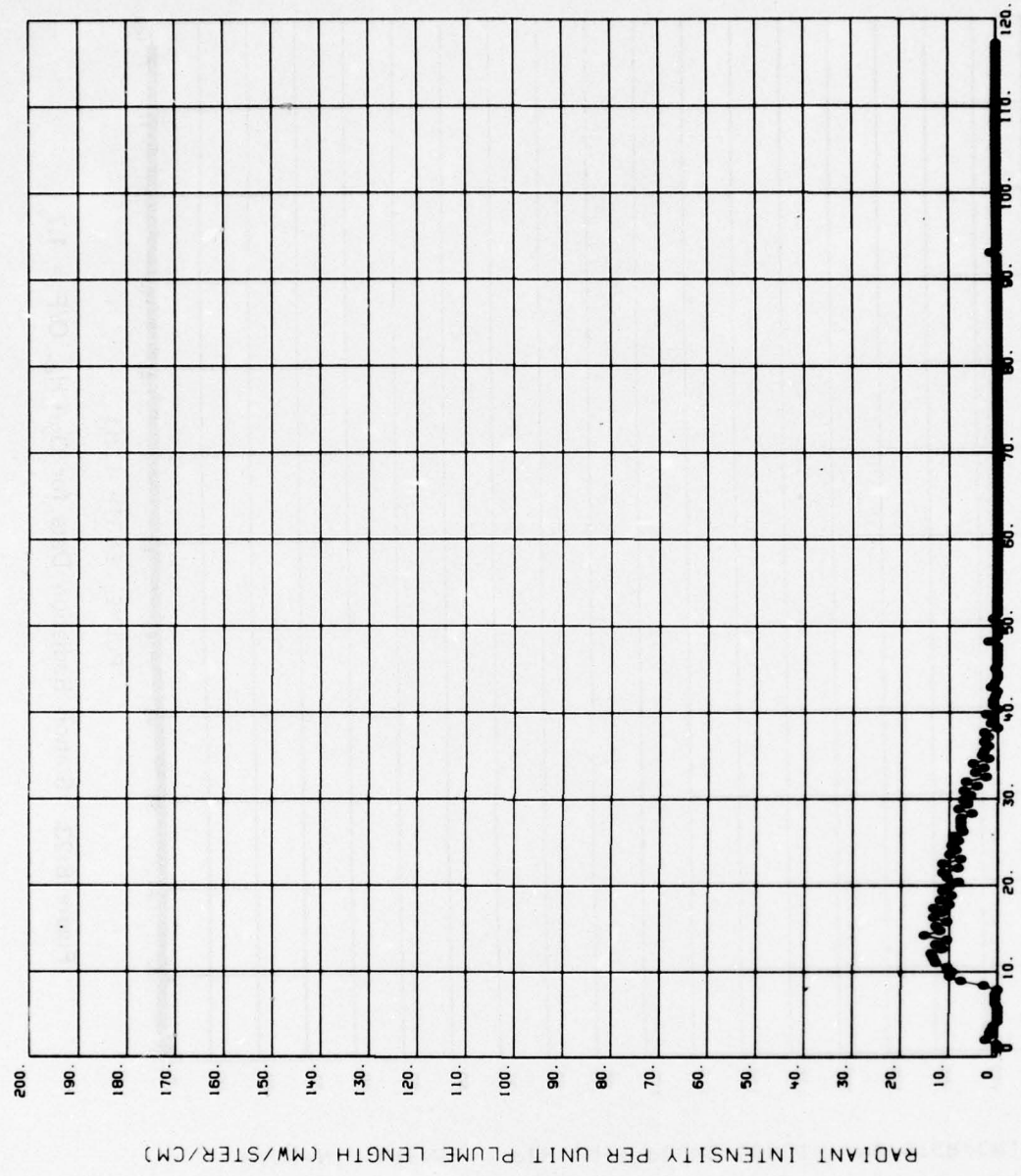

Figure B-22. Station Radiation Data for O_2/C_2H_4, O/F = 6.0

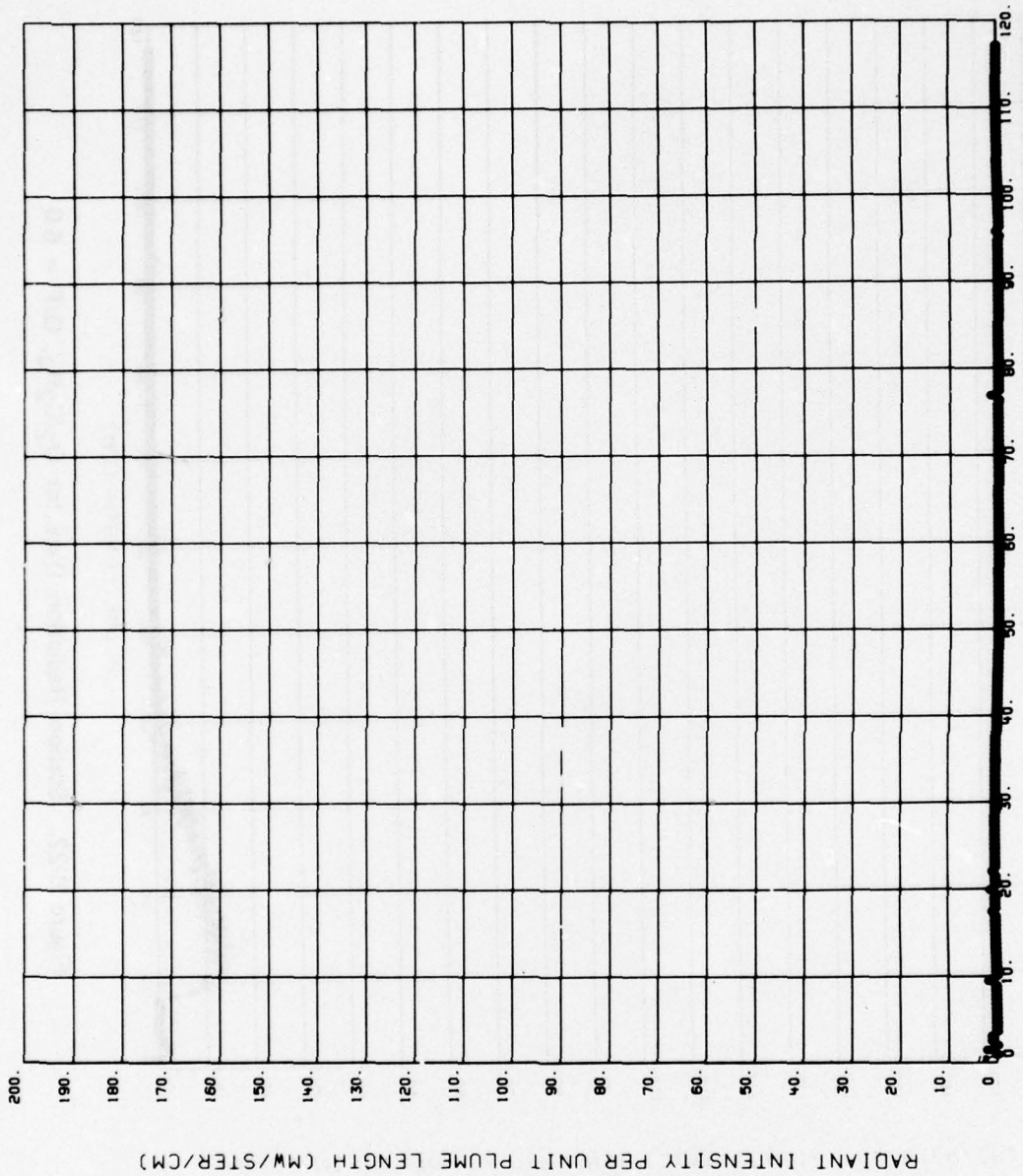

Figure B-23. Station Radiation Data for O_2/CH_4, O/F = 1.7

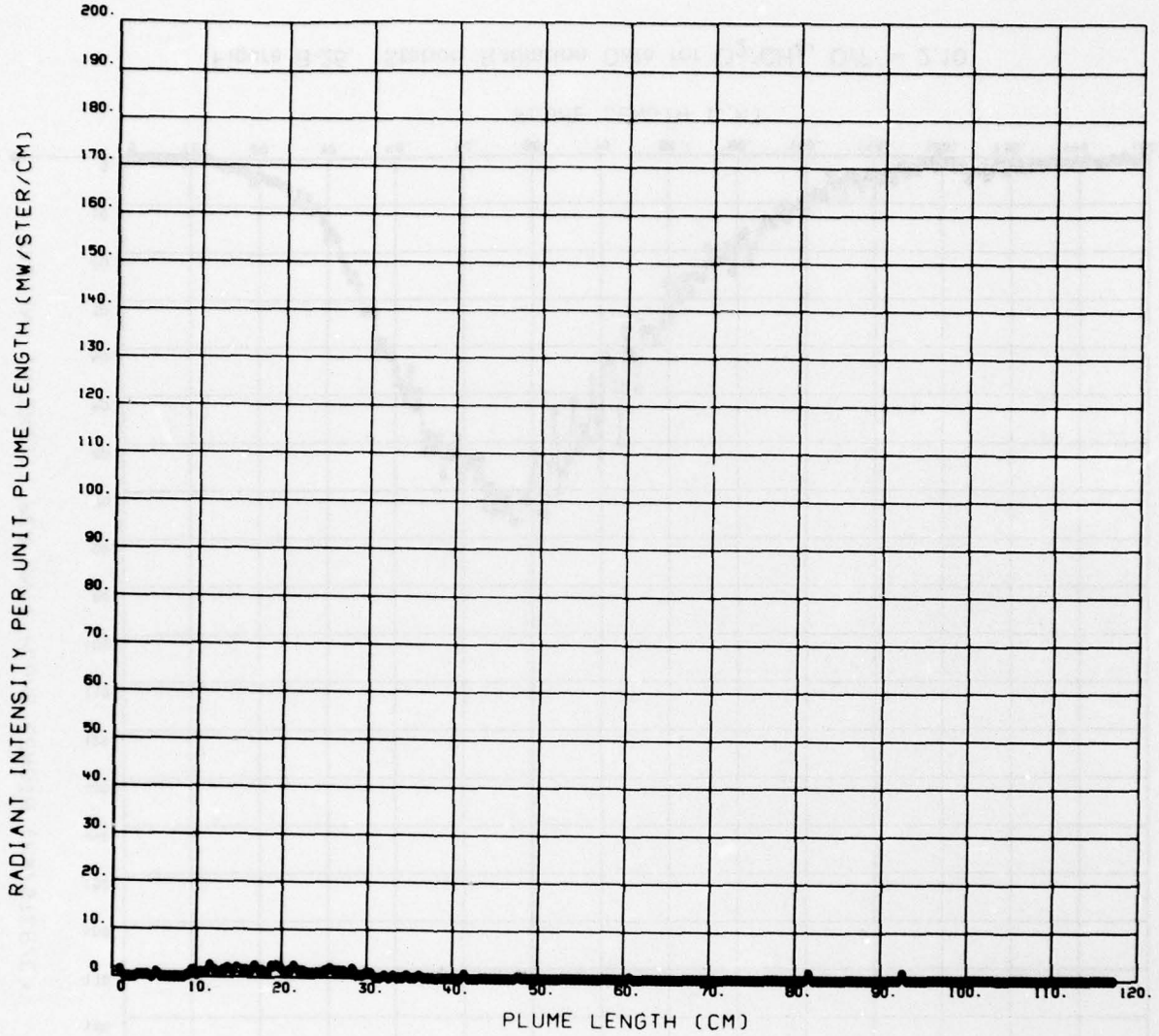

Figure B-24. Station Radiation Data for O_2/CH_4, O/F = 2.0

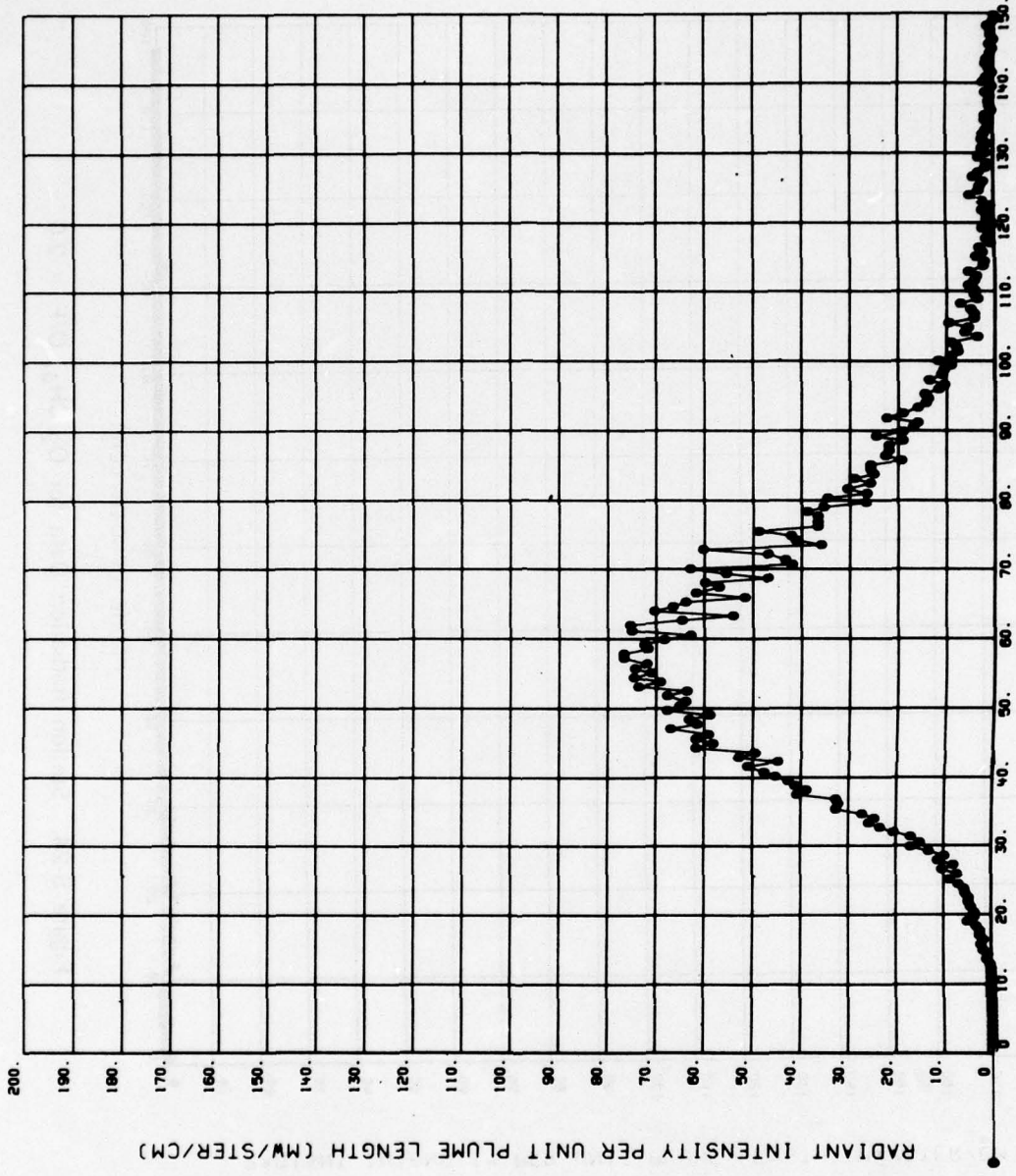

Figure B-25. Station Radiation Data for O_2/CH_4, O/F = 2.10

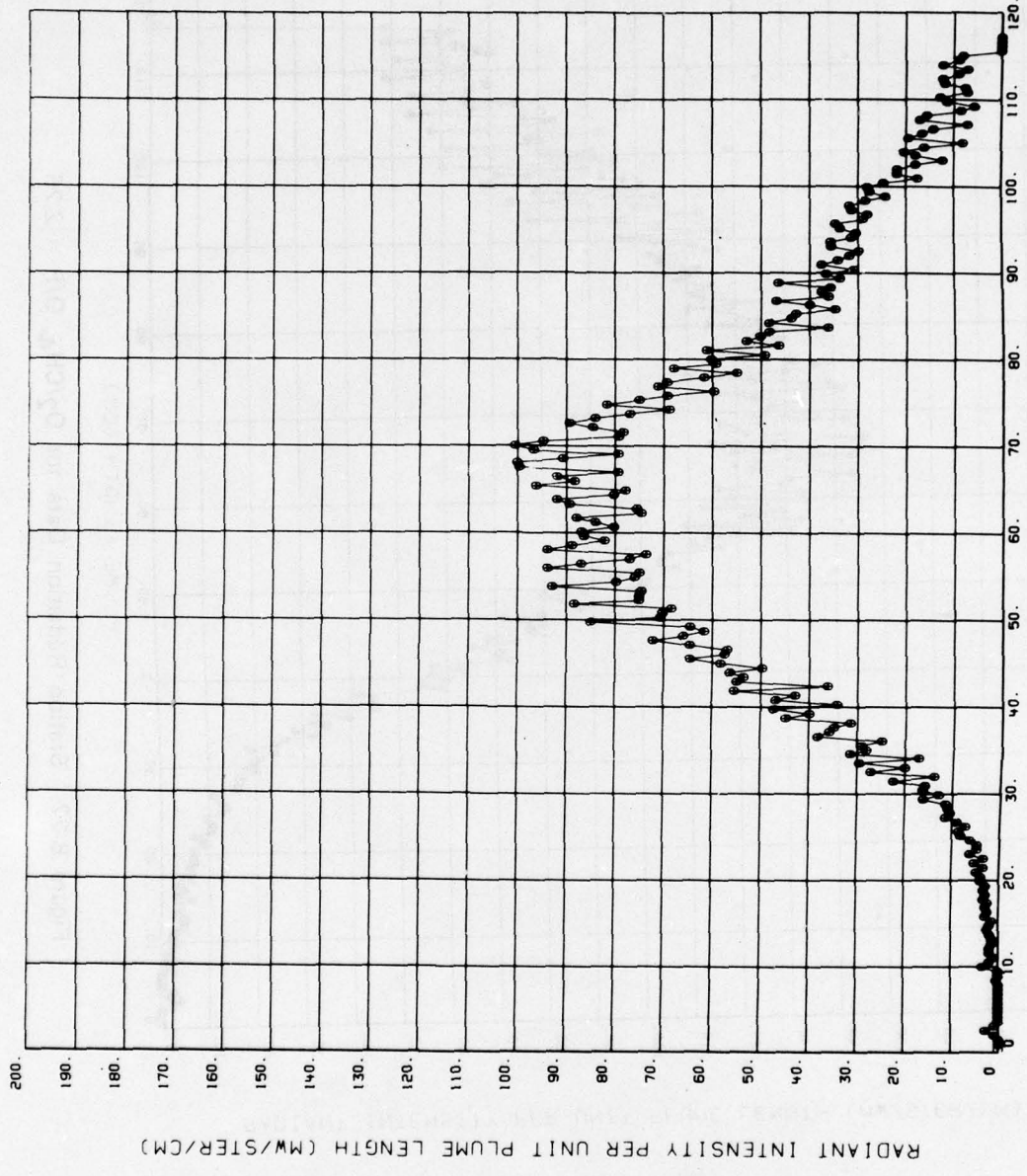

Figure B-26. Station Radiation Data for O_2/CH_4, O/F = 2.2

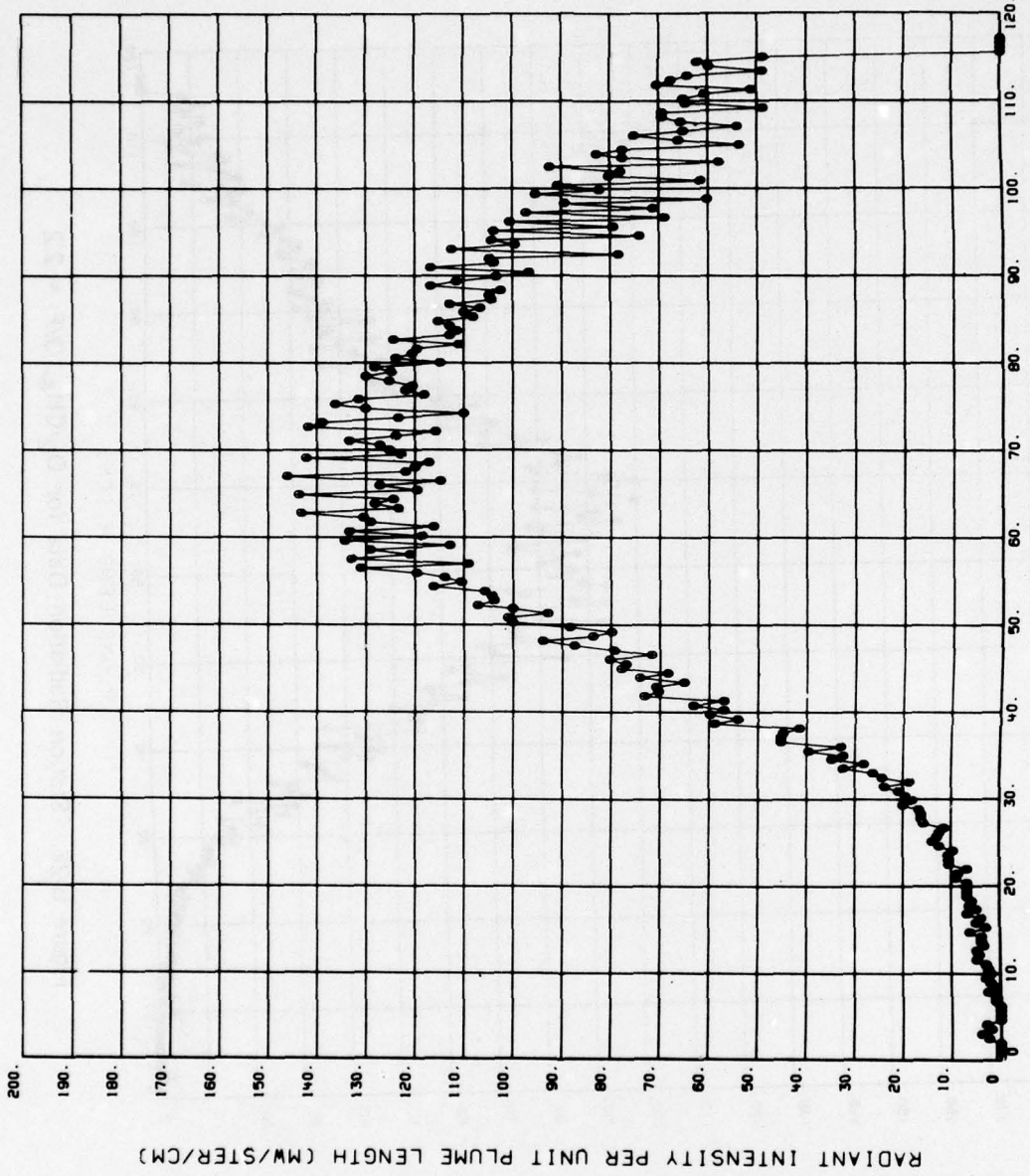

Figure B-27. Station Radiation Data for O_2/CH_4, O/F = 2.26

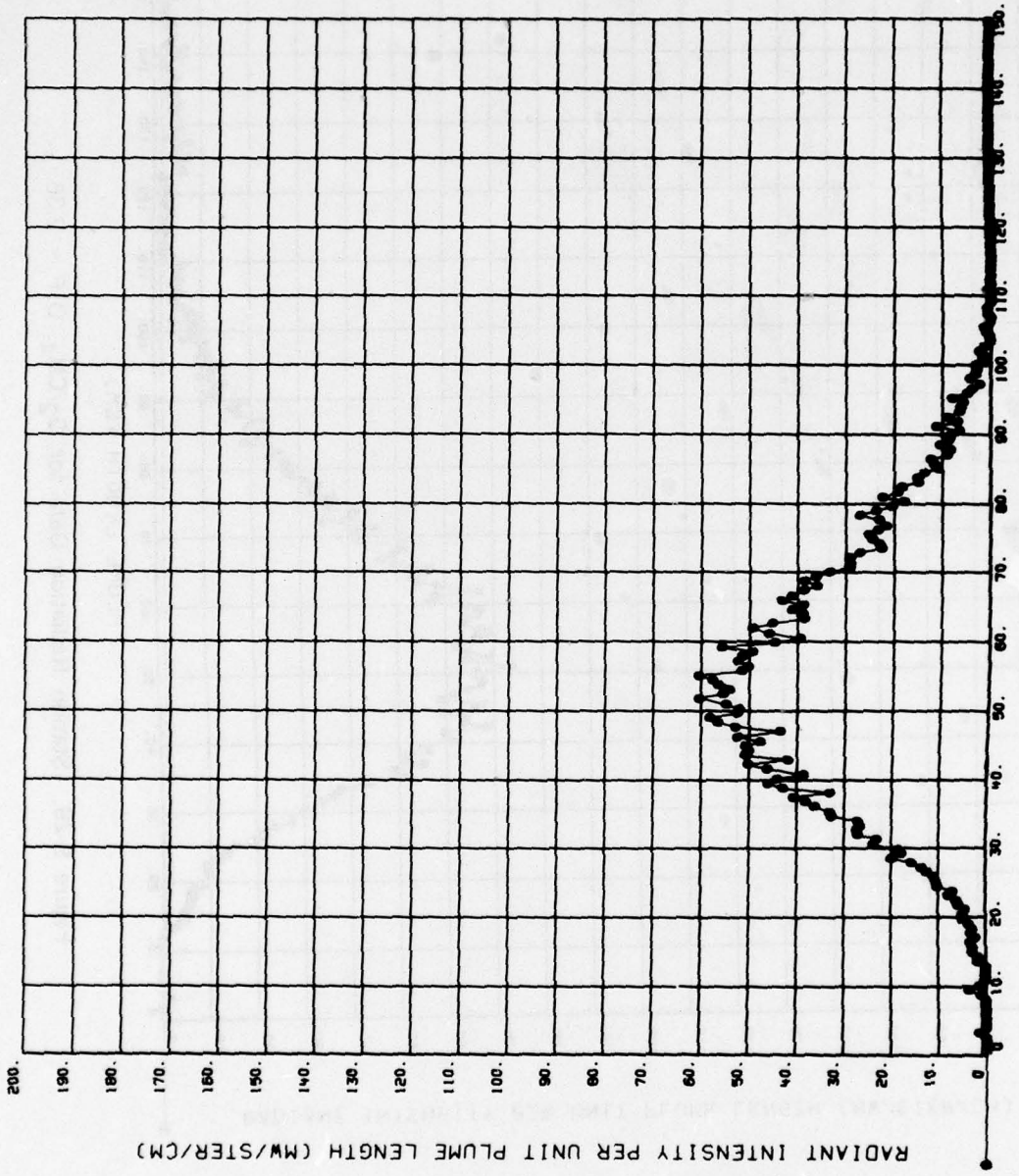

Figure B-28. Station Radiation Data for O_2/CH_4, O/F = 2.32

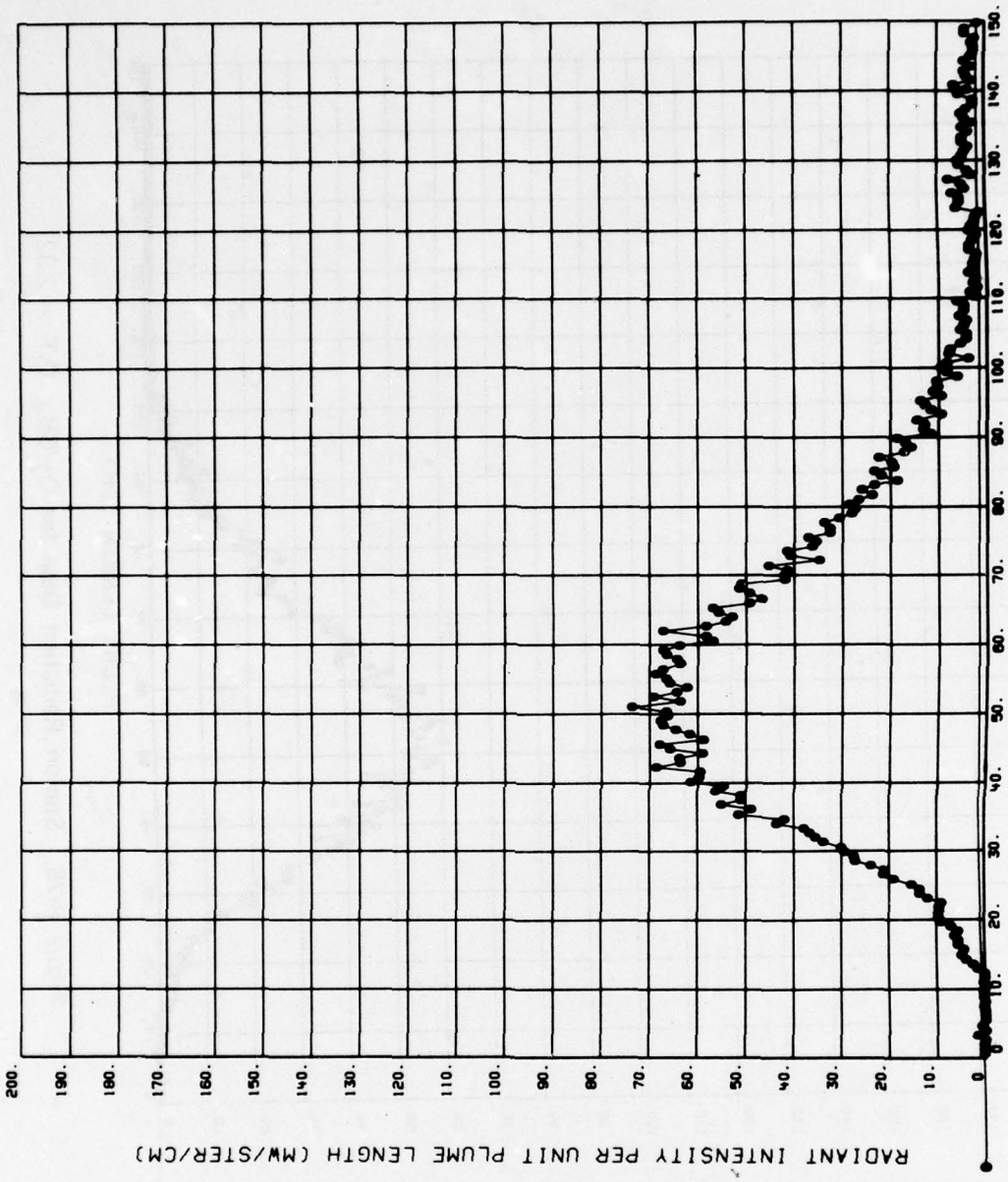

Figure B-29. Station Radiation Data for O_2/CH_4, O/F = 2.36

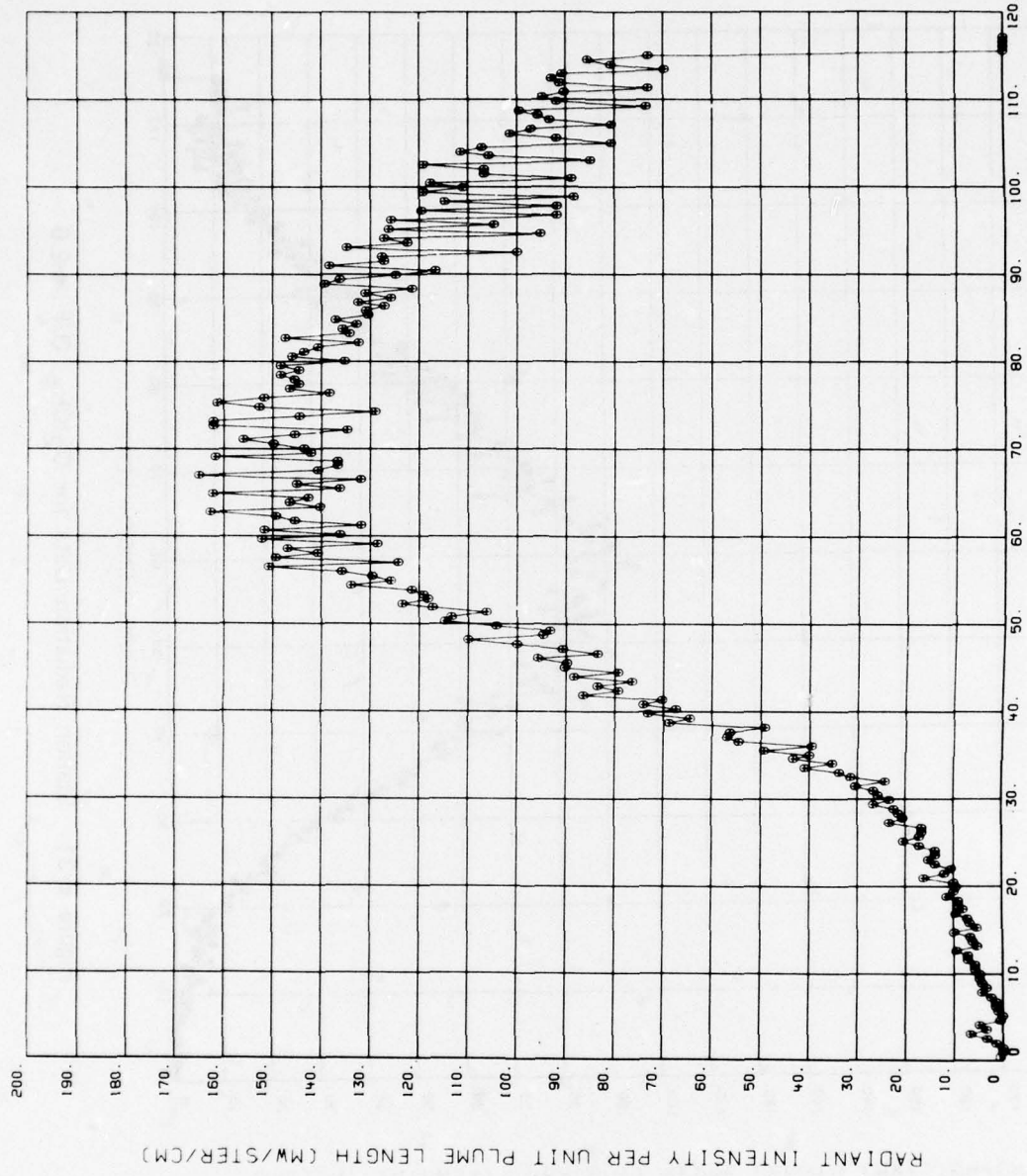

Figure B-30. Station Radiation Data for O_2/CH_4, O/F = 2.5

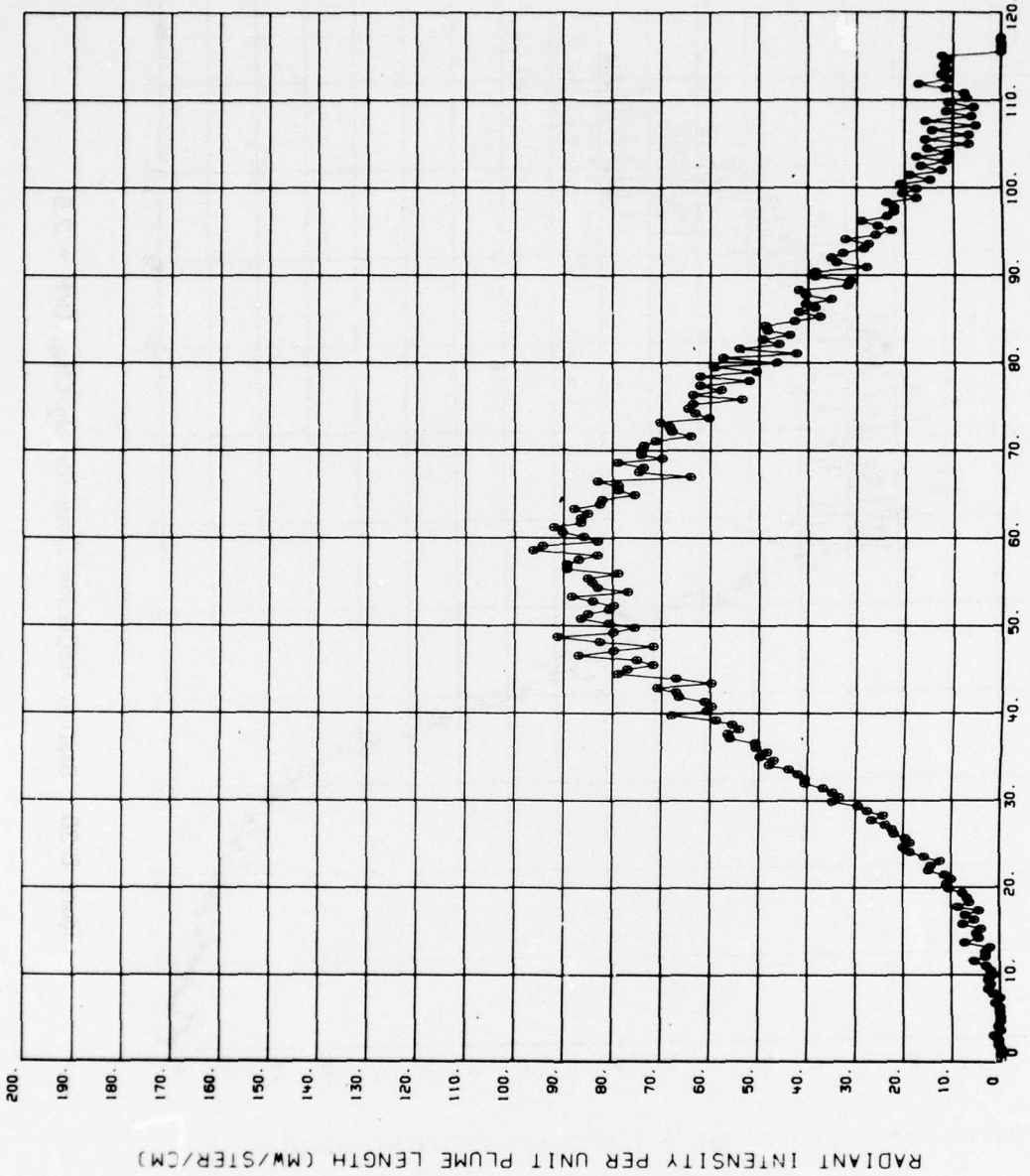

Figure B-31. Station Radiation Data for O_2/CH_4, O/F = 2.6

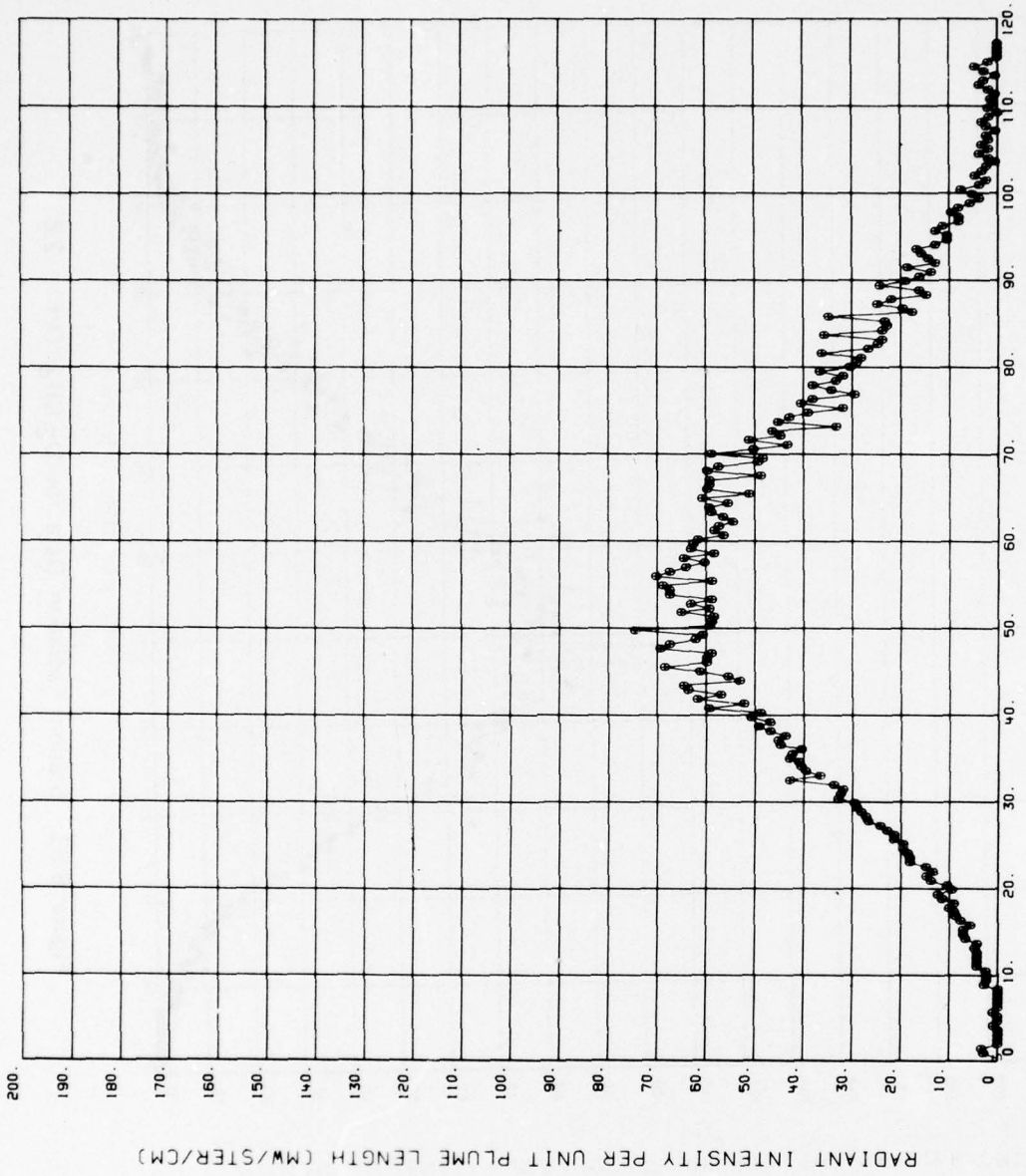

Figure B-32. Station Radiation Data for O_2/CH_4, O/F = 2.71

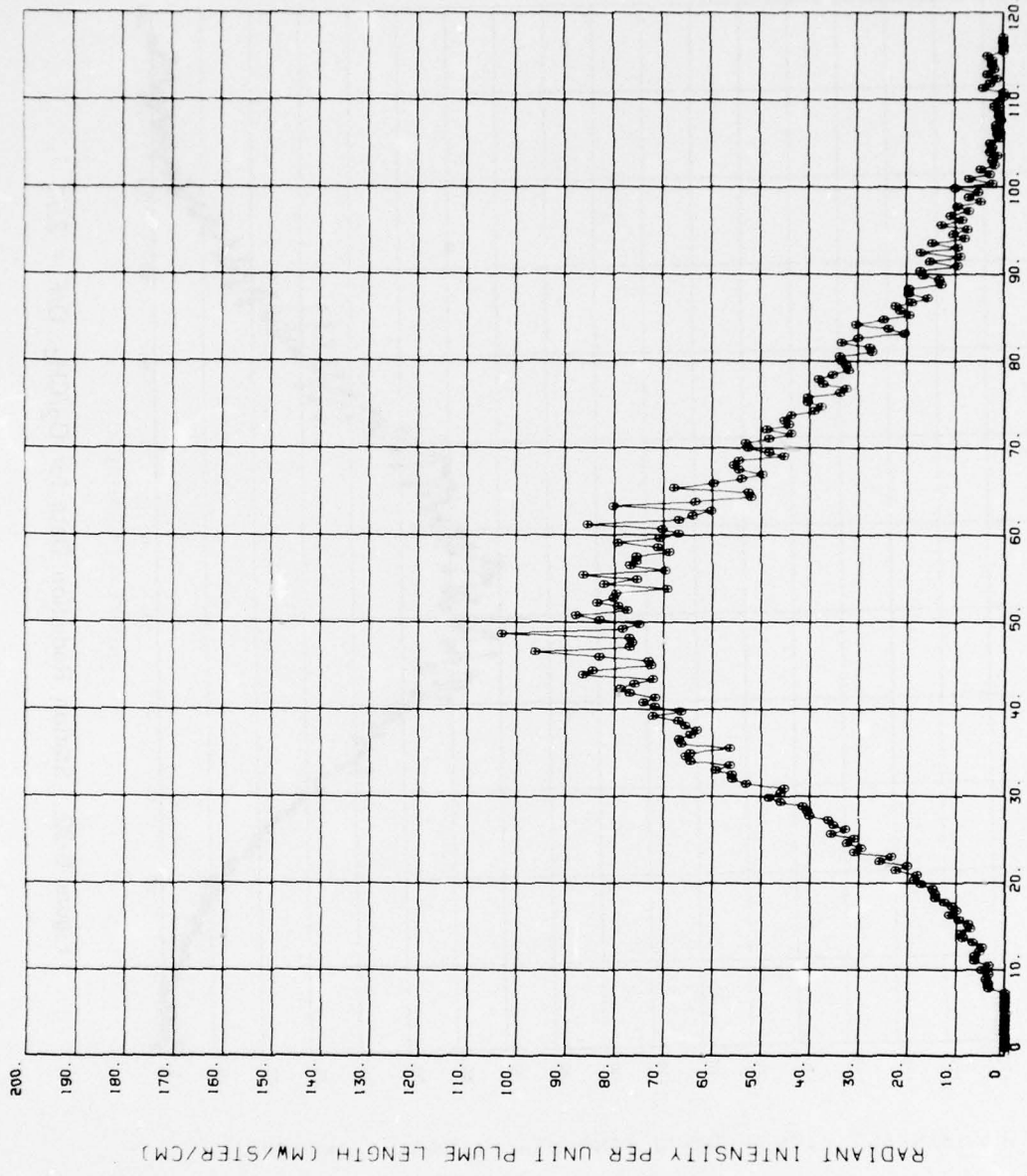

Figure B-33. Station Radiation Data for O_2/CH_4, O/F = 2.8

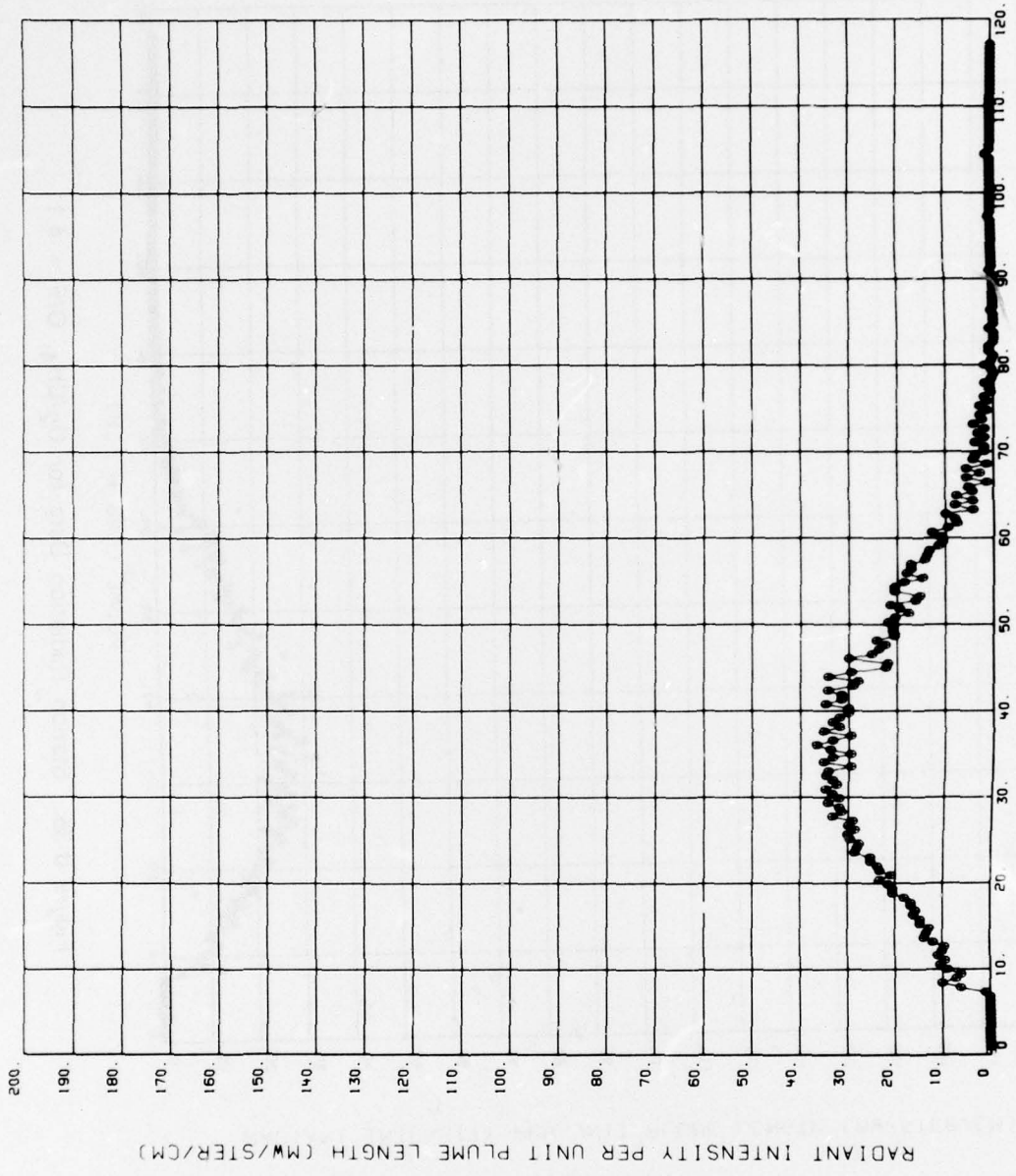

Figure B-34. Station Radiation Data for O_2/CH_4, O/F = 3.6

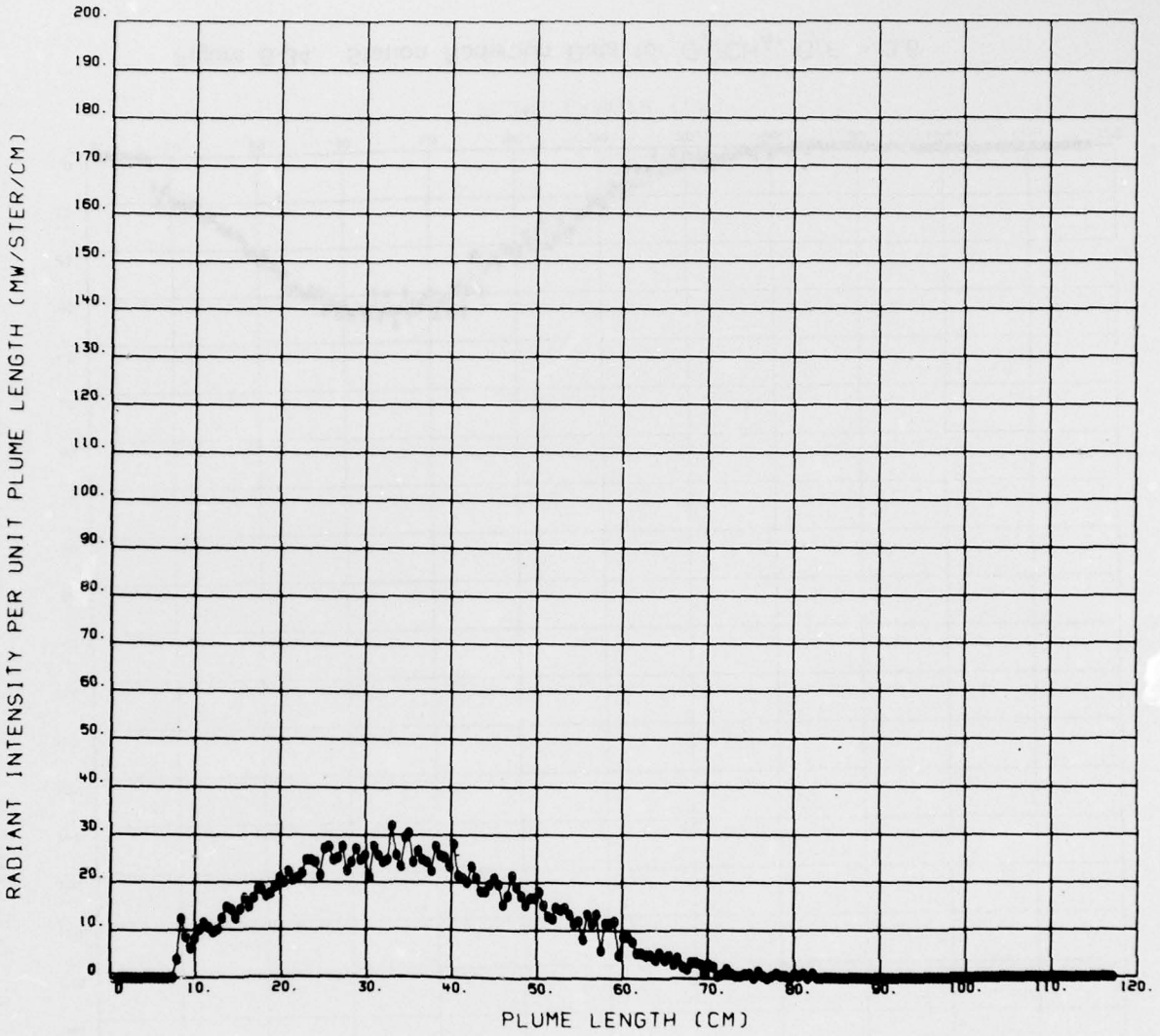

Figure B-35. Station Radiation Data for O_2/CH_4, O/F = 4.1

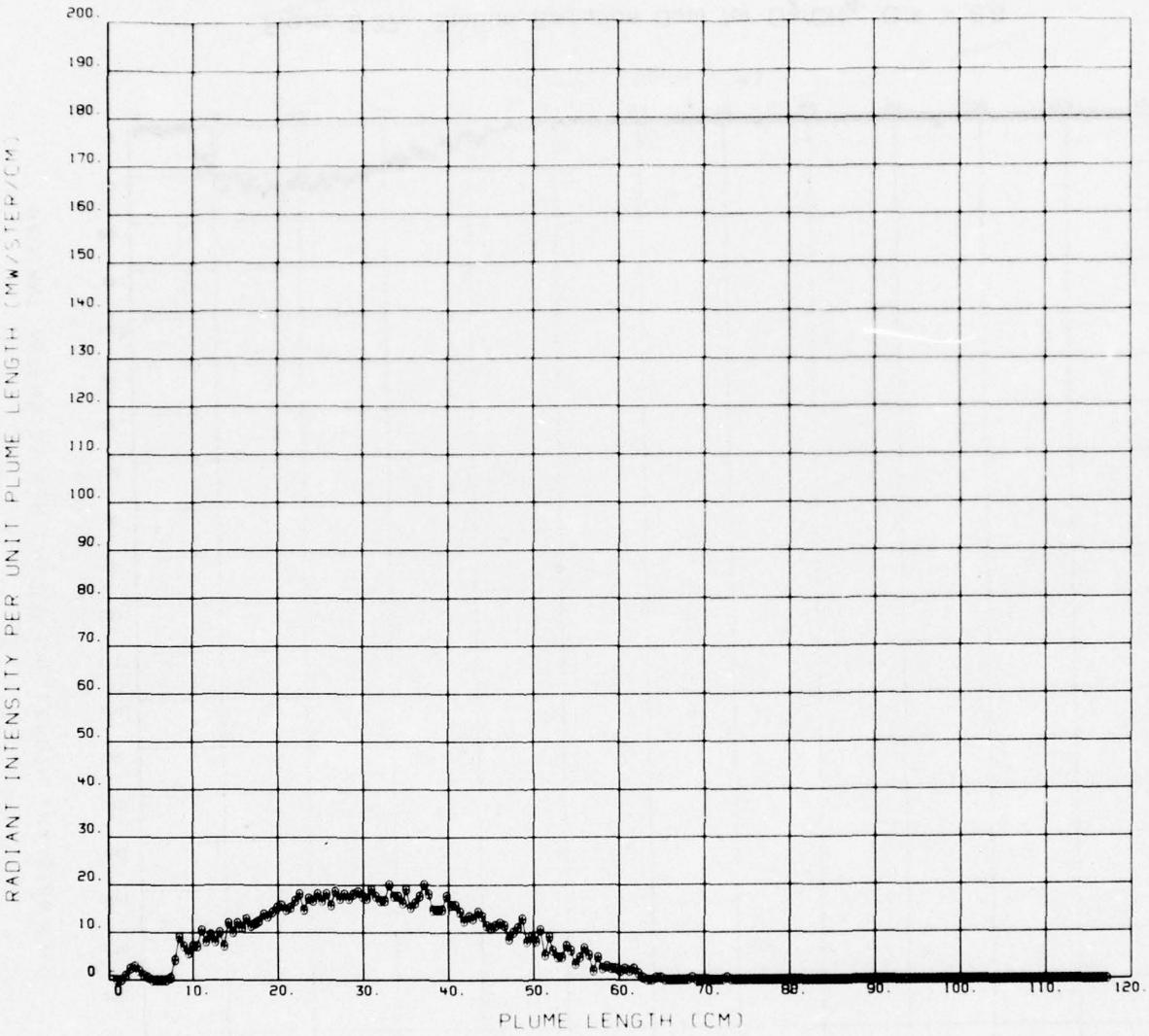

Figure B-36. Station Radiation Data for O_2/CH_4, O/F = 5.1

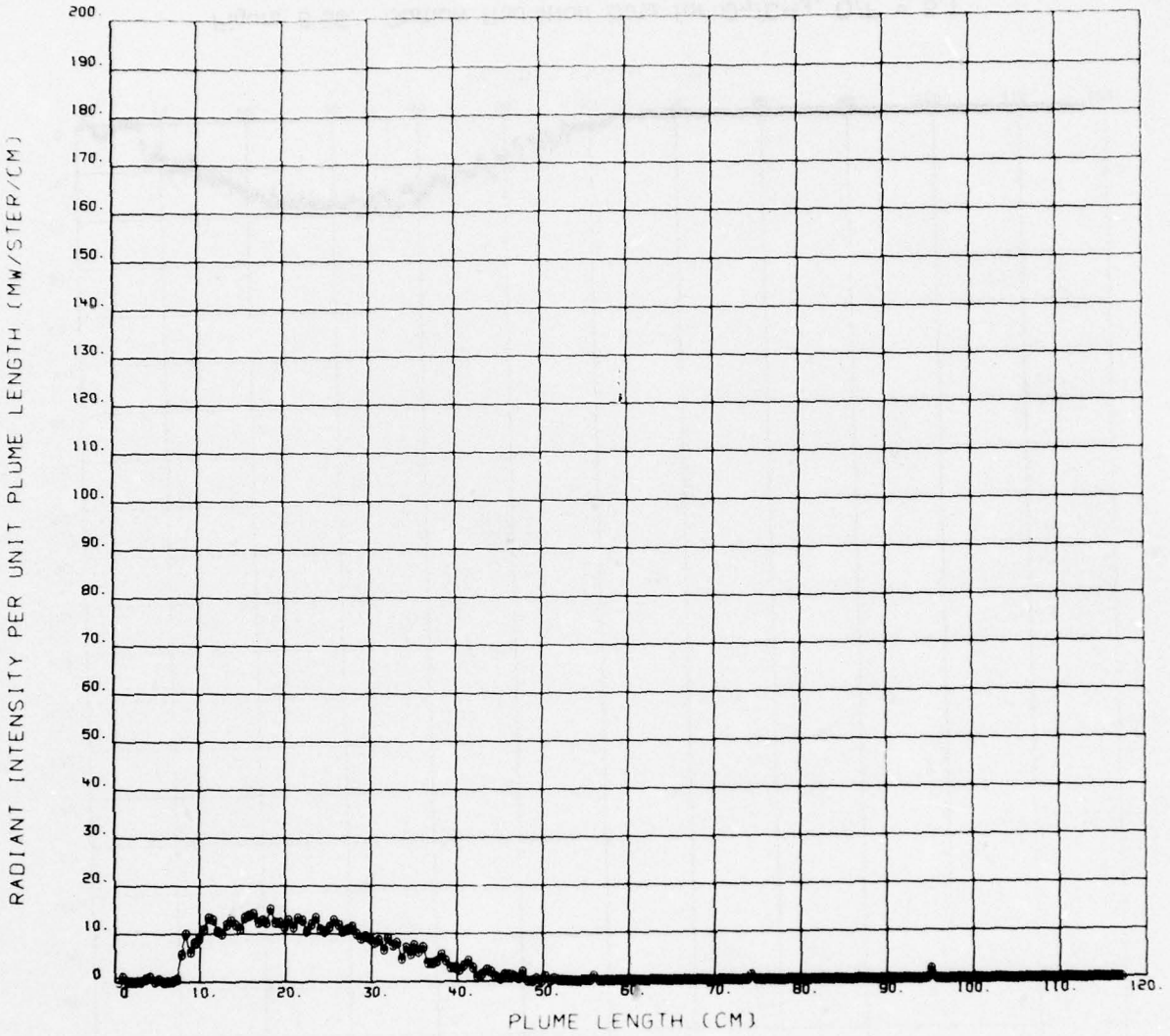

Figure B-37. Station Radiation Data for O_2/CH_4, O/F = 6.6

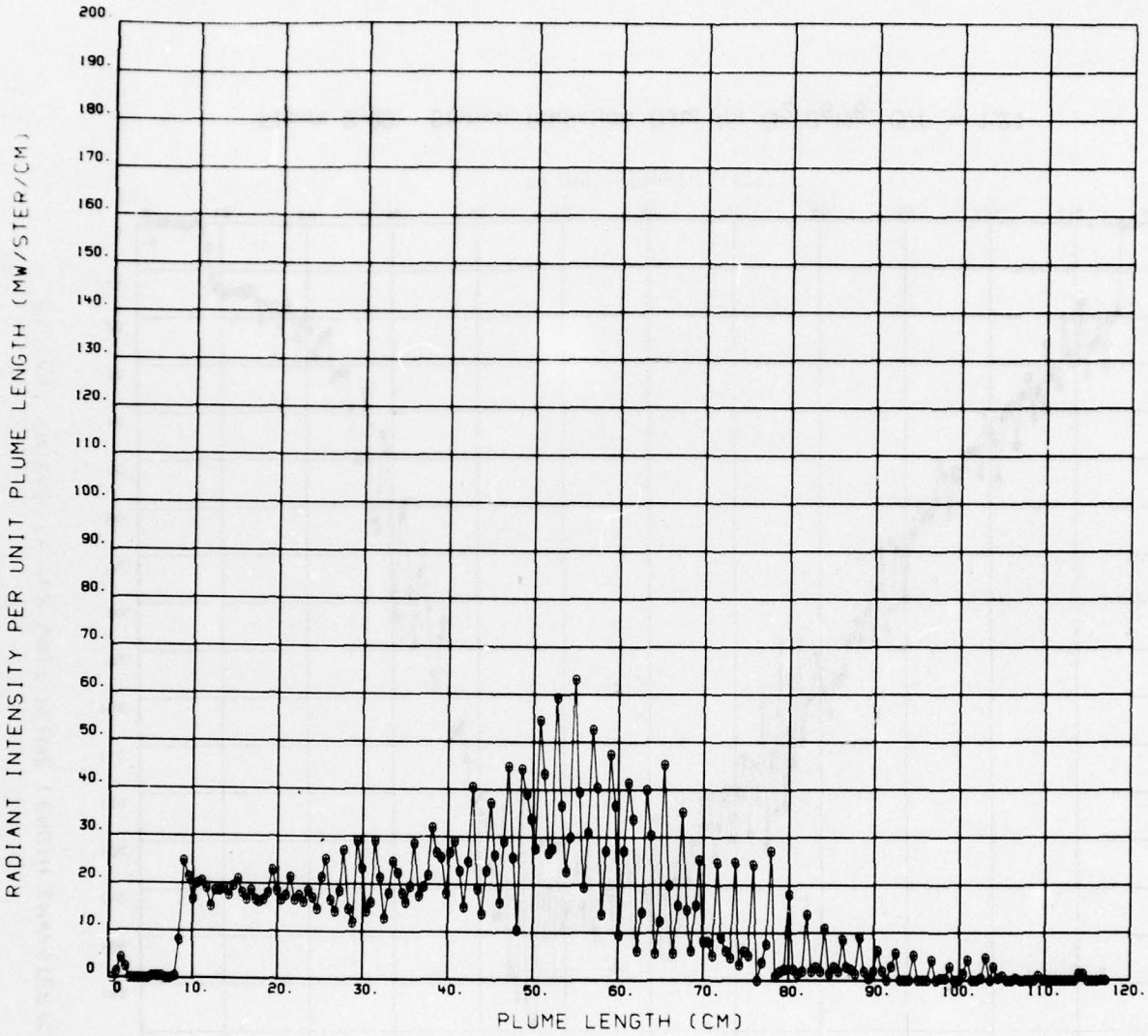

Figure B-38. Station Radiation Data for O_2/C_6H_6, O/F = 1.18

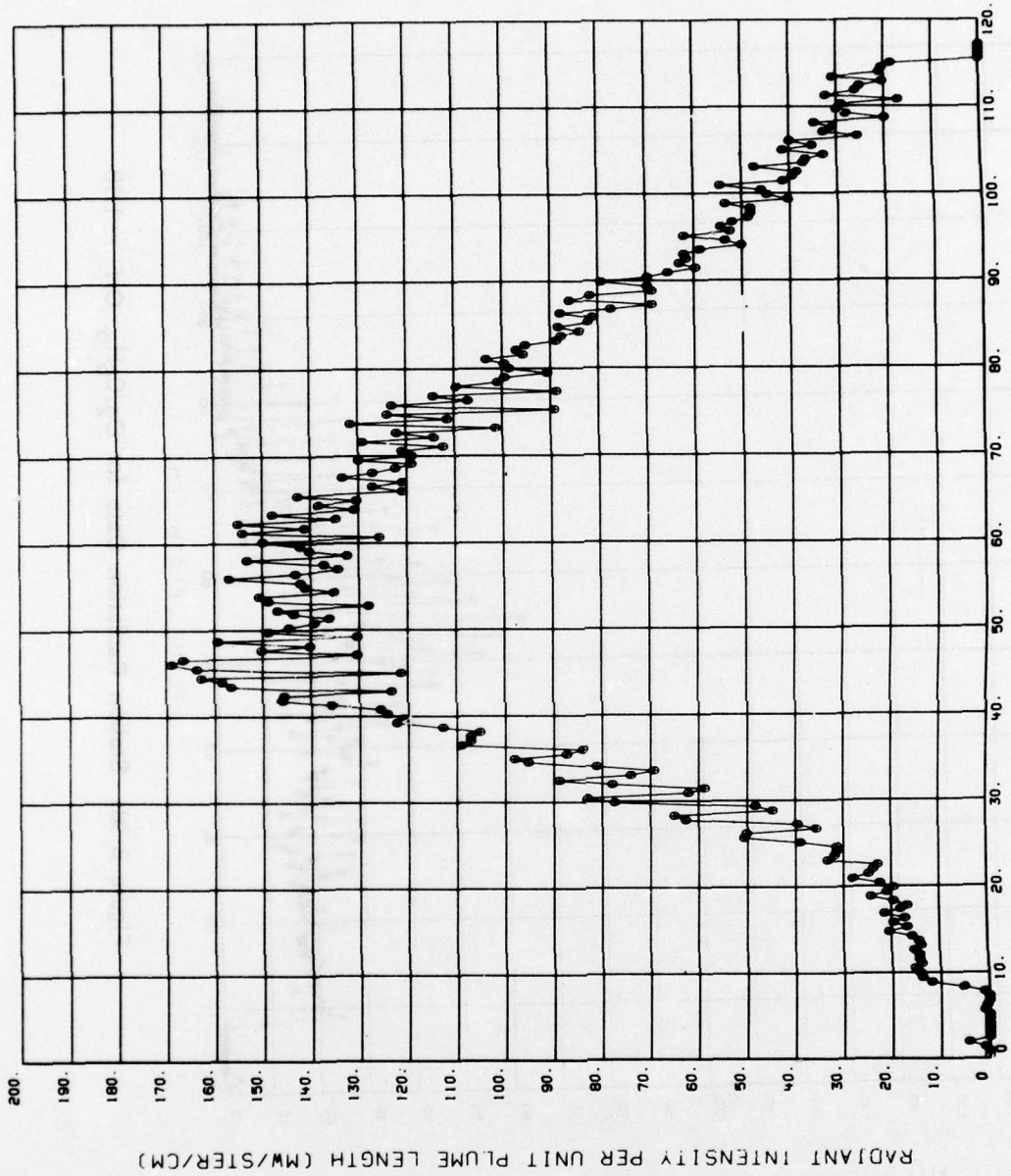

Figure B-39. Station Radiation Data for O_2/C_6H_6, O/F = 1.21

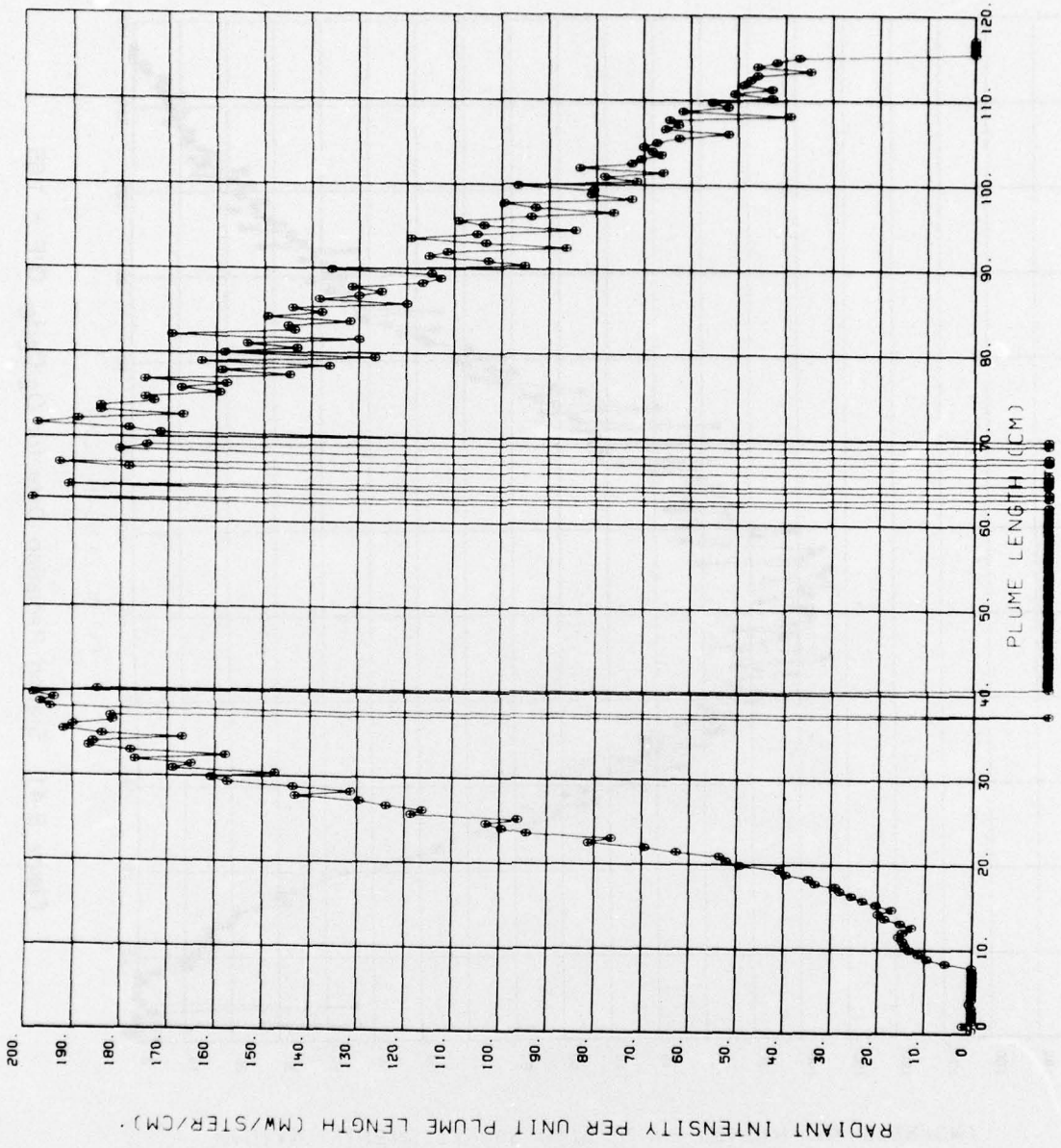

Figure B-40. Station Radiation Data for O_2/C_6H_6, O/F = 1.46

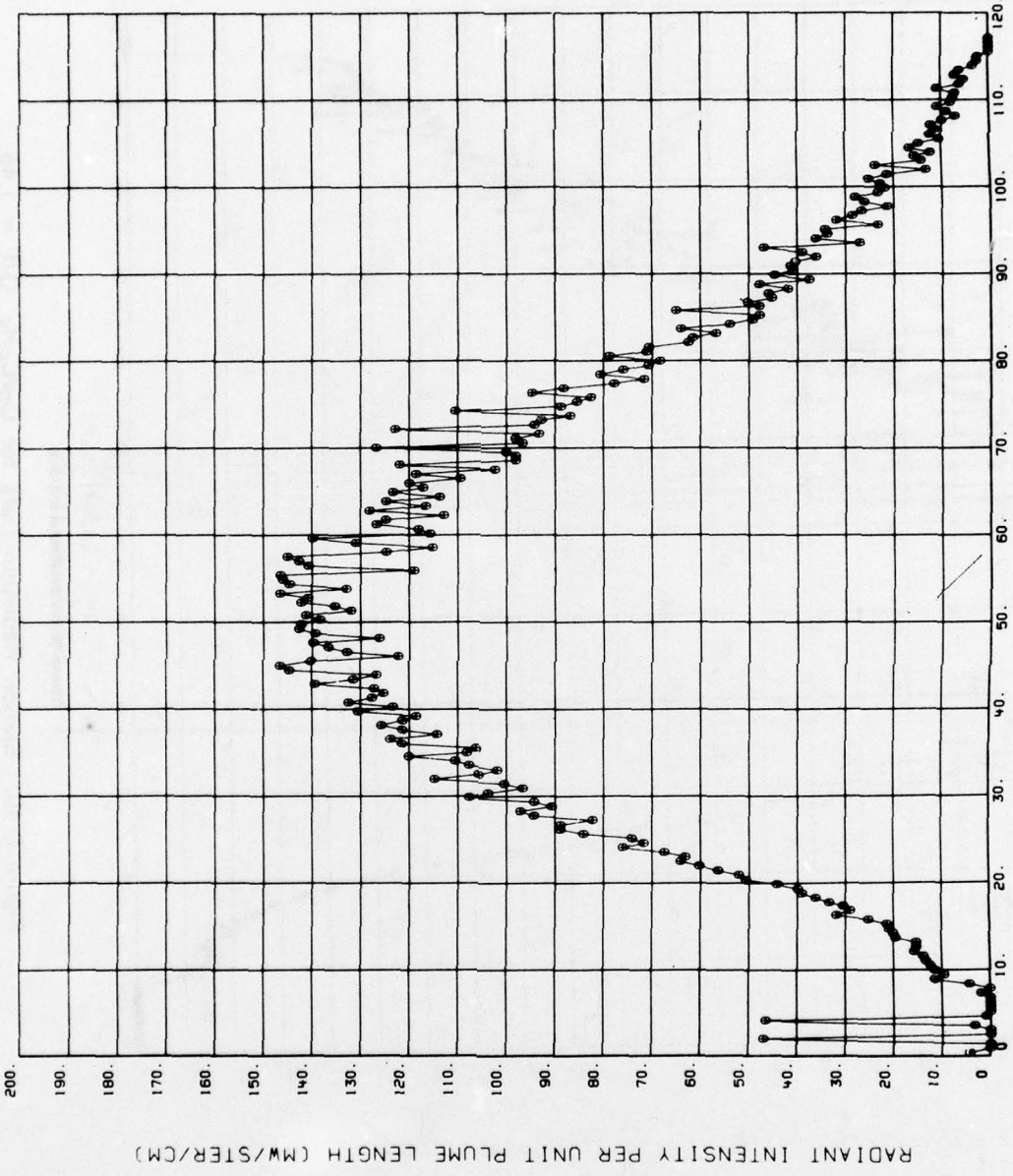

Figure B-41. Station Radiation Data for O_2/C_6H_6, O/F = 1.65

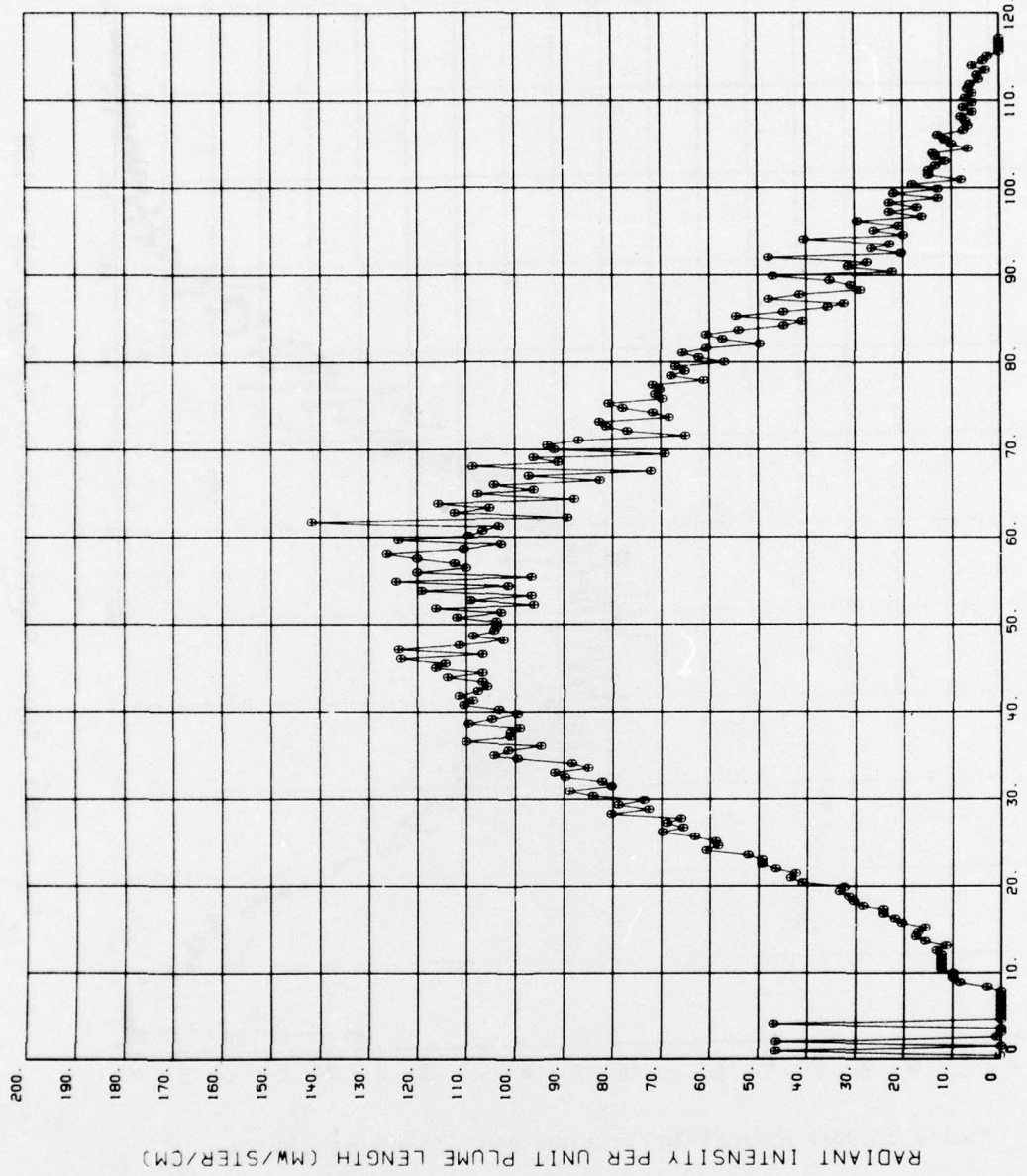

Figure B-42. Station Radiation Data for O_2/C_6H_6, O/F = 1.80

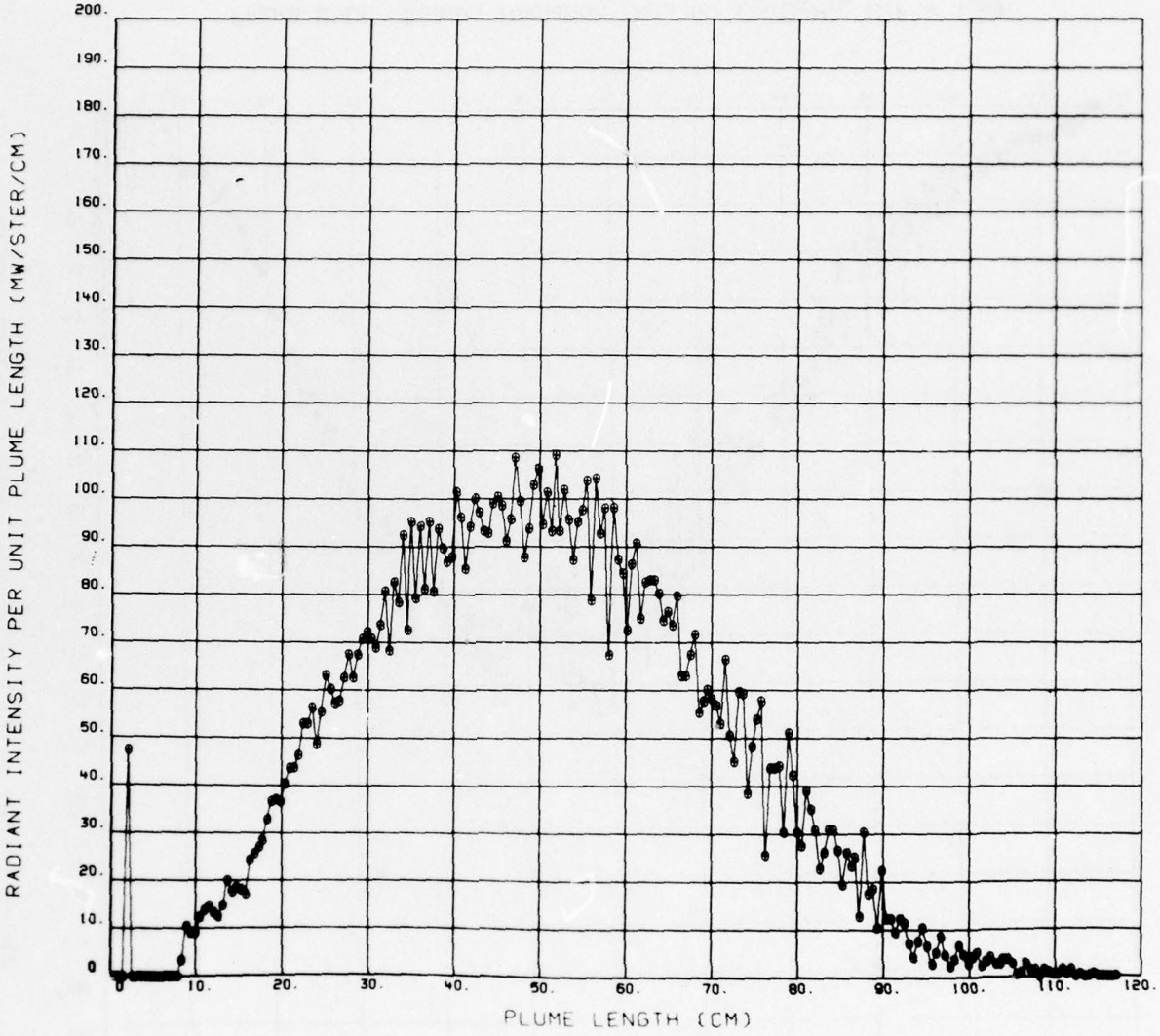

Figure B-43. Station Radiation Data for O_2/C_6H_6, O/F = 1.98

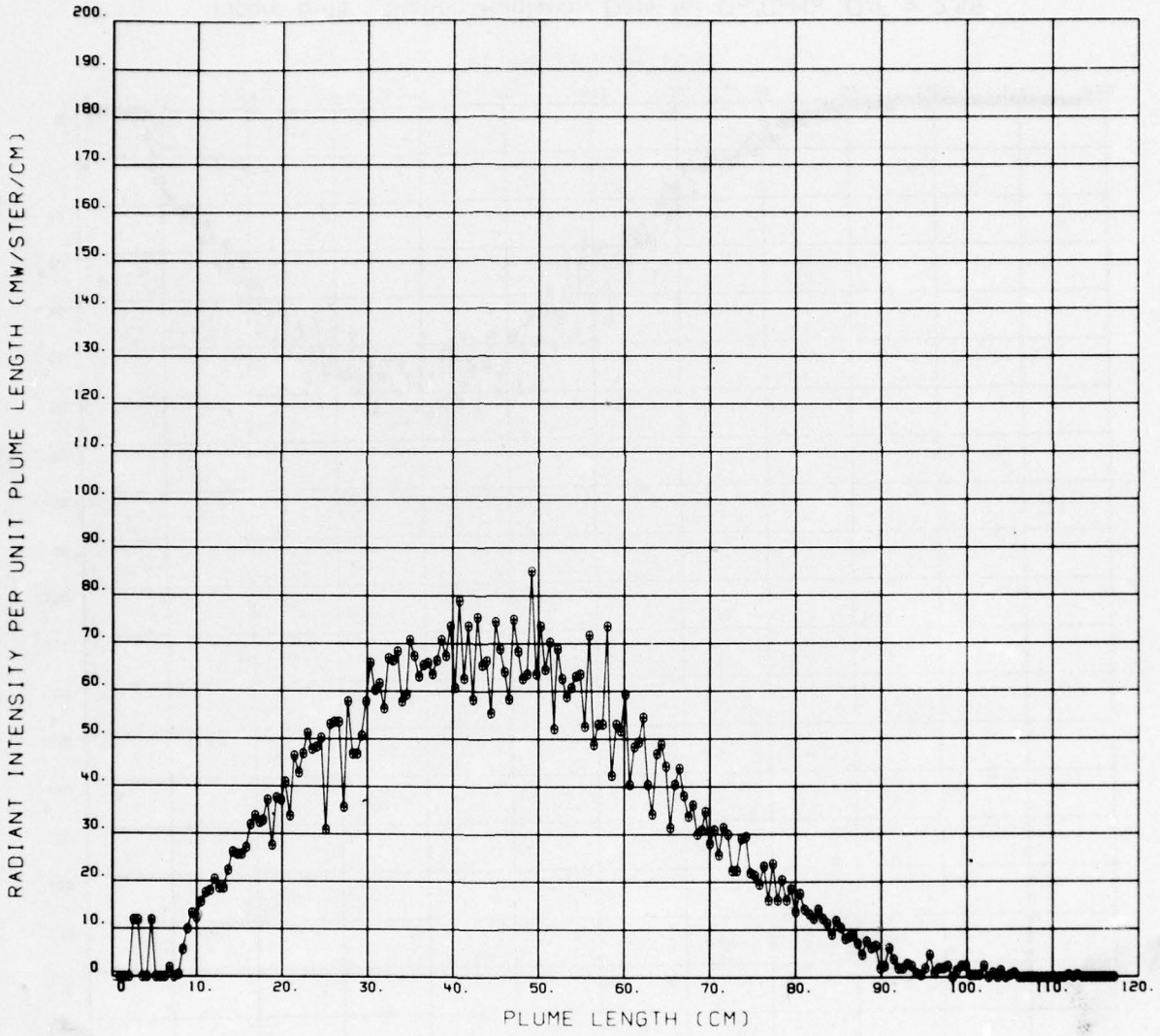

Figure B-44. Station Radiation Data for O_2/C_6H_6, O/F = 2.35

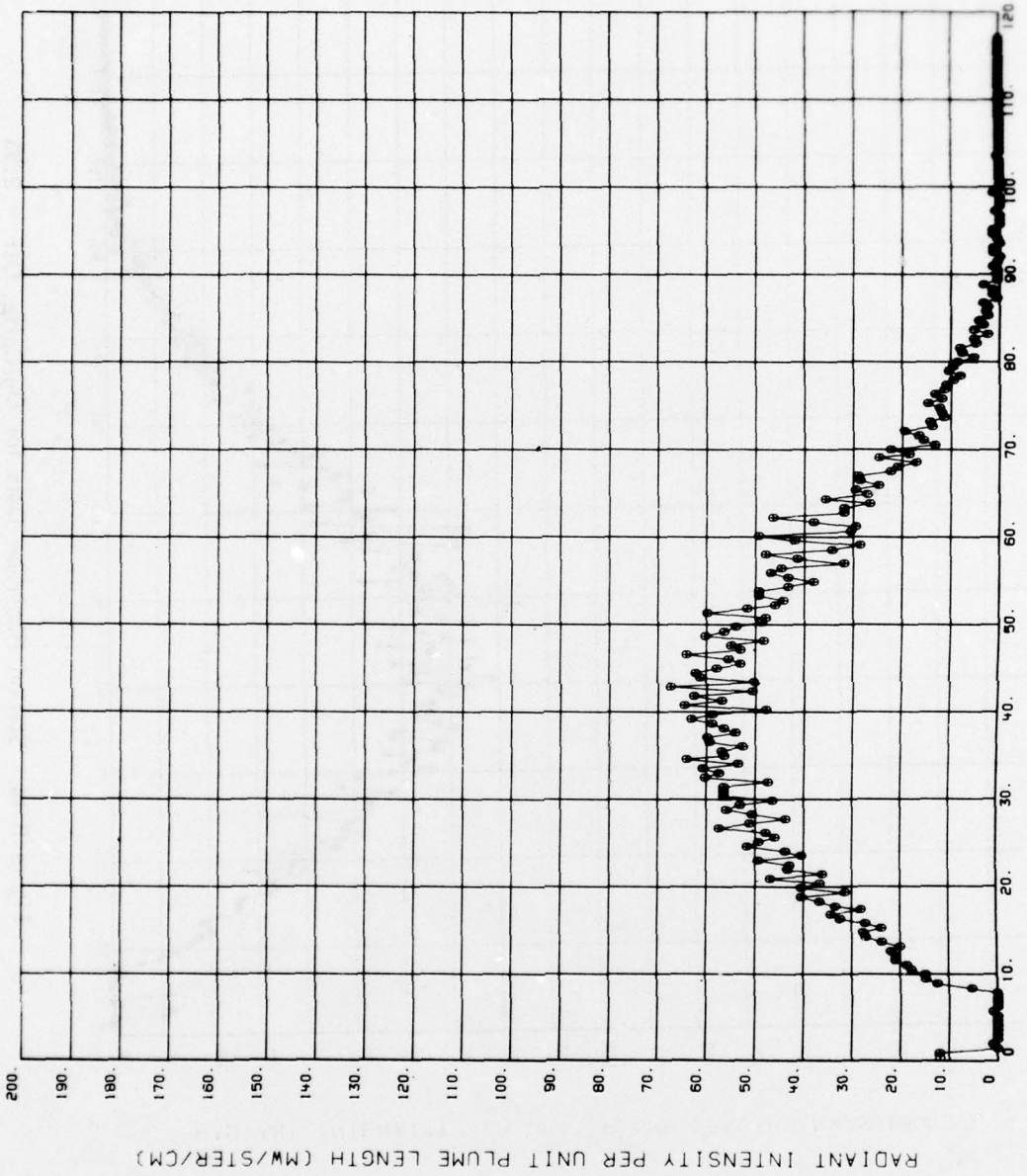

Figure B-45. Station Radiation Data for O_2/C_6H_6, O/F = 2.55

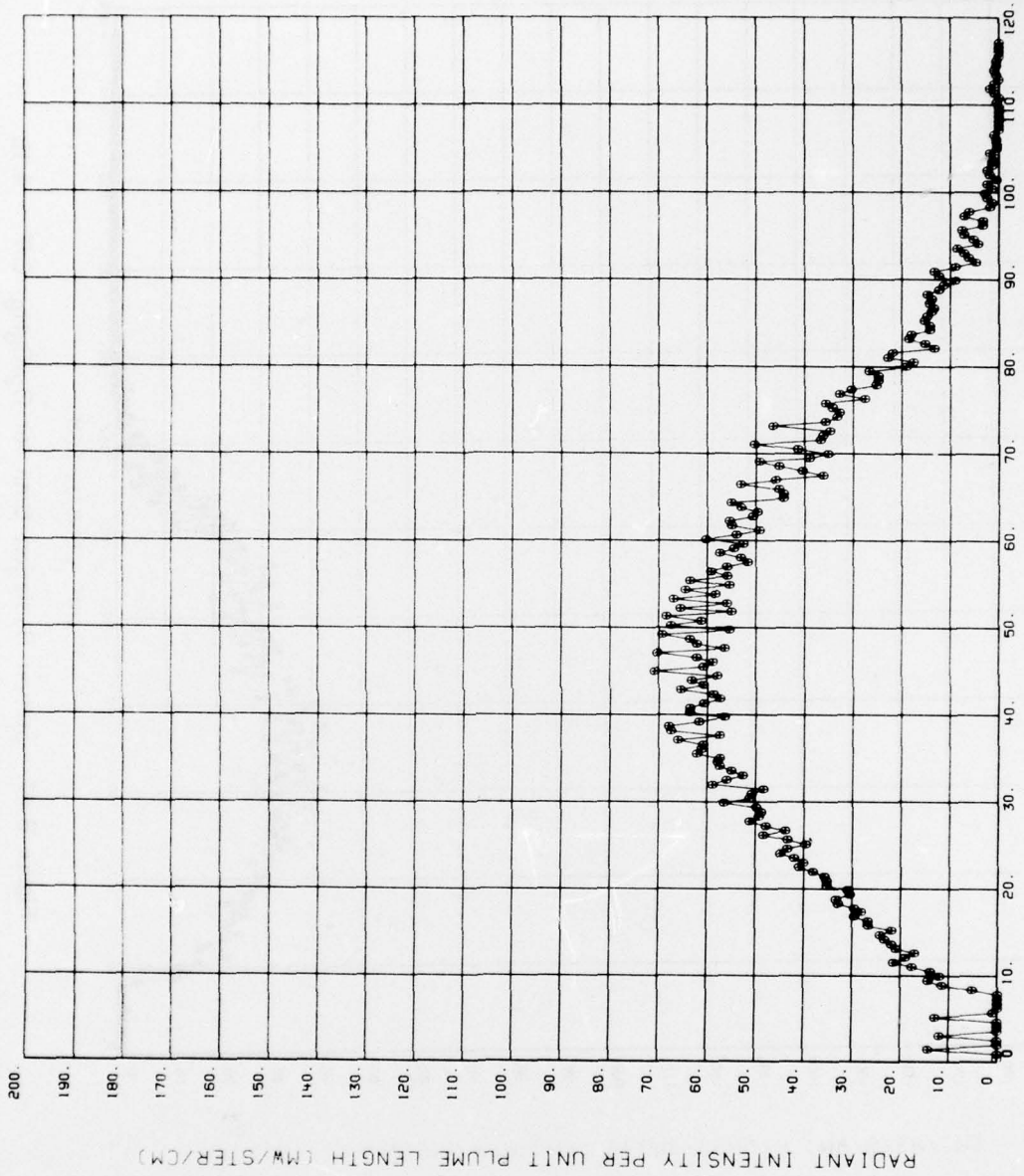

Figure B-46. Station Radiation Data for O_2/C_6H_6, O/F = 2.95

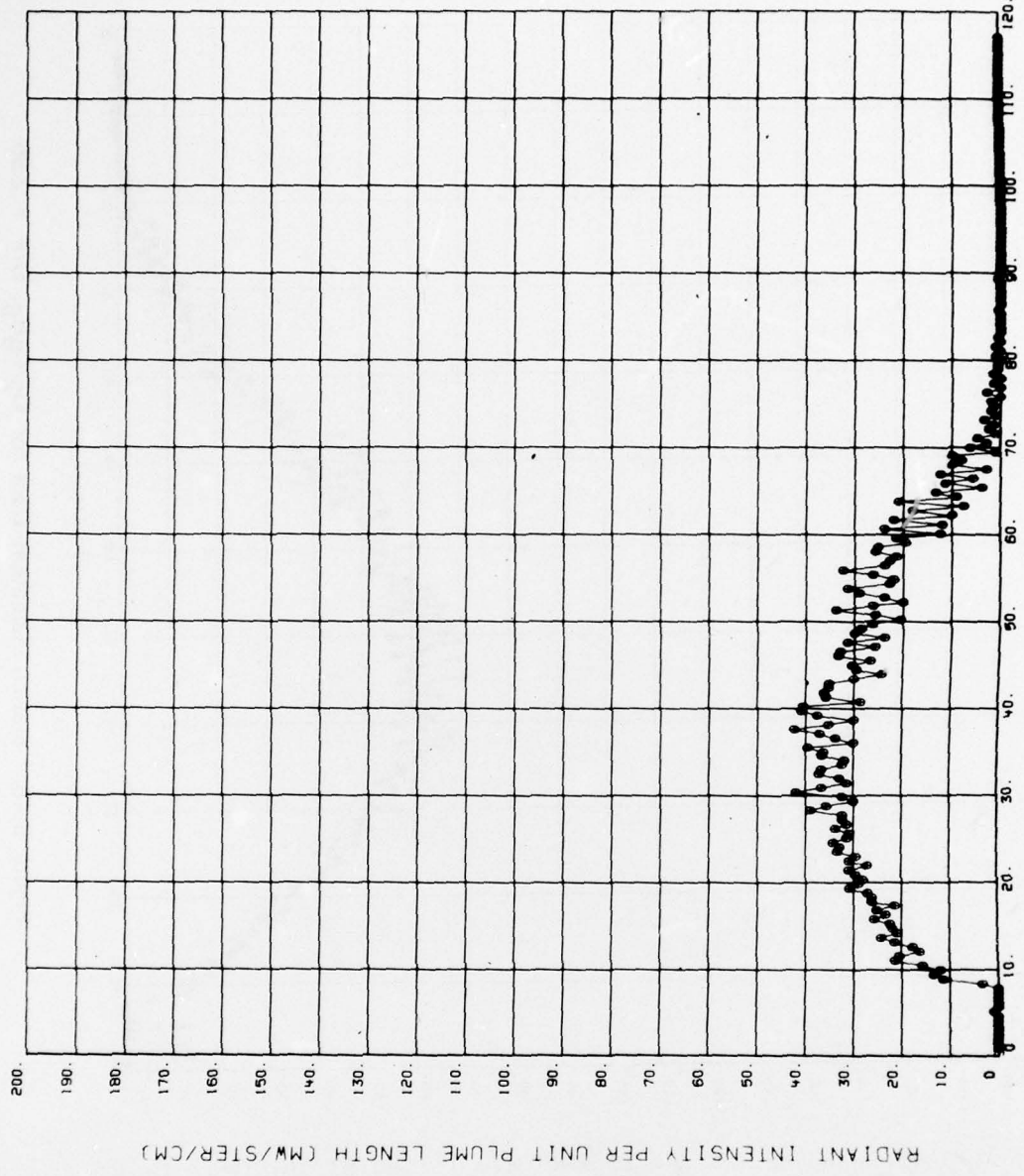

Figure B-47. Station Radiation Data for O_2/C_6H_6, O/F = 4.15

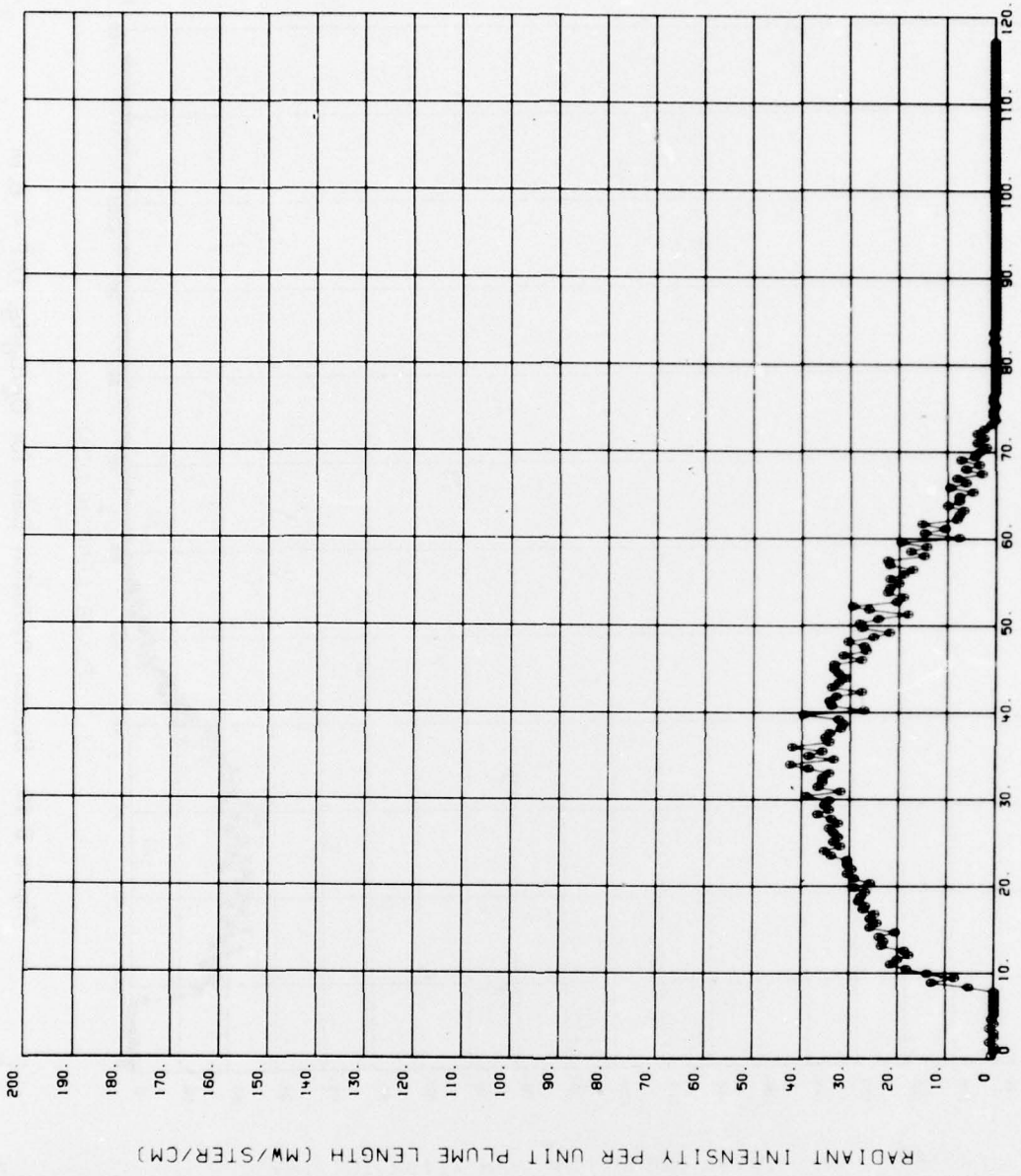

Figure B-48. Station Radiation Data for O_2/C_6H_6, O/F = 4.42

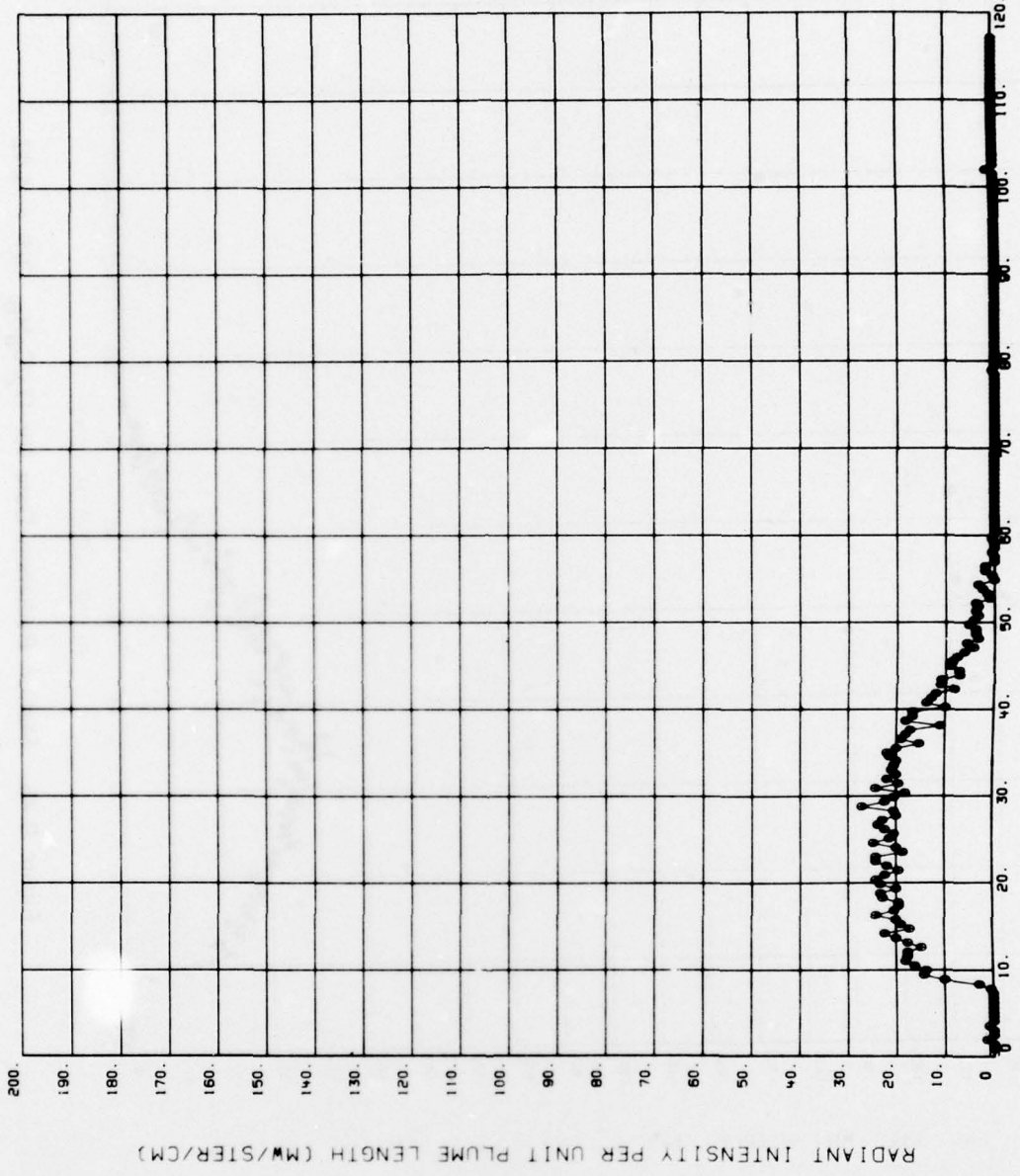

Figure B-49. Station Radiation Data for O_2/C_6H_6, O/F = 6.14

INITIAL DISTRIBUTION

USAF/RDPA	1	AFATL/DLMM	1
USAF/RDQRM	1	AFATL/DLY	1
USAF/XOOFA	1	AFATL/DLJ	1
AFSC/INA	1	AFATL/DLJC	1
AFSC/SDA	1	AFATL/DLOSL	9
AFSC/DLCAW	1	ADTC/SD	1
AFSC/DPSL	1	ADTC/SDW	1
AFSC/SDWM	1	ADTC/SDT	3
TAC/DRA	2	ASD/SDC	1
TAC/XPSY	1	ASD/SDM	1
AFAL/AA	1	AFFDL/FGC	1
AFAL/TEM	1	USAFA, DFAN, Maj Gallington	1
AFAL/RWM	1	SAC/XPHN	2
AFAL/RW	1	SAC/DOXT	1
ASD/YHEV	1	AFAL/NVA-679A	2
ASD/XRE	2	ASD/SD-65	1
ASD/YFEI (Armament)	1	Philco-Ford Aeronutronics Div	1
ASD/ENO	1	Hughes Aircraft Co	1
ASD/ENFEA	1	Martin-Marietta Corp	1
ASD/ENASA	1	The Rand Corporation	1
ASD/YPEX	1	Ogden ALC/MMNOP	2
ASD/RWS	1	USAFE/DOQ	1
ASD/RWR	2	PACAF/DOO	1
ASD/SD (Tech Dir)	1	CIA/John W. Hutson	1
ASD/SD7	2	Inst for Def Analyses/Mr Bieberman	1
ASD/SD5EI	1	Inst for Def Analyses/Dr Wolfhard	1
ASD/SD4T	2	AFOSR/NAE	1
6585TG/GDP	1	FTD/ENDA	1
AUL/AUL-LSE-70-239	1	ASD/XRHP	1
NASC/AIR-5323	1	AFAPL/RJT	1
NASC/AIR-5324	1	AFGL/OP	1
DARPA/TIO	1	AFRPL/DYSP (Dr Stewart)	2
NASC/AIR-360E	1	Sandia Corporation/Tech Lib 3421	1
CO, VX-5 (Code 9020)	1	AEDC/ARO, Inc	1
USAF/AFSC Liaison Office	6	ARO, Inc/Wheeler K. McGregor	1
CO, NWC (Code 456)	2	USA Missile Command/AMSMI-RDK	1
CO, NWC (Code 533)	1	AFOSR/NP	1
CO, NWC (Code 4063)	1	FTD/ETEO	1
CO, NWC (Code 40903)	3	USNMC/Code 5351	1
CO, NWC (Code 3301)	1	CO, NWC (Code 39403)	1
CO, NWC (Code 335)	1	CO, NWC (Code 4513)	2
Redstone Sci Info Cen/Ch Documents	2	CO, NWC (Code 454)	1
CO, USN Weapons Lab/MAL	1	CO, NWC (Code 394)	1
CG, USAMICOM/AMCPM-CT-E	1	Naval Research Lab/Code 4004B	1
DDC	2	ADTC/TEEP	2
CINCPACAF/IGFW	1	AFATL/DLMI	20
ADTC/PP	1	Aerodyne Research, Inc	2
ADTC/TGW	1	Aerochem Research Labs, Inc	2
SOF/DR	1	Aeronautical Research Associates of Princeton, Inc	2
TAWC-DT	1	The Aerospace Corp/Richard H. C. Lee	1
TAWC-FTS	1	The Aerospace Corp/Delbert D. Thomas	1
ADTC/XR	2	Beech Aircraft Corp/Francis C. Chenoweth	1
TRADOC/ADTC/DO	1	Calspan Corp	1
AFATL/DL	1	Grumman Aerospace Corp	2
AFATL/DLB	1	Lockheed Missiles & Space Co	2
AFATL/DLMA	1	Physical Dynamics, Inc	1
AFATL/DLM	1		

Thikol Corp, Wasatch Div	1
TRW Systems Group	1
Brigham Young Univ/L. Douglas Smoot	1
General Applied Research Lab	2
USA/MC (AMSMI-TM)	1
CNO-OP-932E21	1
AFWL/LRL	1
AFTEC/TET	1
AFTEC/TER	1
AFTEC/TE	1
6585TG/RX	1
AFSWC/TEE	1
ODDR&E/OSD/T&E	2
USNMC/Code 5162	1
AFWL/RL	2
ADTC/SD-102	1
TAWC/TW	1
TAWC/TEF	1
TAWC/TERR	1
TAWC/TERA	1
British Defense Staff, British Embassy	3
AFTEC/XR	1
AFTEC/TET	1
USAF/AF-SAMI	1
4950TW/TIHM	1
ADC/DOV	1
CO, USA Missile Comd/AMSMI-TM	1
CO, USA Missile Comd/AMSMI-REI	1
ADWC650th TES	1
CO, Pacific Missile Test Center/Code 1252	1
CO, COMPTREVFOR (Code 713)	1
CO, TFWC/TAF	1
CO, NASC/PMA-247	1
CO, NSWSES/Code 4221	1
CO, NADC/Targets Office	1
Mitre Corp/Mr Greenlee	1
Beech Aircraft Corp/HAST Ofc (Mr Wells)	1
Atlantic Research Corp	1
Teledyne CAE	1
Teledyne Ryan Aeronautical	1
Northrup Ventura	1
Hayes International Corp/Targets Div	1
Sanders Associates Inc	1
Motorola Inc, Govn Elec Div	1
Ordnance Research Inc	1
United Technologies	20
AFIS/INTA	1
Univ of Florida, Dr Richard T. Schneider, Professor of Nuclear Engrg Sciences	1
Avco Systems Div	1
Univ of Maryland, Dept of Aerospace Engineering , Dr J. D. Anderson	1
DARPA	1
AFCRL/OPI	1
ROCKETDYNE	1
Univ of Florida, Dr Roland Anderson, Dept of Engineering Sciences	1
AFAPL/POD	1